Towards Programmable Materials - Tunable Material Properties Through Feedback Control of Conducting Polymers

by

Nathan Scott Wiedenman

B.S., Harvey Mudd College (1993)
M.S., University of California at Berkeley (2003)

Submitted to the Department of Mechanical Engineering
in partial fulfillment of the requirements for the degree of

Doctor of Philosophy in Mechanical Engineering

at the

MASSACHUSETTS INSTITUTE OF TECHNOLOGY

June 2008

Author .....
Department of Mechanical Engineering
May 7, 2008

Certified by .....
Ian W. Hunter
Hatsopoulos Professor of Mechanical Engineering
Thesis Supervisor

Accepted by .....
Lallit Anand
Chairman, Department Committee on Graduate Students

Towards Programmable Materials - Tunable Material Properties Through Feedback Control of Conducting Polymers

by

Nathan Scott Wiedenman

Submitted to the Department of Mechanical Engineering
on May 7, 2008, in partial fulfillment of the
requirements for the degree of
Doctor of Philosophy in Mechanical Engineering

Abstract

Mammalian skeletal muscle is an amazing actuation technology that can controllably modify its force and position outputs as well as its material properties such as stiffness. Unlike muscle, current engineering materials are limited by their intrinsic properties, dictated at the molecular level.

This work is focused on developing an integrated device, called a *programmable material*, which mirrors the capabilities of natural co-fabricated controlled actuation systems such as muscle. While such a device may have the external appearance of a homogeneous material, it can possess unique properties not existing in any currently manufactured material. When actuation, sensing, and control capabilities are integrated within a closed-loop system, the mechanical properties of the system such as stiffness, viscosity, and inertia will arise from the dynamics of the feedback loop rather than from any inherent mechanical properties of the materials from which the device was fabricated. Moreover, these properties may be 'tuned' by altering the feedback parameters embedded in the material system. With this approach properties such as negative stiffness may be generated which do not exist in bulk materials.

The most promising of the existing artificial muscle technologies is actuation with conducting polymer. Additionally, conducting polymer has been used to fabricate the position sensor and control electronics. Creating these components from a single type of material has made it possible to co-fabricate the system into an integrated device. This is the first research to attempt to create a co-fabricated, fully integrated conducting polymer feedback device. This work establishes the feasibility of building the device and answers many of the questions of fabrication and design.

Thesis Supervisor: Ian W. Hunter
Title: Hatsopoulos Professor of Mechanical Engineering

Acknowledgments

The time I have spent at MIT has been an incredible experience. That has largely been due to the excellence of the people with whom I have had the opportunity to collaborate, analyze, experiment, build, tear apart, and absorb. The ideas and knowledge that these people bring to the table are staggering, and their willingness to share their expertise has been a key factor in any success I have been able to achieve.

First and foremost, I must thank Professor Ian Hunter for giving me the chance to work in the amazing environment of the BioInstrumentation Lab. His enthusiasm and seemingly endless capacity for new ideas is an inspiration.

My colleagues in the BioInstrumentation Lab have been irreplaceable in their expertise, willingness to assist, and sense of humor. I have never worked in a more comfortable and collegial environment than this lab, with the overall success of the lab's work and research a priority for all rather than consisting of a collection of independent projects. Thanks to Patrick Anquetil, Cathy Hogan, James Tangorra, and Andrew Taberner for all of their guidance. I could not have survived without the collaboration and decompression opportunities provided by my labmates, including Tim Fofonoff, Rachel Pytel, Nate Vandesteeg, Priam Pillai, Nate Ball, Mike Del Zio, Angela Chen, Brian Hemond, Bryan Ruddy, and Scott McEuen. Thanks also to the undergraduates who have helped me with my biostability research: Arjun Naskar, Ed Jennings, Sarah Sheih, and Nate Sharpe.

Professors Tim Swager, John Joannopoulos, and Karen Gleason have all provided invaluable advice and input. I want to thank John and everyone at the Institute for Soldier Nanotechnologies for providing the funding and many of the resources needed to complete this work. My discussions with Tim about the molecular structure of polypyrrole and how to manipulate it provided me with useful insight. I was very lucky to have the opportunity to work with Karen, who graciously allowed me to utilize her lab facilities in the Department of Chemical Engineering to explore and complete my oCVD work. In the Gleason Lab, Sung Gap Im and Dr. Sreeram

Vaddiraju helped me through the fine points of oCVD.

Thanks also to my committee members, Professors John Leonard and Derek Rowell, for their guidance and feedback throughout this process. Their assistance has been invaluable for maintaining the focus and drive of this work.

I must also thank the U.S. Army for providing me the opportunity to complete this work. Funding for my time at MIT was provided by the Uniformed Army Scientist and Engineer program, and I am sincerely grateful for the chance to do this. Thanks especially to Mrs. Paula Bettes, who was always available for advice and guidance when it came to Army matters.

Finally, I would be lost without my wife Shannon. Her unwavering support has seen me through difficult times. I may have doubted myself, but she never did.

Biographical Note

Nathan S. Wiedenman is currently serving as a major on active duty in the United States Army. As a member of the Uniformed Army Scientist and Engineer program, his role is to serve at the intersection of the military, academia, and industry to foster research that will provide tangible, beneficial results for our nation's soldiers.

Originally from Anaheim, California, Nathan received his bachelor of science degree in engineering from Harvey Mudd College in 1993. He then entered the Army as a second lieutenant, serving as a tank platoon leader and support platoon leader in Germany and as part of the United Nations peacekeeping mission in the Former Yugoslav Republic of Macedonia.

Upon return from his time overseas, Nathan served as the company commander of C Company and Headquarters Company, 3rd Battalion, 67th Armor, at Fort Hood, Texas. In 2001, he moved to the University of California at Berkeley where he received his master of science in mechanical engineering in 2003. He spent the next two years teaching in the Department of Civil and Mechanical Engineering at the United States Military Academy at West Point.

Nathan leaves MIT for an assignment with the Army's Tank and Automotive Research, Development, and Engineering Center in Warren, Michigan.

Contents

List of Figures

List of Tables

Chapter 1

Introduction

1.1 Motivation

At rest, a human being's ankle has a stiffness of approximately 20 $\frac{N \cdot m}{rad}$. When fully flexed, the ankle can have a stiffness up 1000 $\frac{N \cdot m}{rad}$, an increase by a *factor of 50.* This is a remarkable achievement, one that has taken nature billions of years of evolution to accomplish.

The ankle system is just one of many *reflex loops* in the human body. Through the microscopic integration of muscle fibers (actin and myosin filaments), energy delivery and waste removal systems (blood vessels), sensory mechanisms (muscle spindles and Golgi tendon organs), and control capability (nervous system), these reflex loops enable finely controllable motion (see Figure 1-1). By the time we learn to walk as toddlers, we are using a wide variety of these systems without ever being conscious of their use.

No passive material could hope to match the performance of this system. Passive engineering materials are limited by their intrinsic properties, dictated at the atomic and molecular level. Characteristics like inertia, stiffness, and damping which determine the material's response to a mechanical input can only be changed by processing the material (for example, alloying, annealing, drawing, or cross-linking).

To replicate the controllable properties of muscle, an active material is required. Such a material would in fact be an integrated device. It must include an actuator

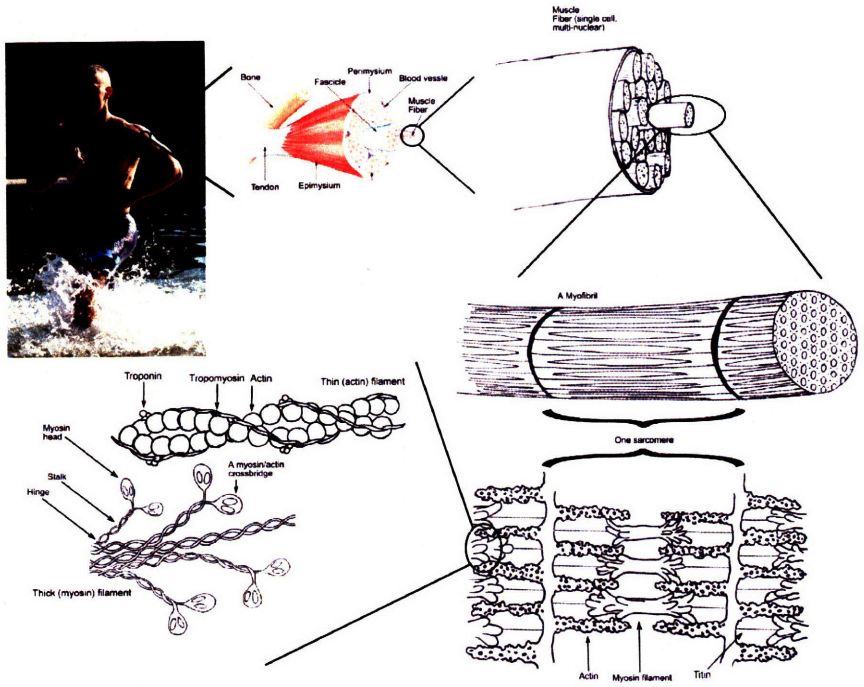

Figure 1-1: Human skeletal muscle is an incredibly intricate co-fabricated system. Through integration of actuation (muscle filaments), sensory (spindles), and control (nervous system) capabilities, a reflex loop is created which can execute extremely fine controlled motions. From [1].

component, along with sensing capability and a control system to read the sensor and drive the actuator to some desired force or position. In engineering these devices are called *servomechanisms*, and they are widely used in situations where a quantity such as position, force, or velocity must be maintained with little or no error. Unfortunately, these systems must traditionally be assembled from distinct individual components (actuator, sensor, control) as shown in Figure 1-2.

Skeletal muscle has the further advantage of being co-fabricated. That is, the various capabilities are fully integrated at the microscopic level to the extent that muscle appears to be a single homogeneous material. If traditional engineering materials and devices are used, the controllable motion performance of muscle can be matched and even exceeded, but the device will never be mistaken for a material unto itself.

This work has been focused on developing an integrated device which mirrors the capabilities of natural co-fabricated controlled actuation systems such as skeletal muscle. While this device may have the external appearance of a homogeneous material,

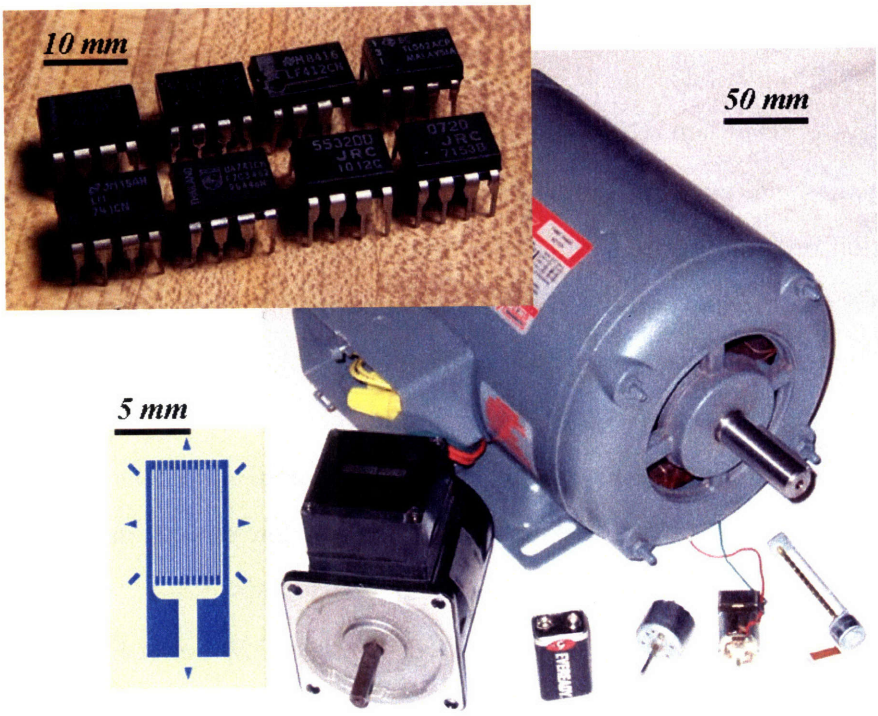

Figure 1-2: To replicate the controllable motion of skeletal muscle, a servomechanism must be fabricated. Accomplishing this with traditional engineering materials and devices requires an actuation system such as an electric motor (right [2]), a sensing device such as a strain gage (lower left [3]), and a control system using silicon-based electronics such as IC operational amplifiers (upper left [4]). No servo system constructed from these devices could be mistaken for muscle.

it will possess unique properties not existing in any currently available engineering material. Since they are controlled through an embedded servo system, the mechanical properties of the device such as stiffness, viscosity, and inertia will arise from the dynamics of the feedback loop rather than from any inherent mechanical properties of the materials from which it was fabricated. Moreover, these properties may be 'tuned' by altering the servo-control parameters embedded in the material system. With this approach properties such as negative stiffness may be generated which do not exist in bulk materials.

Such a device is called a *programmable material.* As mentioned above, traditional actuation technologies such as hydraulics and electromechanical motors are not easily embedded in a material. The actuator needed is one without moving parts - in fact, one that comprises the material itself.

Matching the capabilities of skeletal muscle is the subject of a great deal of ongoing research (see Table 1.1) [5]. The most promising of the existing artificial muscle technologies is actuation with *conducting polymer* [6–13].

Of the artificial muscle technologies reviewed, conducting polymers exhibited the combination of total strain, strain rate, and low power which best matched skeletal muscle. Of the others, liquid crystal elastomers are either too slow or require high electrical fields to actuate. Dielectric elastomers, while fast with good total strains, require very high voltages and fields for useful motion. Ionic polymer metal composites have good bending actuation, but can't be used for linear motion. Carbon nanotube actuators are expensive and have relatively low strains, and shape memory alloys are difficult to control at intermediate actuation states.

Conducting polymers have achieved good strains at low power inputs. The strain rate is still lower than desired, but has improved over recent years and continues to increase. Finally, conducting polymers have no real moving parts. The entire material swells and contracts under the proper electrochemical conditions, so this technology was ideal for the programmable material device application.

Since the goal is to create a device that externally appears to be a homogeneous material, it is necessary to build the device components from materials that are similar in material properties such as density, stiffness, and toughness. Having chosen a conducting polymer from which to make the actuator, it is therefore logical to fabricate the sensing and control capabilities from other polymeric materials.

Such an integrated feedback device has never been fabricated in any previous research. Many researchers have fabricated various components of such a system, and have achieved significant advances in the capabilities of these individual components. As shown in Table 1.1 and discussed in Chapter 2, actuation using conducting polymer is approaching the performance level of natural muscle. As we shall see in Chapters 4 and 5, electronics fabricated from conducing polymers have also begun to compete with some traditional components.

However, these actuation and electronics components have been realized independently of other requirements. Creation of a programmable material will force

Table 1.1: Artificial Muscle Technologies. Assembled in [14] from [5].

Actuator	Active Strain (%)	Active Stress (MPa)	Work Density (kJ/m^3)	Strain Rate (%/s)	Efficiency (%)	Advantages	Disadvantages
Mammalian Skeletal Muscle	20	0.35	8	>50	40	Has systems for heat and waste removal, energy delivery and regeneration	Requires specialized chemical and thermal environment, not synthetically produced
Dielectric Elastomers	Up to 380	1	Up to 3400	4500	30 - 90	Very high strains and strain rates	High voltages (>1 kV) and fields (150 MV/m) required
Liquid Crystal Elastomers	2 - 45	0.01 - 0.5	20	30 - 1000	75	Large strain for thermal materials, fast strains for electrical	Thermal versions are slow; electrical versions require high fields (1-25 MV/m)
Polypyrrole (conducting polymer)	39 reported, 5 reliably	Up to 30	100	12	20	Low voltage (2 V); high stress and strain	Slow (often run at several Hz to achieve full strain)
Ionic Polymer Metal Composites	0.5 - 3	3	Up to 5	3	1.5 - 3	Low voltage (<10 V), mechanical amplification gives large displacements	Only useful for bending (not linear) motion
Carbon Nanotube Actuators	<1	Up to 30	2	20	0.1	Large operating temperature range; low voltage	Materials are expensive, active strains are very low
Thermally Activated Shape Memory Alloys	5	Up to 200	>1000	300	<5	Very high power (>100 kW/kg); low operating voltage	Difficult to control (run between fully contracted and extended but not between)

compromises in the performance levels of each of the individual components of the device. None of these components can currently perform as well as their standalone conducting polymer counterparts (let alone traditional devices such as electromechanical motors and silicon-based electronics), but without these compromises the device will not work at all.

Some researchers have implemented feedback systems using some conducting polymer components [15, 16], but none have before attempted to create a co-fabricated, fully integrated conducting polymer feedback device. This work establishes the feasibility of building the device and answers many of the questions of fabrication and design.

1.2 Conducting Polymers

Conducting polymers were first characterized by Heeger, MacDiarmid, and Shirakawa in 1977 [17], work for which they won the Nobel Prize in Chemistry in 2000 [18]. They created conductive polyacetylene by oxidizing it with a halogen vapor (chorine, bromine, or iodine), resulting in a film that was 10^9 times more conductive than before treatment [17].

There are two requirements for a polymer to be conductive. First, the molecular structure must have a *conjugated* backbone, which consists of alternating single and double bonds. This structure enables delocalization of the π-electrons associated with the double bonds, increasing the mobility of these electrons [18].

Second, a dopant is required. A dopant provides charge carriers in the form of extra electrons or "holes" (a position where an electron is missing). Conducting polymer dopants consist of anions incorporated in the polymer bulk during oxidative deposition (see Chapter 2). These two factors give conducting polymers a remarkable range of realizable conductivities (see Figure 1-3).

Since the discovery of conductive polyacetylene, many other conducting polymers have been used for a wide selection of applications, including actuation, sensing, and electronics [6, 12, 19 21]. Some of the most common of these polymers are shown in

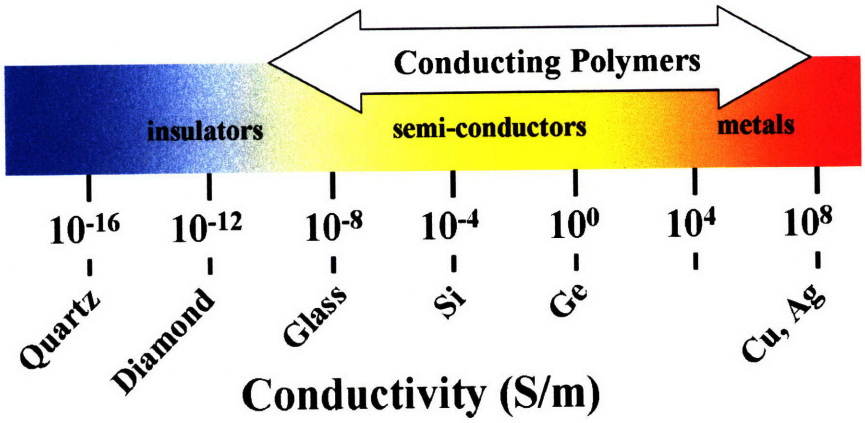

Figure 1-3: Conductivity of conductive polymers compared to those of other materials, from quartz (insulator) to copper (conductor). Polymers may also have conductivities corresponding to those of semiconductors. From [18].

Figure 1-4.

1.3 Thesis Overview

Each of the vital capabilities necessary to the creation of a programmable material will be covered individually, but always with the understanding that each component must be integrated with the others. Therefore, each capability will be discussed in turn before overall integration is examined.

Since the actuation technology was the starting point of the design of a programmable material, the theory and implementation of conducting polymer actuators will be discussed first in Chapter 2. The most promising conducting polymer actuators have been fabricated from polypyrrole, which was chosen as the actuator material for the programmable material.

In order to achieve apparent material homogeneity, the sensor layer will also be fabricated from polypyrrole. Given the proper geometry a film of polypyrrole can serve as a strain gage, converting mechanical deformation into an electrical signal. This is examined in Chapter 3.

Creating control electronics was significantly more difficult. Creating a programmable material with integrated capabilities posed some unique requirements for

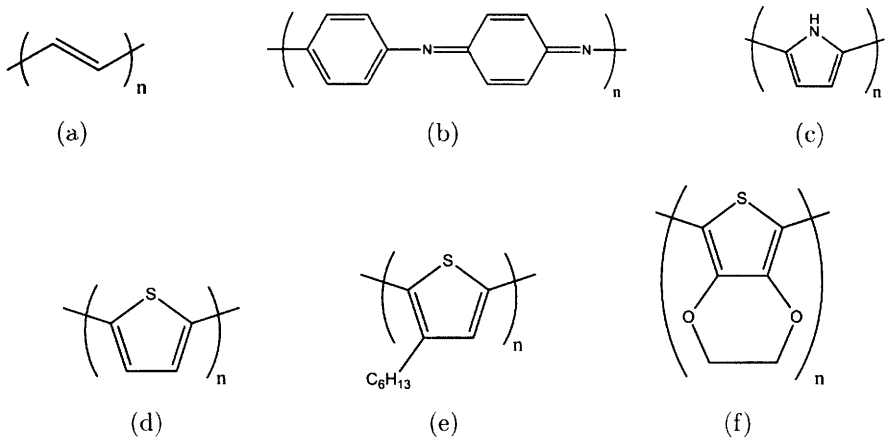

Figure 1-4: Common Conducting Polymers: a) Polyacetylene (PA). b) Polyaniline (PAN). c) Polypyrrole (PPy). d) Polythiophene (PT). e) Poly(3-hexylthiophene (P3HT). f) Poly(3,4-ethyelendioxythiophene) (PEDOT).

the fabrication process. Chapter 4 looks at the various deposition and patterning techniques available for fabricating conducing polymer components and their relative merits for building the programmable material. Finally, this chapter discusses the final selection of the oxidative chemical vapor deposition process and the work done to fabricate conducting polymer electronics using this technique.

Chapter 5 discusses the various electronic components required and how these were fabricated. Once the design and deposition process was refined enough to produce functional components, these devices were tested for their performance characteristics. Finally, individual electronic components were integrated to create functional polymer circuitry and their capabilities were tested.

Bringing all of these pieces together, Chapter 6 examines the work done to integrate the conducting polymer components (actuator, sensor, electronics) into an operational programmable material. The system performance (given the current capabilities of the components) is predicted, along with projections for near-term component improvements and their effects on the overall system.

As a programmable material is fundamentally an integrated controllable actuator, this device is a first step to a practical artificial muscle application. It is therefore of significant interest to examine the biostability and biocompatibility characteristics of such a device. Chapter 7 looks at these possibilities.

Finally, Chapter 8 discusses the results of this work. Directions for future work are examined, along with a possible application.

Chapter 2

Polypyrrole Electrochemistry and Actuation

In this work, the conducting polymer polypyrrole has been used extensively. In this chapter the actuation capability of polypyrrole as part of the larger programmable material system will be addressed (see Figure 2-1), while the sensing capability will be addressed in Chapter 3. The third major component, the control electronics, was implemented with a different conducting polymer and will be addressed in Chapters 4 and 5.

In order to understand how polypyrrole actuates, it is necessary to first understand how the films are fabricated. Both the fabrication and actuation are accomplished using similar electrochemical processes, though it is not necessary that they be identical.

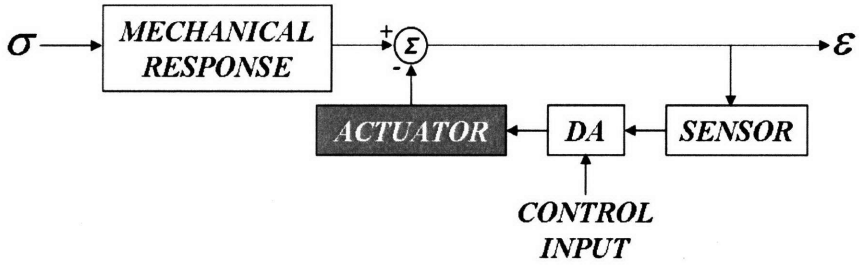

Figure 2-1: System block diagram.

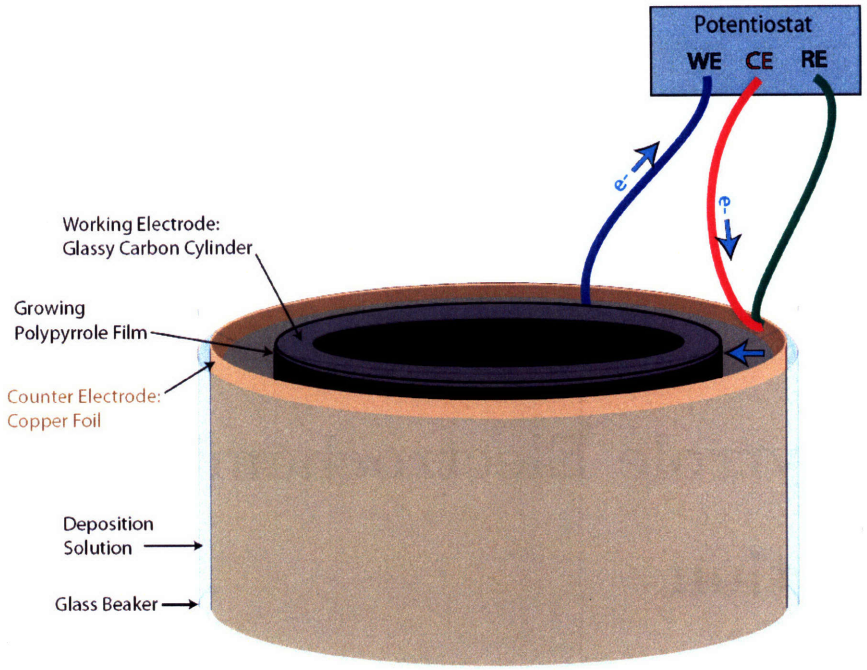

Figure 2-2: The glassy carbon working electrode is positioned concentrically with the copper foil counter electrode in the electrolyte bath. Oxidation of the pyrrole monomer in solution (in contact with the working electrode) leads to polymerization and deposition. From [14].

2.1 Electrochemistry

The polypyrrole films used in this study were fabricated electrochemically. This process produces a free-standing film that is mechanically robust and electrically conductive. The electrochemical deposition process was developed originally by Yamaura [22] and refined in the MIT BioInstrumentation Lab by John Madden, Peter Madden, and Patrick Anquetil [15, 16, 23].

2.1.1 Polypyrrole Fabrication

Electrochemical deposition of polypyrrole is accomplished via the construction of an electrochemical cell (see Fig. 2-2). A solution is mixed consisting of 0.05 M pyrrole monomer (distilled and maintained at -20°C under nitrogen atmosphere protected from light), 0.05 M tetrabutylammonium hexafluorophosphate (TBAP), and 1% distilled water in propylene carbonate.

This solution serves as the electrolyte for the cell, which is constructed with concentric electrodes. The working electrode and deposition target consists of a glassy carbon crucible (75 mm in diameter and 100 mm in height) with Kapton® tape used to define the film's horizontal edges. The counter electrode used is a polished copper sheet, ideally with four times the surface area of the working electrode.

The deposition is completed at -40°C to control the rate of polymerization. The working and counter electrodes are connected to a potentiostat (Princeton VMP2) with the reference electrode contact connected to the counter electrode. After allowing the temperature to equalize, the film is deposited galvanostatically using a current density of 1.5 $\frac{A}{m^2}$ for 8-15 hours. The deposition is controlled using EC-Lab® software version 9.45 from Bio-Logic® Science Instruments.

This galvanostatic condition causes the working electrode to be positively charged relative to the counter electrode. This allows monomer in solution in contact with the working electrode to oxidize, losing an electron. As shown in Figure 2-3, this enables the formation of a dimer. This dimer then oxidizes again at the working electrode, and the process is repeated to create a long polymer chain.

The positively charged working electrode serves a second, vital purpose in the deposition of this conducting polymer. Negatively charged ions from the salt in the electrolyte solution (the hexafluorophosphate ions, in this case) are attracted to the working electrode and are incorporated into the oxidized film as it is deposited. This intercalation of anions (the film is doped with these ions) enables the polymer to achieve as-deposited conductivities on the order of 10^5 $\frac{S}{m}$ [24].

Depositions using this technique result in films with thicknesses from 10 to 30 μm. These films have been optimized for mechanical robustness and the ability to reliably actuate for long periods of time. Depositions with different variables (dopant ions, solvent, deposition temperature) will be discussed in Chapter 7.

2.1.2 Polypyrrole Actuation

Functional actuation of polypyrrole is achieved in an electrochemical environment very similar to that used for deposition. An electrolyte solution (using propylene

Synthesis of Polypyrrole

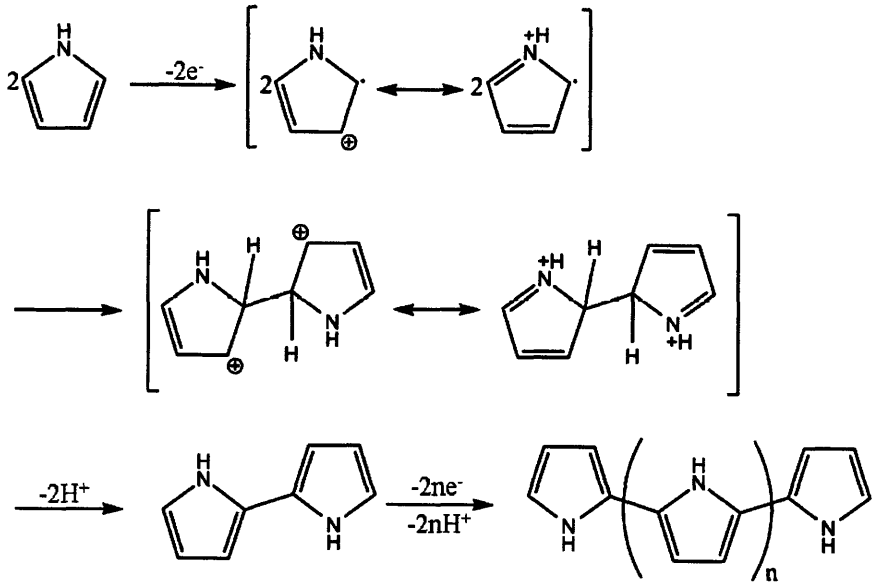

The last step is in fact a repetition of the first steps beginning with oxidation, followed by coupling to either end of the polymer, and finally elimination of H^+. The electrons are either removed via an electrode (electrochemical deposition) or chemically, e.g.

$$Fe^{+++} \xrightarrow{e^-} Fe^{++}$$

Note that the polymerization does not generally result in a neutral polymer shown above, but rather the backbone is charged, as below, such that the total number of electrons transferred per monomer is $2+a$ where a is generally between 0.2 and 0.5:

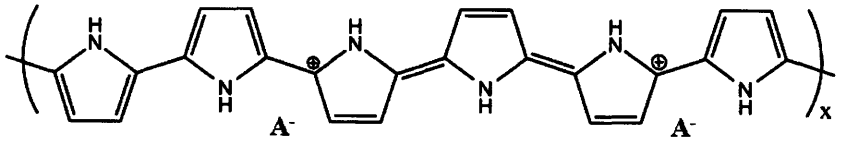

where A^- is an anion or dopant. Here $a = 1/3$. During the initial phases of electrodeposition the oligomers remain in solution, eventually precipitating to form a solid with intercalated anions.

Figure 2-3: The electrochemical deposition process for polypyrrole results in an oxidized film with intercalated anions. These films typically have conductivities on the order of $10^5 \frac{S}{m}$. From [15].

carbonate, water, or some other solvent) containing a salt is needed to provide dopant ions and the medium through which the ions move. The actuation environment may be the same as the deposition environment (minus the monomer), thoough in many cases it is beneficial to use different ions to optimize actuation behavior.

As a voltage is applied between the polypyrrole and a counter electrode, an electrostatic field is established which creates a capacitive double layer at the surface of the polypyrrole. If the potential between the actuator and the counter electrode is negative, the polypyrrole undergoes reduction. This generally causes the intercalation of cations in solution and the de-intercalation of anions within the polymer (actual ion movement is governed by several factors, including the potential difference, ion size and the diffusion coefficient). Due to the loss of anions, the reduced state is the low conductivity state of conducting polymers.

Similarly, if the actuator-counter electrode potential is positive the polymer undergoes an oxidation reaction. This causes an influx of anions and an outflux of cations (increasing the polymer conductivity) [14, 15, 25].

The incorporation of ions into the polymer bulk (intercalation) causes expansion of the polypyrrole, while loss of ions into the solution causes contraction. Systems are commonly designed to take advantage of a cation-anion pair of significantly differing sizes [7,26]. Smaller ions move more easily, but if the ion is too small it will not result in useful actuation. Ideally, one of the ions is very large in order to greatly reduce its rate of diffusion and thus effectively render it immobile. The other ion is small enough to move easily but large enough to produce useful expansion and contraction.

For example, in the deposition and actuation electrochemical system discussed above, tetrabutylammonium hexafluorophosphate is dissolved in propylene carbonate at a concentration of 0.05 M (a system normally designated TBAP/PC). The cation of this system, tetrabutylammonium, has nearly twice the radius (0.415 nm) of the anion, hexafluorophosphate (0.254 nm) [27]. Actuation in a TBAP/PC environment is the result of motion of the hexafluorophosphate anion, since the tetrabutylammonium cation is significantly less mobile.

The ion movement involved in polypyrrole actuation as a function of time is shown

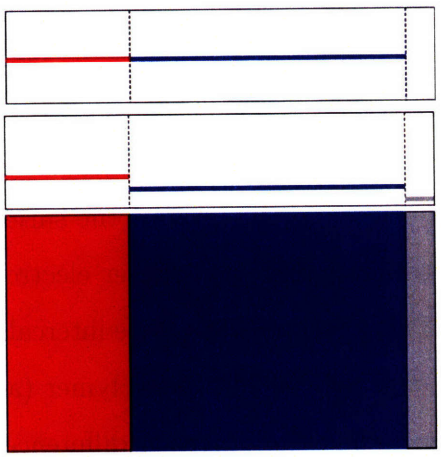

(a) The polymer at rest. There is a voltage difference at the interface between the polymer and the electrolyte and at the interface between the electrolyte and the counter electrode.

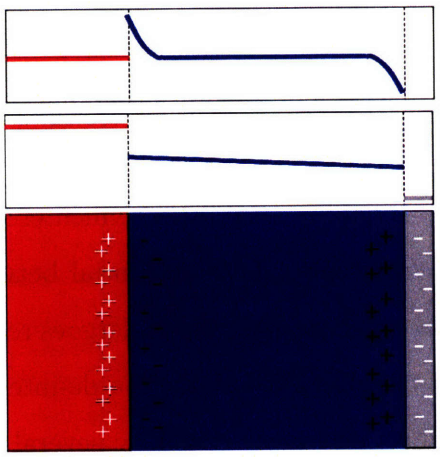

(b) When a potential is applied, a current begins to flow through the electrolyte and ionic charge builds up in the double layers.

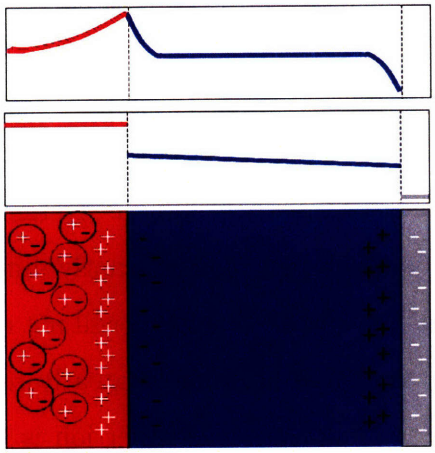

(c) The concentration of ions at the polymer surface drives the diffusion of ions into the polymer. Inside the polymer, the ions are paired with holes or electrons to form neutral species.

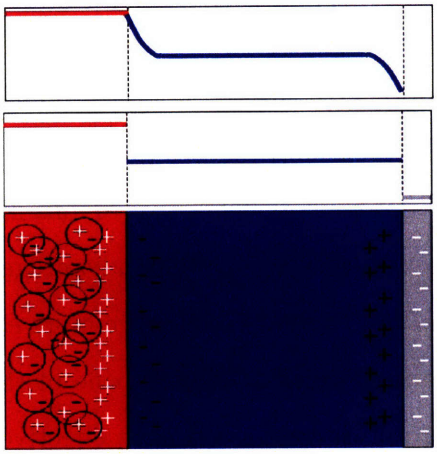

(d) The polymer if fully charged when the concentration of ions in the polymer is equal to the concentration of ions in the double layer at the polymer electrolyte interface.

Figure 2-4: Charging of the conducting polymer drives ion motion, resulting in conductivity changes and actuation. The upper two plots of each figure show the ion concentration and the voltage in the polymer (polypyrrole, red), in the electrolyte (blue), and the in the counter electrode (gray). The figure depicts charging for single ion (anion) movement into and out of the polymer. From [16].

in Figure 2-4. The application of a potential between the polymer and the counter electrode first results in the creation of the capacitive double layer. As the polymer is oxidized, anions in solution are attracted and begin to diffuse into the bulk of the polymer. This results in expansion of the polymer (assuming mobile anions and immobile cations). As the ion concentration within the polymer reaches that in the double layer, diffusion ceases [16].

2.2 Polypyrrole Actuation Model

The relationship between the voltage input and the strain output of the actuator is necessary in order to model the overall system behavior (see Figure 2-1). The voltage output from the control electronics is an amplification of the error between the desired strain of the actuator (given by the overall system input as a voltage) and the actual strain (transduced to a voltage by the sensor). This voltage is then used as the driving input of the actuator.

John Madden [15] derived an admittance model of a polypyrrole actuator, called the Diffusive-Elastic-Metal (DEM) model. The DEM model was based on the fact that the polypyrrole actuator acts as a distributed capacitance, and uses a transmission line model to represent this. The actuator admittance is then stated as,

$$Y(s) \cdot R = s \cdot \frac{\frac{\sqrt{D}}{\delta} \cdot tanh\left(\frac{a}{2}\sqrt{\frac{s}{D}}\right) + \sqrt{s}}{\frac{\sqrt{s}}{RC} + s^{3/2} + \frac{\sqrt{D}}{\delta} \cdot s \cdot tanh\left(\frac{a}{2}\sqrt{\frac{s}{D}}\right)}, \tag{2.1}$$

where D is the diffusion coefficient, δ is the thickness of the capacitive double layer formed at the surface of the polymer, C is the double layer capacitance, R is the polymer resistance, a is the polymer thickness, and s is the Laplace variable. This can be expressed more usefully in terms of time constants:

$$Y(s) \cdot R = s \cdot \frac{\frac{1}{\sqrt{\tau_C}} \cdot tanh\left(\sqrt{s\tau_D}\right) + \sqrt{s}}{\frac{\sqrt{s}}{\tau_{RC}} + s^{3/2} + \frac{1}{\tau_C} \cdot s \cdot tanh\left(\sqrt{s\tau_D}\right)}, \tag{2.2}$$

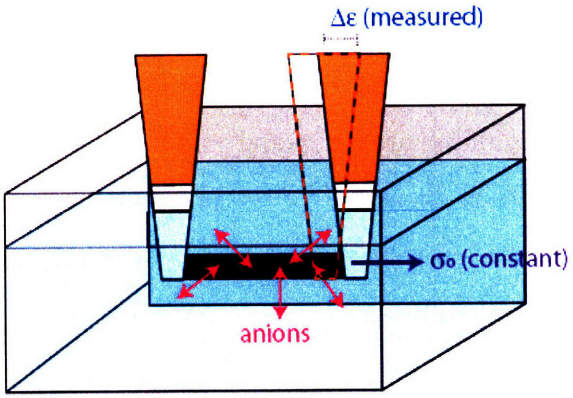

Figure 2-5: By maintaining a constant stress through force feedback, an isotonic linear actuation test is completed. From [14].

where

$$\begin{aligned} \tau_D &= \frac{a^2}{4D}, \\ \tau_{RC} &= RC, \ and \\ \tau_C &= \frac{\delta^2}{D}. \end{aligned} \tag{2.3}$$

These time constants determine the dominant rate limiting process at a given frequency or time. The first, τ_D, represents the diffusion time in the polymer, the second, τ_{RC} is the charging time for the capacitive double layer, and the third, τ_C, is the double layer diffusion discharge time [15].

2.3 Functional Polypyrrole Actuators

Many researchers have created actuators using polypyrrole [7–9, 11, 14, 15, 25, 28–42]. By manipulating deposition and actuation system variables, they have been able to increase the total strain achievable, while improving strain rate and total force. Novel actuator geometries have been developed to amplify strain and force.

2.3.1 Actuator Capabilities

The simplest polypyrrole actuator is a linear actuator. Figure 2-5 shows the test setup for measuring total linear strain under isotonic (constant force) conditions. Films deposited using the conditions described above normally actuate with 2-4% linear strain [14].

Modifications to the deposition electrochemistry and the actuation environment can produce significantly higher strains. By depositing polypyrrole from a methyl benzoate solution of 1,2-dimethyl-3-propylimidazolium tris (trifluoromethylsulfonyl) methide (DMPIMe) and actuating in a propylene carbonate/water solution of lithium bis (nonafluorobutylsulfonyl) imide, $Li(C_4F_9SO_2)_2N$ (LiNFSI), Kaneto has demonstrated strains as high as 36.7% [42], albeit for a single actuation cycle. Among the highest strains achieved and sustained over many cycles was 14%, accomplished by Patrick Anquetil et al. in the MIT BioInstrumentation Lab using films deposited using the PC/TBAP environment described above and actuated in ionic liquid (1-Butyl-3-methyl-imidazolium tetrafluoroborate, or BMIMBF4) [39].

2.3.2 Actuator Geometries

In order to amplify the strain provided by a polypyrrole actuator, many researchers have used a bimorph geometry [26,33,43–49]. A bimorph, or bilayer, geometry consists of one layer of conducting polymer bonded to a second layer of passive (non-actuating) material. The passive layer serves as something for the CP to 'push off' against - that is, when the CP expands due to ion influx, the bilayer bends towards the passive layer. When the CP contracts, the bilayer bends towards the polymer layer (see Figure 2-6).

However, the bilayer geometry requires a counter electrode placed near the actuator in order to complete the electrochemical circuit. This type of actuator also must be immersed in electrolyte solution, precluding use in air.

As a result, the most common method for amplifying polypyrrole actuator strain is the trilayer. The simplest trilayer consists of two conducting polymer films separated by a passive thin electronic insulator. This trilayer must be immersed in an

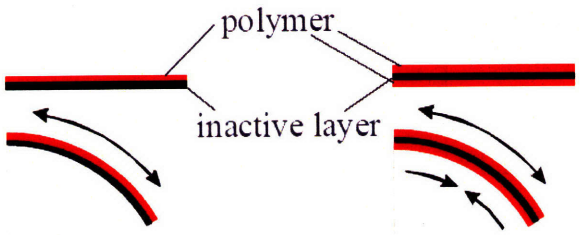

Figure 2-6: Bilayer (left) and Trilayer (right) Geometries. Arrows indicate polymer expansion and contraction. From [16].

electrolyte solution with a counter electrode as the two actuating films do not ionically communicate directly. When opposing potentials are applied to the polypyrrole layers, the trilayer bends towards the contracting polypyrrole layer (see Figure 2-6).

For a trilayer to operate in air, an ionic transport layer must replace the passive insulator between the actuating layers. Since the middle layer serves as both an ionic reservoir and diffusion pathway, this actuator geometry can be taken out of the liquid electrolyte bath [16, 41]. One example of an ionic transport layer material is the electrolyte gel used by Angela Chen [41] in the MIT BioInstrumentation Lab, which consisted of a liquid salt (BMIMBF4) in a gel polymer (methacrylate). Another effective technique that tends to last longer is that employed by Spinks et al. [50], which uses a polyvinylidene fluoride (PVDF) polymer membrane as the ionic transport medium. By sputter coating gold on both sides of the membrane, polypyrrole can be deposited directly onto the membrane surface.

Chen's trilayers were successfully used to construct a prototype biomimetic robotic fish fin (see Figure 2-7). It was important to generate a cupping motion in the fin [51], and this was accomplished by incorporating the fin rays directly into a specially shaped trilayer actuator. Rather than incorporating the actuator into the fin webbing, the trilayer serves as the webbing itself.

Instead of amplifying strain through actuator geometry, it is also possible to amplify the force output through parallel actuation. Tim Fofonoff has pioneered a technique in the MIT BioInstrumentation Lab for producing long (>10 m) gold-backed polypyrrole ribbons. Using a serpentine arrangement, he was able to achieve much

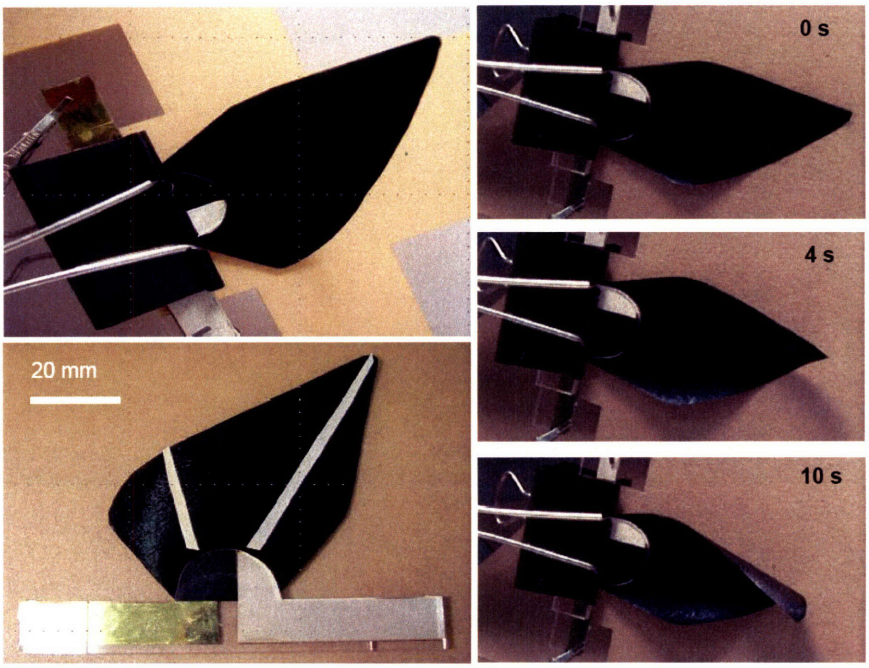

Figure 2-7: An all polymer fin with light ribs affixed to the back to increase fin stiffness in the spanwise direction. This fin was able to cup the dorsal and ventral edges, and to create a sweep motion [51].

higher forces than is possible using a single linear actuator (see Figure 2-8) [51].

2.4 Actuation in the Programmable Material

In the current work, a uniaxial actuation geometry is visualized as the basic mode of the programmable material. In this configuration, the device consists of a single actuation layer with one surface open to an electrolyte and counter electrode. The opposite surface of the actuator is coated with a barrier material before the sensor and control electronics layers are deposited, as discussed in Chapter 6.

As discussed above, the Madden DEM admittance model relates the input voltage to the current into the actuator. By integrating this we get the charge injected into the actuator, which we can then relate to the linear strain. By defining a strain to charge ratio, α, and further assuming that α is independent of load [52], Madden found that the relationship

$$\epsilon = \rho\alpha \tag{2.4}$$

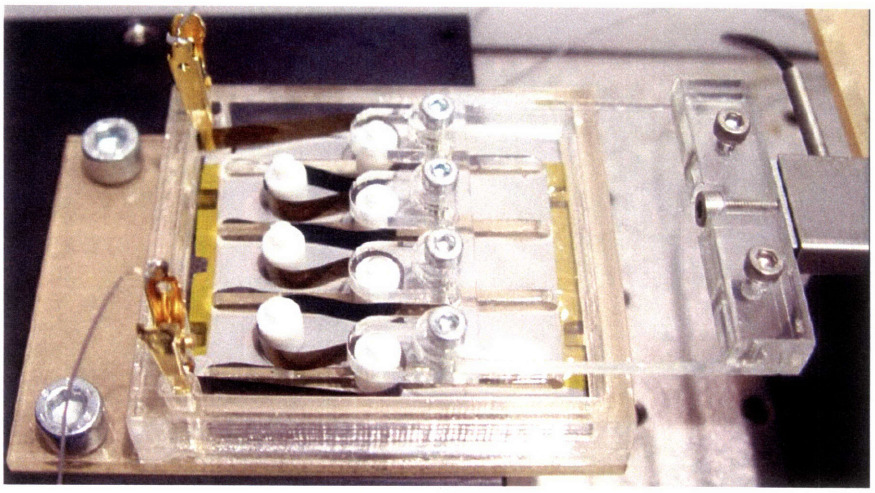

Figure 2-8: To increase the actuation force from a polypyrrole film, multiple actuators are placed in parallel. In this case, a single gold backed film is snaked around Teflon bearings to create the equivalent of 8 films acting in parallel. This device generated forces in excess of 2 N. From [51].

gives a typical value of α for polypyrrole of 500×10^{-12} $\frac{m^3}{C}$. Since $\rho = \frac{q}{V}$, where q is charge and V is the polymer volume, the overall strain resulting from actuation under loaded conditions is

$$\epsilon = \frac{\alpha q}{LWh} + \frac{\sigma}{E}, \tag{2.5}$$

where L, W, and h are the length, width, and thickness of the polymer actuator, respectively, σ is the applied stress, and E is the polymer Young's modulus. This equation is used to represent the actuator performance under uniaxial stress conditions.

The linear configuration is useful for controlling the apparent stiffness of the programmable material. However, the system can also be used as a position-controlled device. To get useful displacements, the small strains of the actuator must be amplified through a different configuration. As mentioned previously, an excellent and simple configuration for accomplishing this is the trilayer (see Figure 2-9).

As discussed in Chapter 6 (and similarly to the linear configuration), one of the two actuator layers in the trilayer will have the sensor and control electronics deposited on its outside surface. To determine the mathematical representation of the trilayer deflection for the overall system model, it is necessary to account for these extra

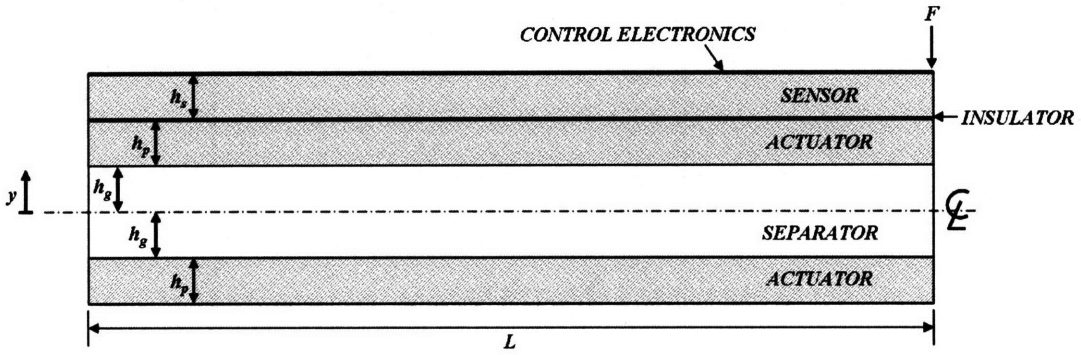

Figure 2-9: This design for a programmable material is based on a trilayer actuator device. The control electronics and insulator layers are two orders of magnitude thinner than the actuator and sensor layers, and can be neglected in the elastic beam analysis of the device. Diagram based on [16].

layers. For the purposes of this analysis, the insulation and control electronics layers are neglected as they are two orders of magnitude thinner than the actuator and sensor layers.

Based on Peter Madden's trilayer deflection analysis [16], the starting point is a beam of uniform cross-section. It is assumed that the ion flux is uniform along the length of the actuation layers. That is, there are no significant ohmic losses along the length of the actuator which would lead to potential differences. Further, it is assumed that the charge density in the top actuator layer is equal and opposite to the charge density in the bottom layer, and that the charge density in each actuator layer is uniform through the actuator thickness.

The device has length L and width W (into the page). Measuring distance y from the centerline of the separator layer, thicknesses are as shown in Figure 2-9. The gel separator layer has a Young's modulus of E_g, while the polymer layers (both actuator layers and the sensor layer) have a Young's modulus of E_p as they are all implemented with polypyrrole. The device's total thickness is thus $2h_g + 2h_p + h_s$.

Assuming that the beam bends with uniform curvature [26], the strain is given by

$$\epsilon(y) = \kappa y, \tag{2.6}$$

where ϵ is the strain, κ is the curvature, and y is the distance from the centerline of

the separator layer (the line of zero strain).

Since all torques resulting from external forces or internal stresses must sum to zero for equilibrium,

$$\sum_i \tau_i = 0. \tag{2.7}$$

For a force F applied at the end of the device and small curvatures,

$$\sum_i \tau_i = W \int \sigma(y) \cdot W \cdot y \cdot dy + F \cdot L = 0, \tag{2.8}$$

where σ is the internal stress resulting from elastic deformation. The material constitutive equations give

$$\begin{aligned} \sigma_g(y) &= E_g \epsilon_g(y), \\ \sigma_p(y) &= E_p \epsilon_p(y) + E_p \alpha \rho, \ and \\ \sigma_s(y) &= E_p \epsilon_s(y), \end{aligned} \tag{2.9}$$

where ϵ_g, ϵ_p, and ϵ_s are the local strain of the separator, actuator, and sensor layers, respectively. Recall that the Young's modulus of the sensor layer is the same as that of the actuator layers. These can be substituted along with geometric dimensions, and the torque balance equation is then rewritten as

$$\begin{aligned} 0 = &\int_{-h_p-h_g}^{-h_g} \left[E_p \kappa y^2 - E_p \alpha \rho y\right] dy + \int_{-h_g}^{h_g} E_g \kappa y^2 dy \\ &+ \int_{h_g}^{h_g+h_p} \left[E_p \kappa y^2 + E_p \alpha \rho y\right] dy + \int_{h_g+h_p}^{h_g+h_p+h_s} E_p \kappa y^2 dy - \frac{F \cdot L}{W}. \end{aligned} \tag{2.10}$$

Integrating Equation 2.10 and solving for the force gives

$$F = C_{spring} \cdot \kappa + C_{charge} \cdot \rho, \tag{2.11}$$

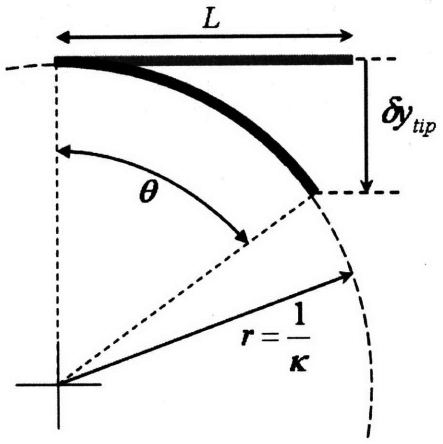

Figure 2-10: As the trilayer device actuates from a rest position (shown in gray) to a curved position (black), it covers an arc of length L on a circle of circumference $\frac{2\pi}{\kappa}$. The angle θ is the fraction of the total circumference covered by the device length.

where

$$C_{spring} = \frac{WE_p}{3L} h_g^3 \left[\left(1 + \frac{h_p}{h_g} + \frac{h_s}{h_g}\right)^3 + \left(1 + \frac{h_p}{h_g}\right)^3 - 2 + 2\frac{E_g}{E_p} \right], \tag{2.12}$$

and

$$C_{charge} = \frac{WE_p\rho}{L} h_g^2 \left[\left(1 + \frac{h_p}{h_g}\right)^2 - 1 \right]. \tag{2.13}$$

Assuming free deflection (no external force is applied at the end of the beam), rearranging gives the curvature to charge density ratio:

$$\frac{\kappa}{\rho} = -\frac{C_{charge}}{C_{spring}} = -\frac{3\alpha}{h_g} \left[\frac{\left(1 + \frac{h_p}{h_g}\right)^2 - 1}{\left(1 + \frac{h_p}{h_g} + \frac{h_s}{h_g}\right)^3 + \left(1 + \frac{h_p}{h_g}\right)^3 + 2\left(\frac{E_g}{E_p} - 1\right)} \right]. \tag{2.14}$$

Multiplying this by the charge and actuator volume gives the resultant device curvature.

The device tip deflection, δy_{tip}, is a function of the curvature and length. As shown in Figure 2-10, the actuated device covers an arc of length L on a circle of circumference $2\pi r$ (or $\frac{2\pi}{\kappa}$). The angle θ then is equivalent to this arc length as a

fraction of the total circumference:

$$\theta = 2\pi\frac{L}{C} = L\kappa. \tag{2.15}$$

The total tip deflection is thus

$$\delta y_{tip} = \frac{1}{\kappa} - \frac{1}{\kappa}cos\left(L\kappa\right). \tag{2.16}$$

Equations 2.5 and 2.16 will be used in Chapter 6 to relate the current (charge) input to the actuators to the linear extension of the sensor, and the resultant tip deflection of a trilayer device.

Chapter 3

Sensing

The second important component of the programmable material's feedback system is the position sensor (shown in Figure 3-1). In order to control the actuator, it is essential that we are able to sense the actuator's resultant strain. This is accomplished by means of a strain gage, which converts the mechanical displacement of the actuator into an electrical signal usable by the control electronics to drive the actuator.

As in any simple feedback control system, comparison of the desired value (strain in this case, represented by the input voltage) to the actual value (generated by the position sensor by converting strain to voltage) results in the position error which is amplified by the control electronics to drive the actuator. The ultimate goal is to minimize the error, or equivalently, to position the actuator to the desired strain.

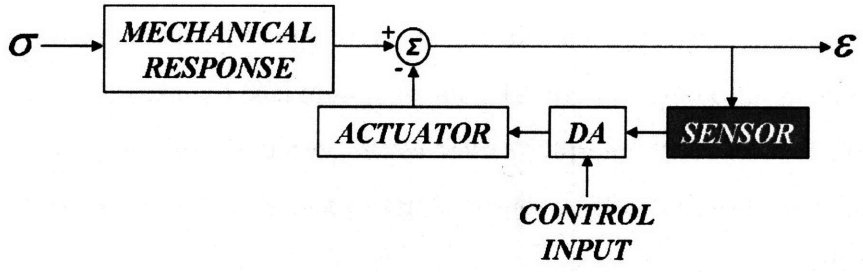

Figure 3-1: System block diagram.

Figure 3-2: Spinks et al. were able to sense the flexure of each finger using the variable resistance of the CP/fabric strain gage mounted on the back of each glove finger (from [37]).

3.1 Previous Work

Other researchers have previously created strain gage-type position sensors using conducting polymers, though all have used these polymers deposited onto an elastic fabric substrate. For example, De Rossi [53] was the first to create a glove with conducting polymer/fabric strain gages attached to the fingers for position sensing. Spinks was able to create a similar device using sensors with a gage factor of approximately 2 (see Figure 3-2) [37], where the gage factor GF is defined as

$$GF = \frac{\Delta R/R_G}{\epsilon}, \tag{3.1}$$

where R_G is the resistance of the undeformed strain gage, ΔR is the change in resistance resulting from the strain, and ϵ is the applied strain.

Peter Madden fabricated a strain gage from polypyrrole deposited on Lycra® fabric, which he used to build a feedback control system (see Figure 3-3). In his system, a polypyrrole trilayer (or 'trimorph') served as the actuator, and the polypyrrole/fabric strain gage served as the position sensor. These sensors displayed gage factors between 6 and 10 [16].

Since the current work is focused on creating co-fabricated, integrated devices

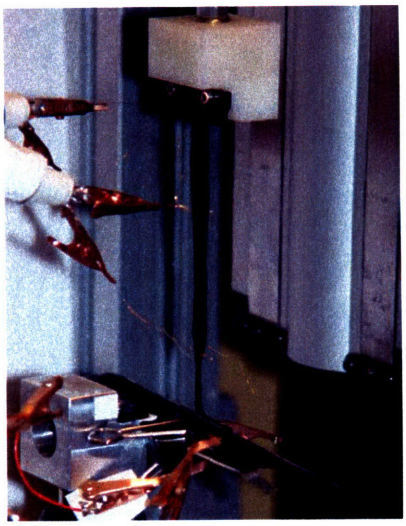

(a) CP feedback system showing strain gage attached to wide trilayer actuator at bottom of figure.

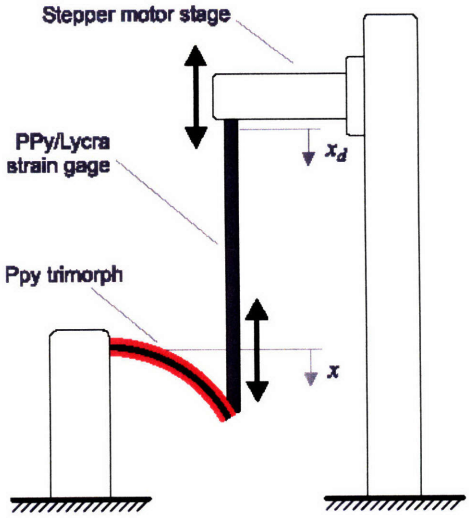

(b) Diagram of actuator and sensor portions of feedback system.

Figure 3-3: Peter Madden's functional feedback system utilizing polypyrrole as actuator and polypyrrole-coated fabric as sensor [16] is shown. Electronic components to implement feedback control were external and not fabricated from conducting polymer.

realized completely from conducting polymers, a fabric-based strain gage was inappropriate. Thus, the focus was entirely on strain gages fabricated strictly from polypyrrole films. Prior to this work, John Madden was the only researcher to examine polypyrrole film strain sensors [15].

3.2 Viscoelastic Behavior

In order to accurately control the device, the viscoelastic properties of the polypyrrole strain gage must be understood. Therefore, a study was undertaken to model the creep behavior of the sensor that will then be incorporated into the integrated system model to account for these effects.

John Madden et al. [54] examined the creep behavior of polypyrrole without deriving a mathematical model to account for the creep behavior. Based on their experiments they found that a wet polypyrrole film (one submerged in solvent, in this case propylene carbonate) has an elastic modulus of 800 MPa at small strains and a

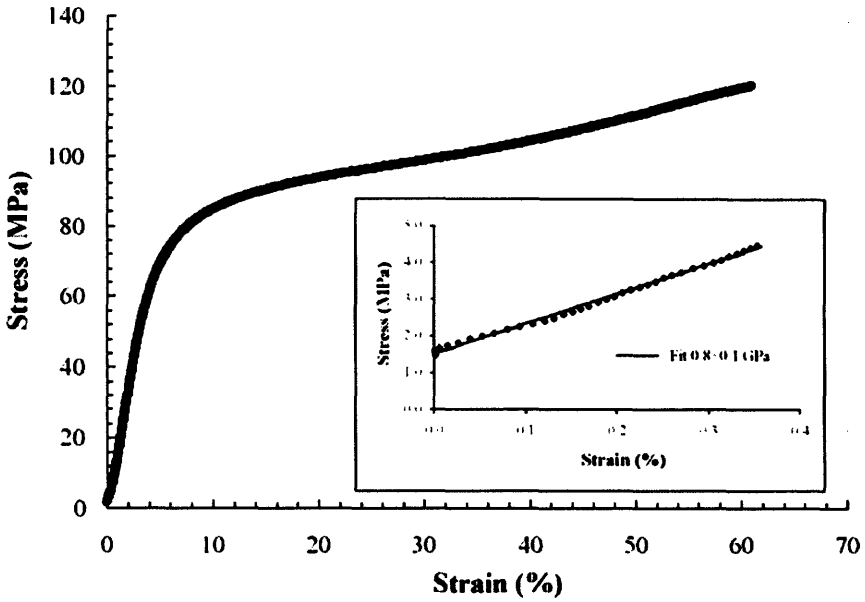

Figure 3-4: These stress-strain results are for a polypyrrole wet film drawn at 5 MPa/min. From [54].

tensile strength of 120 MPa (see Figure 3-4). Dry films may have tensile strengths as high as 150 MPa.

The creep behavior of polypyrrole on timescales up to 1000 seconds has been shown to be linear and viscoelastic [33,55]. On time scales over 12,000 seconds, creep behavior was shown to be non-linear and history dependent [54]. The current work will be limited to the linear viscoelastic case.

3.2.1 Theoretical Modeling of Viscoelasticity

A common and effective model for the viscoelastic behavior of polymers is the standard linear solid model (SLS). As shown in Figure 3-5, the SLS model consists of a spring in parallel with a spring and damper in series. Each of these elements is, as the model name suggests, linear. The springs have stiffnesses represented by E_a and E_b, while the damper has a coefficient of η_c. Springs a and b account for the immediate strain response upon application of a step stress input. Over time the strain from the extension of spring b is transferred to damper c, which accounts for the creep behavior of the polymer.

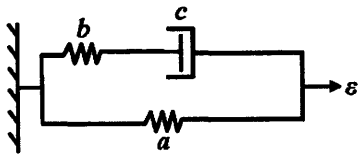

Figure 3-5: Standard Linear Solid Model.

The strain response of a polymer modeled with an SLS to a step stress input is then

$$\epsilon(t) = \left[\frac{1}{E_a} - \left\{\frac{1}{E_a} - \frac{1}{E_a + E_b}\right\} e^{-t/\tau_d}\right] \sigma_o h(t), \tag{3.2}$$

where σ_o represents the magnitude of the step stress input, $h(t)$ is the unit step function, and τ_d is defined as the retardation time:

$$\tau_d \equiv \frac{\eta(E_a + E_b)}{E_a E_b}. \tag{3.3}$$

Unfortunately, the SLS model was found experimentally to be inadequate to model the creep behavior of polypyrrole. There was a second time constant apparent, which prompted the evaluation of a generalized Maxwell model with two SLS units (as shown in Figure 3-5) in parallel. The undamped springs (a in Figure 3-5), sum in the Maxwell model to a single parallel undamped spring. This produces the model shown in Figure 3-6.

The Maxwell model is governed by the differential equation:

$$\left(1 + \frac{E_a}{E_b}\right)\dot{\epsilon} + \frac{E_c}{E_b}\dot{\epsilon}_c + \frac{E_a}{\eta_d}\epsilon + \frac{E_c}{\eta_d}\epsilon_c = \frac{1}{E_b}\dot{\sigma} + \frac{1}{\eta_d}\sigma. \tag{3.4}$$

It is first important to eliminate the terms dependent upon ϵ_c. Given a step stress input:

$$\sigma(t) = \sigma_o h(t) \qquad \dot{\sigma} = \sigma_o \delta(t), \tag{3.5}$$

where $\delta(t)$ is the Dirac delta function, the terms involving ϵ_c are then:

$$\epsilon_c = \epsilon_o h(t) \qquad \dot{\epsilon}_c = \epsilon_o \delta(t) e^{\tau_1 t} + \epsilon_o h(t) \tau_1 e^{\tau_1 t}, \tag{3.6}$$

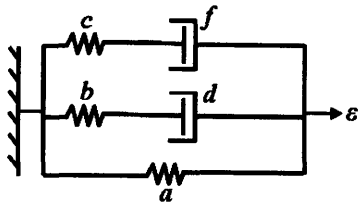

Figure 3-6: Generalized Maxwell model with two damper units.

where $\tau_1 = -\frac{E_c}{\eta_f}$. Making the small strain rate assumption as $t \rightarrow \infty$, any terms containing $\delta(t)$ in Equation 3.6 go to zero. Substituting and rearranging, we get (keeping in mind that for $t = 0^+$, $\dot{\sigma}(t) = 0$ and $\sigma(t) = \sigma_o$):

$$\dot{\epsilon} + \left(\frac{E_a E_b}{\eta_d (E_a + E_b)}\right)\epsilon = \left(\frac{E_b}{\eta_d (E_a + E_b)}\right)\sigma_o - \left(\frac{E_b E_c + \eta_d E_c \tau_1}{\eta_d (E_a + E_b)}\right)\epsilon_o e^{\tau_1 t}. \tag{3.7}$$

Solving this differential equation, we arrive at:

$$\epsilon(t) = C_1 e^{-\tau_1 t} + C_2 e^{-\tau_2 t} + C_3, \tag{3.8}$$

where

$$\begin{aligned}
C_1 &= \frac{E_c (E_b \eta_f - E_c \eta_d)}{\eta_d \eta_f (E_a + E_b)}, \\
C_2 &= \left[\frac{1}{E_a + E_b + E_c} - \frac{E_b}{\eta_d (E_a + E_b)}\right]\sigma_o + \left[\frac{E_c (E_b \eta_f - E_c \eta_d)}{\eta_d \eta_f (E_a + E_b)}\right]\epsilon_o, \\
C_3 &= \left(\frac{E_b}{\eta_d (E_a + E_b)}\right)\sigma_o, \\
\tau_1 &= \frac{E_c}{\eta_f}, \text{ and} \\
\tau_2 &= \frac{E_a E_b}{\eta_d (E_a + E_b)}.
\end{aligned} \tag{3.9}$$

3.2.2 Viscoelasticity Experimental Work

In order to verify the models delineated above, the creep behavior of polypyrrole was examined experimentally. This was done using the dynamic mechanical analyzer (DMA) designed and built in the lab by Nathan Vandesteeg [25] as shown in Figure

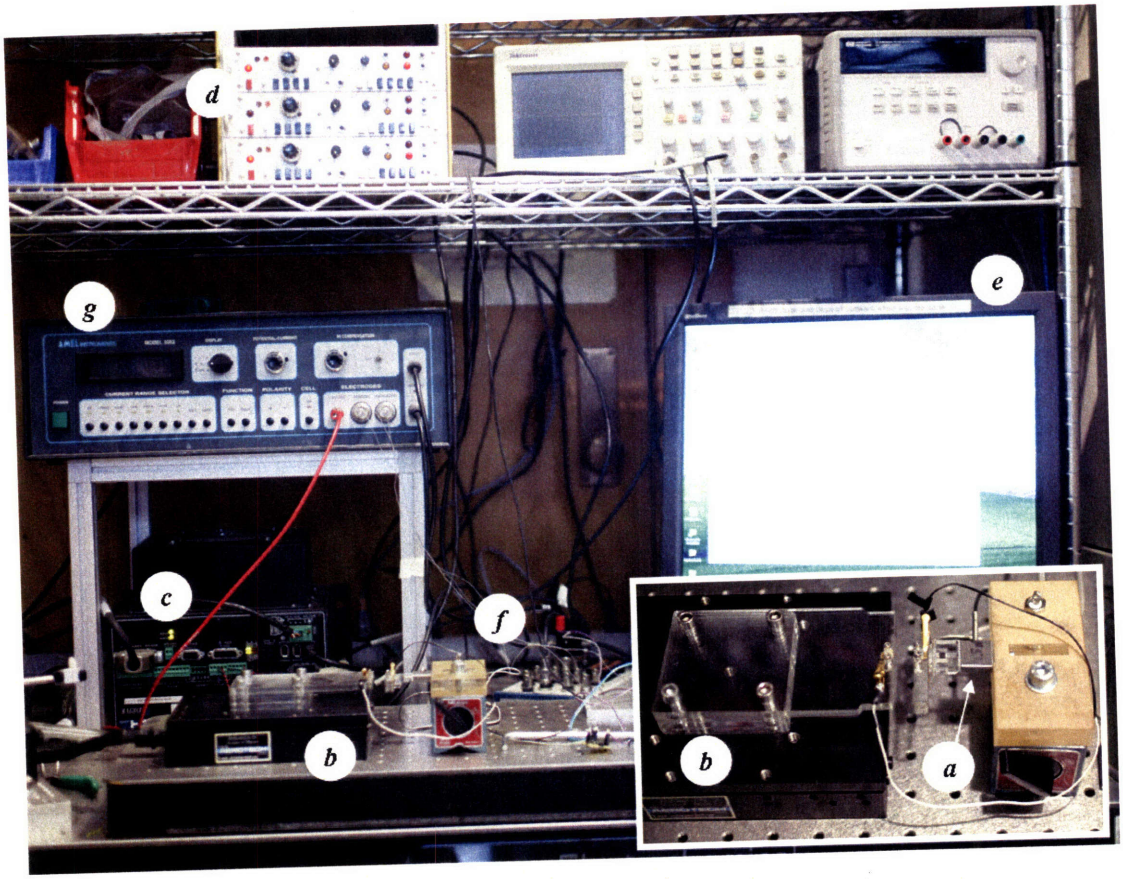

Figure 3-7: Large figure shows dynamic mechanical analyzer (DMA) custom built in the BioInstrumentation Lab by Nate Vandesteeg [25]. Inset shows gold clamp system with force sensor (a) to hold and make electrical contact with the polypyrrole sample. Also shown are (b) stage, (c) stage controller, (d) signal conditioning amplifier (for force sensor), (e) computer screen with DMA software, (f) data acquisition board, and (g) potentiostat (for electrochemical experiments).

3-7.

Using software written in the Microsoft® Visual Basic environment, the DMA utilizes a force sensor to implement force feedback and maintain a constant stress. The Aerotech® ALS130-050 stage and controller enable position control to within 500 nm. The inset of Figure 3-7 shows a close-up image of the clamping system designed and built for this work. These clamps allow stiff mechanical clamping of the sensor sample while providing electrical contact for a four-point measurement of the sample resistance, which was important for measuring the strain-resistance relationship.

Using the DMA, measurements of polypyrrole creep response were taken on film

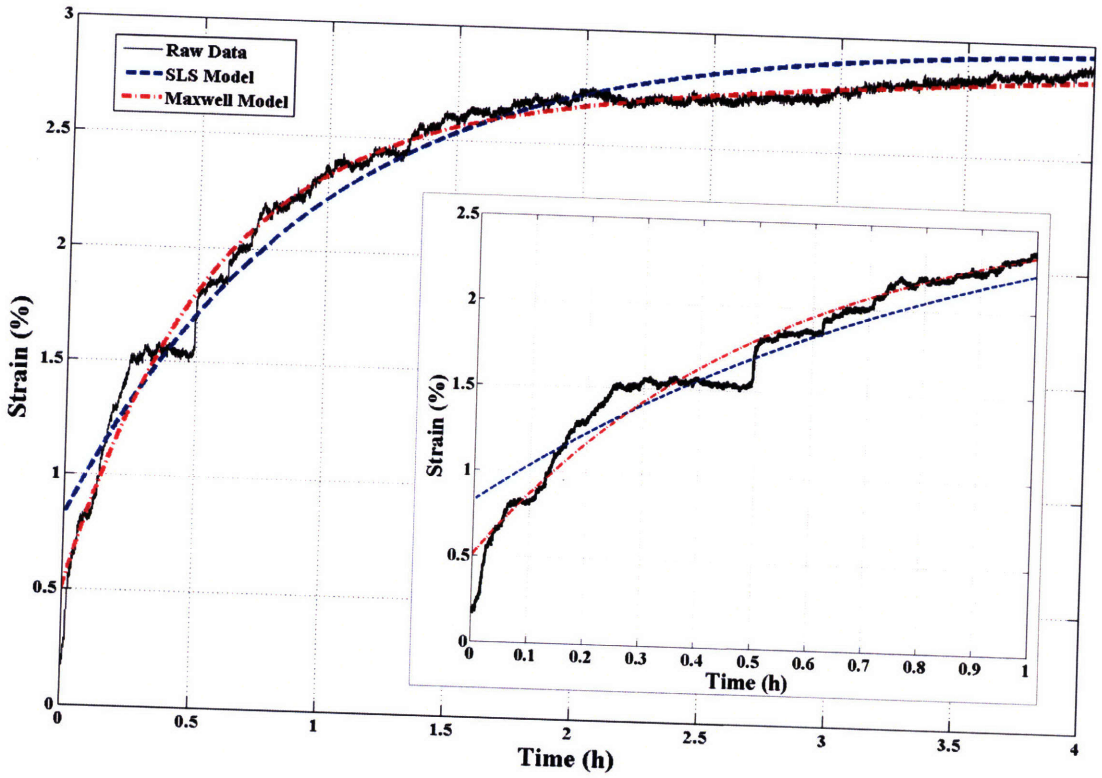

Figure 3-8: As can be seen from this plot of the creep behavior of polypyrrole, the Maxwell model is a significantly better representation of the polymer creep behavior than the SLS model. Inset shows close-up of transient behavior (first hour), emphasizing model differences.

samples deposited under the conditions given in Chapter 2. These films were allowed to air dry for 24 hours before removal from the deposition electrode and subsequent testing. Figure 3-8 shows the experimental creep response of a polypyrrole sample under a 1 MPa load (sample length 10.5 mm between inner contacts, width 1.5 mm, thickness 28 μm).

As can be seen, the generalized Maxwell model more accurately reflects the creep behavior of the material than the SLS model.

3.3 Strain-Resistance Relationship

3.3.1 Theoretical Modeling of Strain-Resistance

To model the relationship between strain and polymer resistance, the sensor was assumed to be an elastic beam. Direction coordinates are assigned based upon the expected aspect ratio of the sensor film (the sensor will consist of a film with length measured in centimeters, width in millimeters, and thickness in micrometers). The strain on the sensor will be applied along the length, which is assigned to be the x-direction. The width is thus the y-direction, and the thickness is the z-direction.

Under elastic beam theory, when an object is subjected uniaxial stress it experiences strains both in the direction of application as well as the lateral directions. The magnitude of these lateral strains is governed by the Poisson's ratio (ν) of the material, which in the case of polypyrrole is 0.426 [33].

Starting with the fundamental linear stress-strain relationships:

$$\begin{aligned} \epsilon_x &= \frac{1}{E}\left[\sigma_{xx} - \nu\left(\sigma_{yy} + \sigma_{zz}\right)\right], \\ \epsilon_y &= \frac{1}{E}\left[\sigma_{yy} - \nu\left(\sigma_{xx} + \sigma_{zz}\right)\right], \text{ and} \\ \epsilon_z &= \frac{1}{E}\left[\sigma_{zz} - \nu\left(\sigma_{xx} + \sigma_{yy}\right)\right], \end{aligned} \tag{3.10}$$

we then apply the assumption of uniaxial stress, where $\sigma_{xx} = \sigma$ and $\sigma_{yy} = \sigma_{zz} = 0$, to get:

$$\begin{aligned} \epsilon_x &= \frac{1}{E}\sigma, \\ \epsilon_y &= \frac{-\nu}{E}\sigma = -\nu\epsilon_x, \text{ and} \\ \epsilon_z &= \frac{-\nu}{E}\sigma = -\nu\epsilon_x. \end{aligned} \tag{3.11}$$

The cross-sectional area of the sensor is simply $A = yz = (y_o + \delta_y)(z_o + \delta_z)$, where δ_y and δ_z represent the deformation in the y- and z-directions. Since $\epsilon_i = \frac{\delta_i}{x_i}$, we can

substitute this into the definition of the area and we arrive at:

$$A = A_o \left(1 - \nu \epsilon_x\right)^2, \tag{3.12}$$

where A_o is the cross-sectional area of the initial, unstrained sensor. It is now necessary to make a further assumption, this regarding the conductivity of the polymer. While significant work has been done into the affects of large strains on the conductivity of polypyrrole films [14], this work is restricted to a small strains and it can thus be assumed that the conductivity remains constant. Using σ_c to represent conductivity and a subscript of 'o' to represent initial values, the conductivity is

$$\sigma_c = \frac{i_o x_o}{V_o A_o} = \frac{x_o}{R_o A_o}, \tag{3.13}$$

where i is current, x is length, V is voltage, and R is resistance. Solving for resistance,

$$R = \frac{x}{\sigma_c A} = \frac{x_o + \delta_x}{\left(\frac{x_o}{R_o A_o}\right) A_o \left(1 - \nu \epsilon_x\right)^2}. \tag{3.14}$$

Rearranging finally gives

$$R_s = R_c \frac{x_o + \delta_x}{x_o \left(1 - \nu \frac{\delta_x}{x_o}\right)^2} = R_c \frac{1 + \epsilon_x}{\left(1 - \nu \epsilon_x\right)^2}. \tag{3.15}$$

This is the relationship (referred to as the Poisson model) which will be incorporated into the system model (see Figure 3-1).

3.3.2 Strain-Resistance Experimental Work

Using the Vandesteeg DMA in Figure 3-7, measurements were taken to find the relationship between the applied strain and the resulting change in resistance of the sensor sample. To accomplish this, it was important that accurate resistance measurements were taken simultaneously with the deformation application.

As mentioned above, the clamps designed for this work (see inset in Figure 3-7)

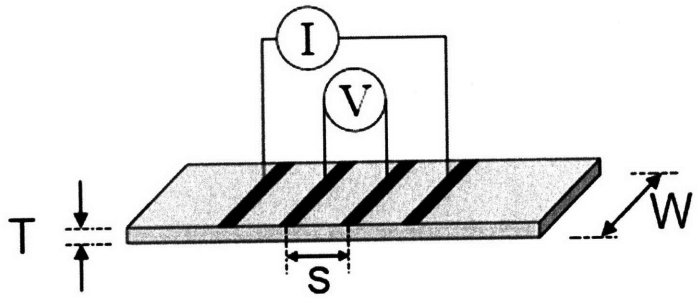

Figure 3-9: Contact configuration for four-wire measurement for a sample of width W, thickness T, and contact spacing S. From [25].

incorporated a four-point resistance measurement configuration using gold contacts. While measuring resistance with two contact points is simplest, this method unfortunately does not account for the contact resistance within the contact probes and between the probes and the sample. Using the four-wire measurement method shown in Figure 3-9 reduces the effect of contact resistance to a negligible level by applying a known current between the outer contact points and measuring the resulting voltage across the inner contacts. The voltage measurement draws a very small current, thus minimizing the effects of the contact resistance.

The film used in this testing was approximately two months old, having been stored in a sealed container since deposition. Samples were cut to be approximately 1.5 mm in width and 30 mm in length. The film was 25 μm thick and had a conductivity of 12.5×10^3 $\frac{S}{m}$.

The applied strain was sinusoidal with frequency of 0.05 Hz and a magnitude of 2%. Figure 3-10 shows the strain-resistance relationship for 150 cycles of a typical sample. The model prediction is also shown (0.38 $\Omega/\%$, in the case of this sample), displaying agreement with experimental results.

To generate an output that is usable by the control electronics, this small change in resistance must be amplified and converted into a voltage. This is done through the utilization of a full Wheatstone bridge, as shown in Figure 3-11. The sensor layer of the programmable material serves as one leg of the bridge. Three resistors of equal and constant values (equal to the resistance of the sensor at rest) form the remainder of the bridge. A constant input voltage is applied and the output voltage varies as a

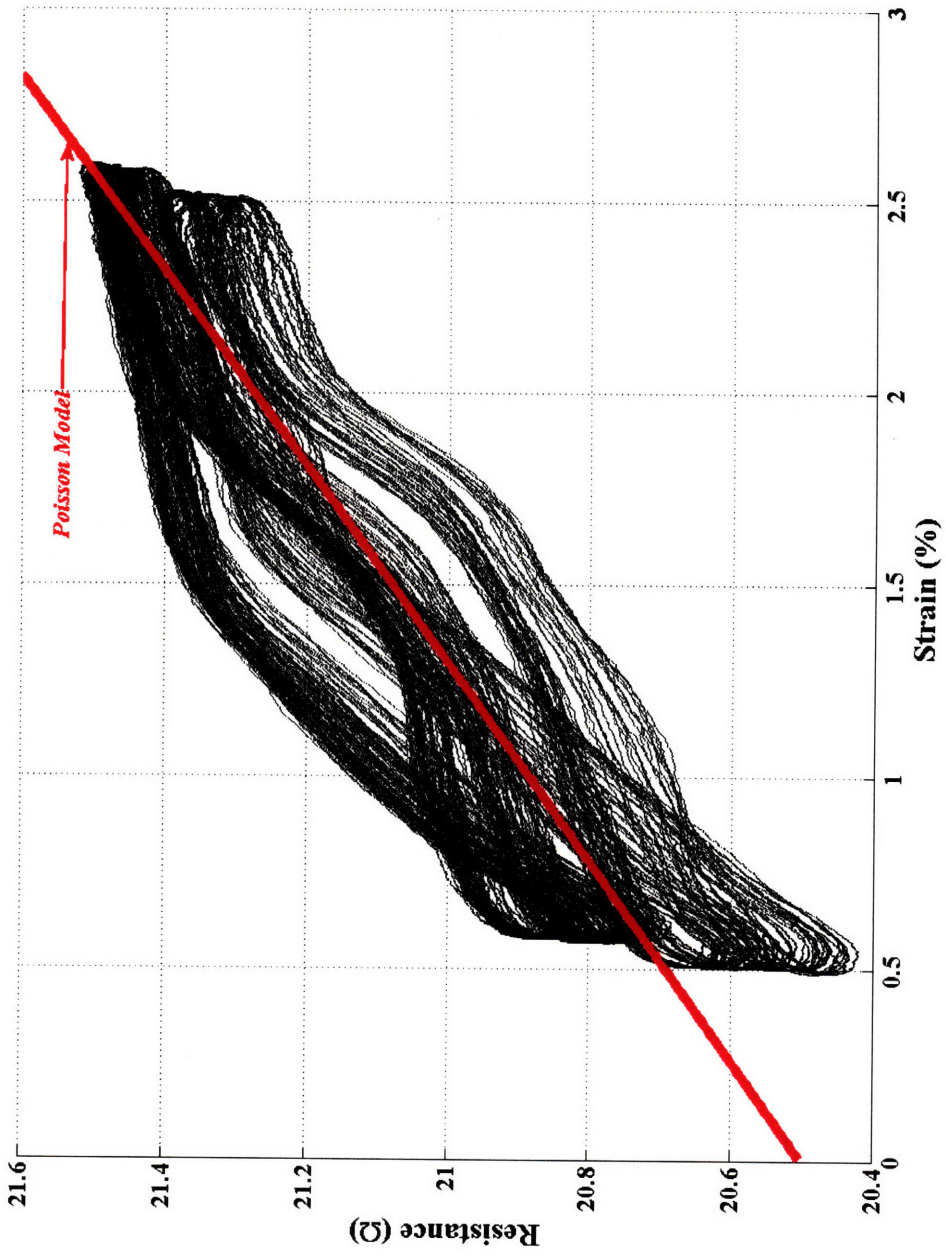

Figure 3-10: Experimental test results for polypyrrole film strain gage response show that the Poisson model is a good predictor of the strain-resistance relationship. Sample was 1.5 mm wide with 25.5 mm between inner contact points. Input was 2% strain sinusoid at 0.05 Hz; three subsequent tests of 50 cycles each are shown.

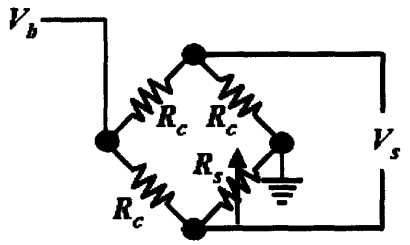

Figure 3-11: The full Wheatstone bridge was used to convert the variable resistance of the sensor into a voltage to be used by the control electronics. The sensor (R_s) forms one leg of the bridge, and the remaining are formed by constant and equal resistors (R_c). A constant voltage, V_s, is applied, and the variable output V_b provides an input to the control electronics.

function of the sensor resistance:

$$V_b = V_s \left(\frac{R_s}{R_s + R_c} - \frac{1}{2} \right), \tag{3.16}$$

where R_s is the sensor variable resistance, R_c is the constant resistance value, V_s is the sensor input voltage, and V_b is the bridge output voltage.

For an R_c value of 25 Ω and a V_s value of 20 V, the bridge output is linear between $\pm 2\%$ strain, as shown in Figure 3-12. The gain for these bridge parameters is 0.93 $\frac{V}{\% \, strain}$. This is the set of values used in the programmable material system model in Chapter 6.

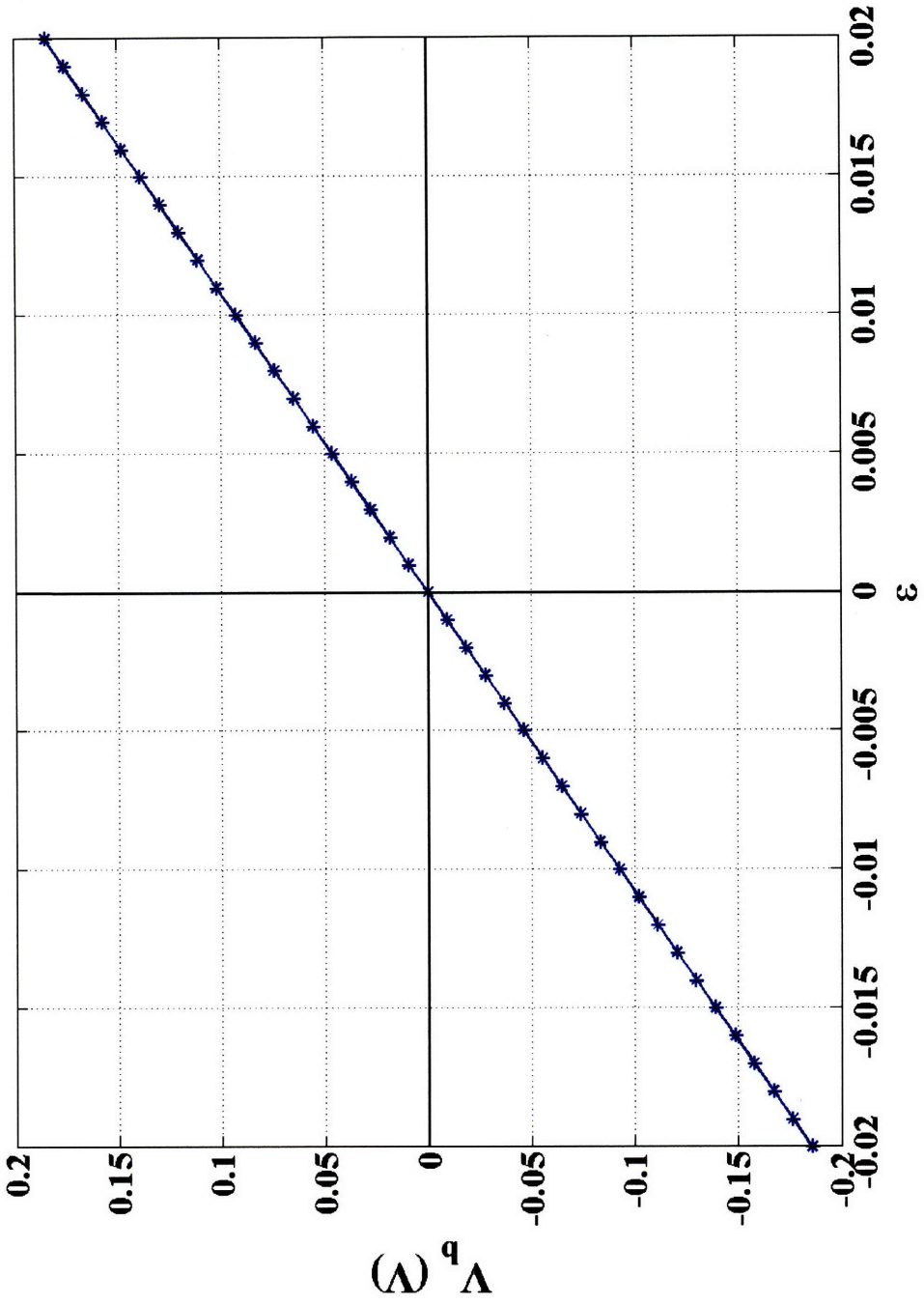

Figure 3-12: When the polypyrrole sensor is used as one leg of a full Wheatstone bridge, the output voltage is a linear function of the sensor strain over the range of interest. Here, using an R_c value of 25 Ω and a V_s value of 20 V, the bridge output has a gain of 0.93 $\frac{V}{\%\ strain}$.

Chapter 4

Deposition and Patterning of Control Electronics

The key component of a programmable material is the feedback loop embedded within it. This loop requires the fabrication of electronic components from polymeric materials that can be co-fabricated with the sensor and actuator elements. This co-fabrication requirement severely restricts the choice of fabrication techniques. This chapter reviews techniques available and discusses the final choice of the oxidative chemical vapor deposition process for device deposition used to fabricate the differential amplifier (as shown in Figure 4-1). Issues with deposition and measures taken to overcome those issues are also discussed.

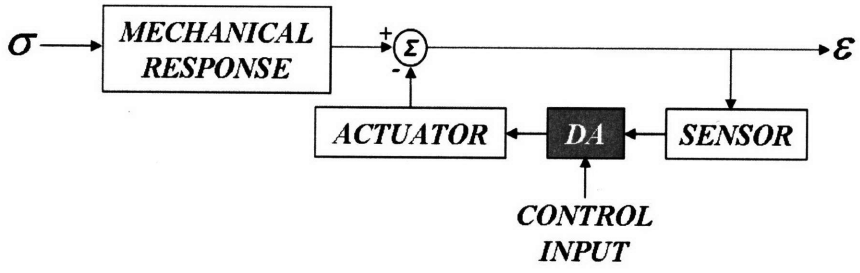

Figure 4-1: System block diagram.

4.1 Deposition and Patterning Techniques

There are a limited number of methods by which a conducting polymer can be deposited. The techniques for patterning the conducting polymer control electronics are closely related to the deposition method, so these will be examined simultaneously. There were several requirements that a method had to satisfy in order to be deemed appropriate for this work.

- First, the fabrication of the control electronics could not damage the actuator or sensor components. As discussed in Chapter 6, co-fabrication of the integrated programmable material requires patterned conducting polymer deposition onto a flexible and somewhat fragile conducting polymer-based substrate. If either the deposition process or the patterning technique (to include pattern removal) damages the underlying conducting polymer, the method will not work.

- Second, it is important to keep the overall size of the device small. Since the speed of actuation in polypyrrole is diffusion-limited (see Chapter 2), it is important to keep the dimension normal to the electrolyte interface (usually the thickness) very small while maintaining mechanical robustness. To prevent significant ohmic losses within the actuator, which results in thermal loading of the actuator and uneven actuation [25, 56], it is important to keep the width and length of the device small. This limits the available footprint upon which the electronics may be fabricated, and therefore limits the complexity of the control implementation.

- Third, the technique or techniques chosen must allow deposition of both conducting and non-conducing polymer layers, or there must be a complementary method for non-conducting polymer deposition. The non-conducting layers will serve as electronic and ionic insulators between the actuator, sensor, and electronics layers.

- Fourth, the deposition process should be as simple and robust as possible. Since the goal is to create a programmable material consisting completely of con-

Table 4.1: Processing Hazards for Polypyrrole. Reprinted from [57].

Damaging	Use care, test first	Harmless
Cr etchant	Acids	Au etchant
High temperatures		Hot plate at 100°C
Developer (KOH), Bases	Solvents	Photoresist
Resist Stripper/Remover		UV light in mask aligner

ducting and non-conducting polymers, silicon or metal substrates are to be avoided. Further, a deposition method and accompanying patterning technique with fewer variables allows for easier optimization.

- Finally, the deposition technique must be capable of depositing conducting polymer onto a non-conductive substrate. This is important to allow adequate electronic isolation between the functional layers of the device.

As mentioned in the first bullet, it would be self-defeating to use a fabrication process to create the control electronics which damaged the underlying conducting polymer components (i.e. sensor and actuator). Smela [57] examined the risks to polypyrrole resulting from various processing techniques, chemicals, and conditions. As shown in Table 4.1, the use of one of the primary methods for patterning micrometer-sized components (photolithography) is severely limited by the sensitivity of polypyrrole to photoresist developers. The other hazards shown were considered in evaluation of the various methods.

There are six basic methods for depositing patterned conducting polymers [58,59]. Each of these were evaluated for their effectiveness and the ease with which the control electronics could be created.

4.1.1 Electroless Deposition

Among the simplest deposition methods is the electroless technique, so called due to the lack of an electrical potential driving force in the depositon. This method can deposit onto nearly any surface (conductive or non-conductive) simply by immersing

(a) Electroless solution with target material.

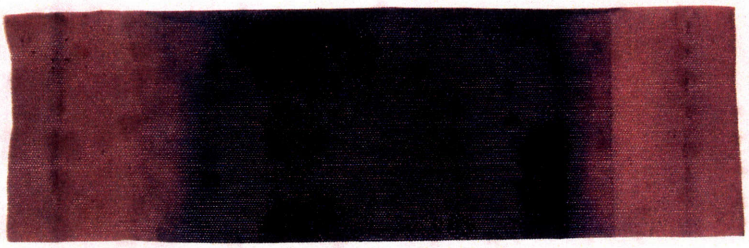

(b) Fabric Target after electroless deposition.

Figure 4-2: After several hours of electroless deposition in a water solution at 4°C, the submerged portions of the target have a uniform coating of polypyrrole.

the target into a prepared solution. For example, to deposit polypyrrole using this method, the solution contains 0.02 M of pyrrole monomer (previously distilled), 0.046 M of an oxidizing agent (for example, iron (III) chloride, $FeCl_3$, which also provides the Cl^- anions for doping), and 0.006 M of an initiator (such as 1,5-naphthalene disulfonic acid tetrahydrate) (see Figure 4-2).

In order to pattern an electroless deposition, a removable conformal pattern must be applied to the target prior to deposition. The difficulty arises in the need to remove the mask following deposition. Photoresist was considered as one possible masking material, but the removal process would have damaged the underlying polypyrrole substrate. Early experiments on fabric targets using various adhesive masking materials proved inadequate (see Figure 4-3).

As no appropriate patterning technique was found, the electroless deposition process was rejected as inappropriate.

4.1.2 Electrochemical Deposition

The process of electrochemically depositing polypyrrole (and similarly, other conducting polymers) is discussed in depth in Chapter 2. This section deals only with this methods applicability to deposition and patterning of a programmable material's control electronics.

Electrochemical deposition (ECD) requires a conductive target to serve as the

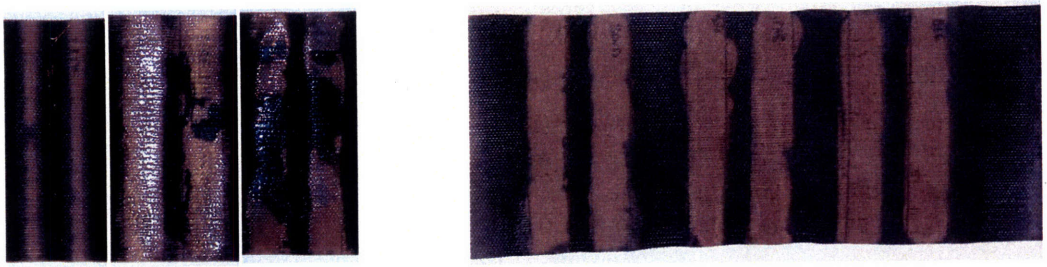

(a) Adhesive mask results on fabric target.

(b) Wax mask results on fabric target.

Figure 4-3: In order to pattern an electroless deposition, different adhesive masks were tested. In subfigure a, the masking materials used were (left to right) Kapton® tape, urethane, and epoxy. In subfigure b, the masking materials used were varying types of wax. The urethane and epoxy were permanently adhered to the substrate and did a reasonable job of blocking the deposition. The tape was easy to remove, but did not effectively block deposition. The waxes blocked deposition and could be removed, but the removal was slow, difficult, and imperfect.

working electrode. If the conductive target is selectively coated with conducting polymer by applying a pattern prior to ECD [60–63], the conducting polymer traces will not be electrically isolated unless the continuous substrate is then etched away. This can be damaging to the original deposition. A more realistic option is to pattern the conductive substrate itself prior to ECD, removing areas where we do not wish conducting polymer to be deposited.

Establishing this pattern can be done several ways, including masked crosslinking, patterned target electrodes, photoresist-patterned electrodeposition, reactive ion etching, selective destruction, and selective doping. Based on the criteria listed above, the only method that might meet the requirements of this work is patterned target electrodes (the other methods require significant processing or post-deposition treatment with harmful chemicals). Of course, this requires patterning of the target electrodes in the first place, which must be done photolithographically.

Jager et al. [64] were able to use photolithographic methods to fabricate arrays of bilayer (see Chapter 2) microactuators (see Figure 4-4), based on earlier work by Smela and others [44, 65]. These devices were deposited on a silicon substrate and required gold, titanium, and chromium layers, which violate the criteria above. Ultimately, it was decided that photolithographic patterning was incompatible with

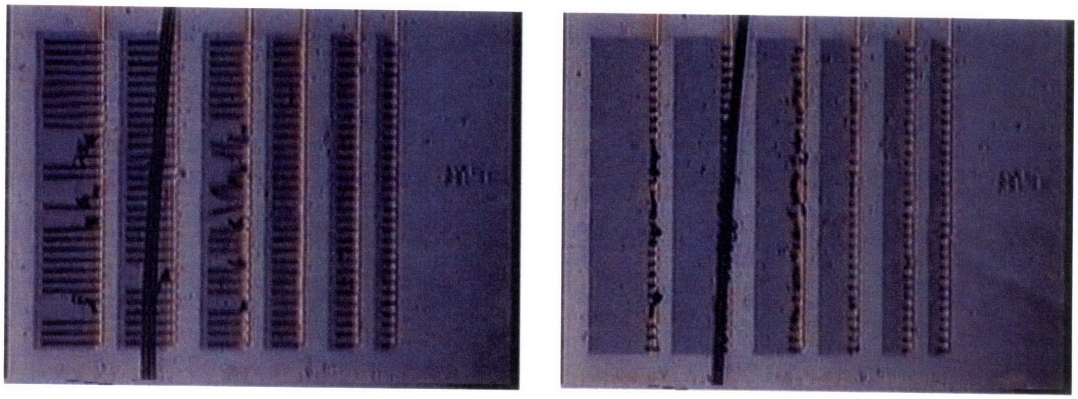

Figure 4-4: Smela et al. created bilayer microactuators through photolithographic atterning. Figure on the left shows the microactuators stretched flat, with a 30 μm fiber for comparison. Figure on the right shows microactuators curled up, grabbing the fiber. From [64].

the requirements for this work. The risks posed by the photoresist developer and the complexity of the deposition process led to rejection of this method. The results that could be achieved using photolithography could be realized using simpler techniques.

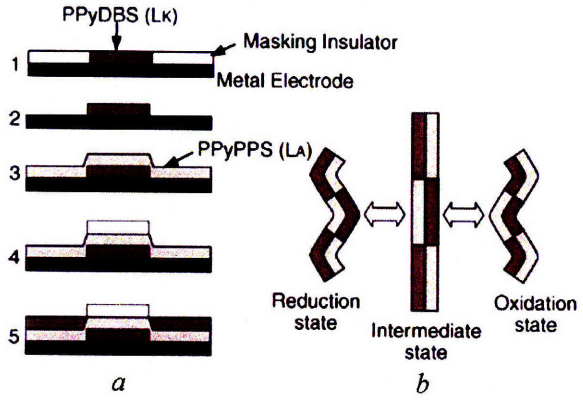

Figure 4-5: Takashima et al. patterned a bi-ionic actuator using insulating tape. Left figure shows deposition sequence, and right figure shows actuation of completed device. From [66].

Another patterning technique for ECD that was considered was that used by Takashima et al. [66]. By selectively and sequentially emplacing insulating adhesive tape, they were able to create a 'bi-ionic' actuator (see Figure 4-5). This actuator is bi-ionic in the sense that due to the two different polypyrrole chemistries deposited, different parts of the actuator contract and expand simultaneously under the same

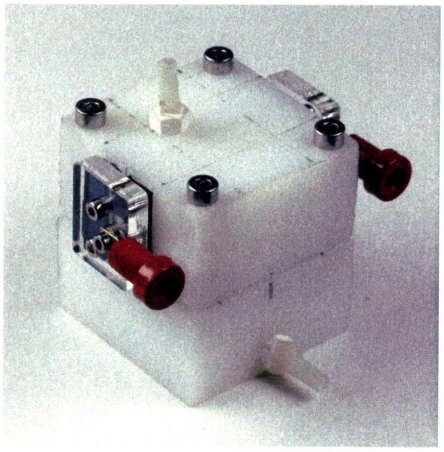

Figure 4-6: A bath was fabricated which allowed passivation of polypyrrole. When an alkaline solution is flushed over the film contained within the bath, the resulting change in conductivity is measured at the contact points on the sides. Subsequent immersion of the sample in an acid solution restored some of the conductivity.

electrochemical conditions. This patterning technique was ultimately rejected due to the difficulty of ensuring complete adhesive removal and the fragility of the polymer substrate.

4.1.3 Selective Passivation

Conducting polymers can undergo a large reduction in conductivity (passivation) when the conductive mechanism is interrupted through chemical treatment. Pei and Qian demonstrated a reduction in the conductivity of polypyrrole by four orders of magnitude after deprotonation of the molecular chain resulting from exposure to a basic solution [24].

To examine the potential for using selective passivation as a patterning technique for polypyrrole, a small bath was fabricated (see Figure 4-6) that enabled the successive immersion of a polypyrrole sample in basic, acidic, and neutral solutions while measuring the sample resistance.

Using this test apparatus, a change of well over one order of magnitude was achieved in the sample conductivity (see Figure 4-7). Unfortunately, these solution treatments resulted in a significant change in the sample geometry, causing samples to contract (enough to break, in some cases) when immersed in the alkaline solution.

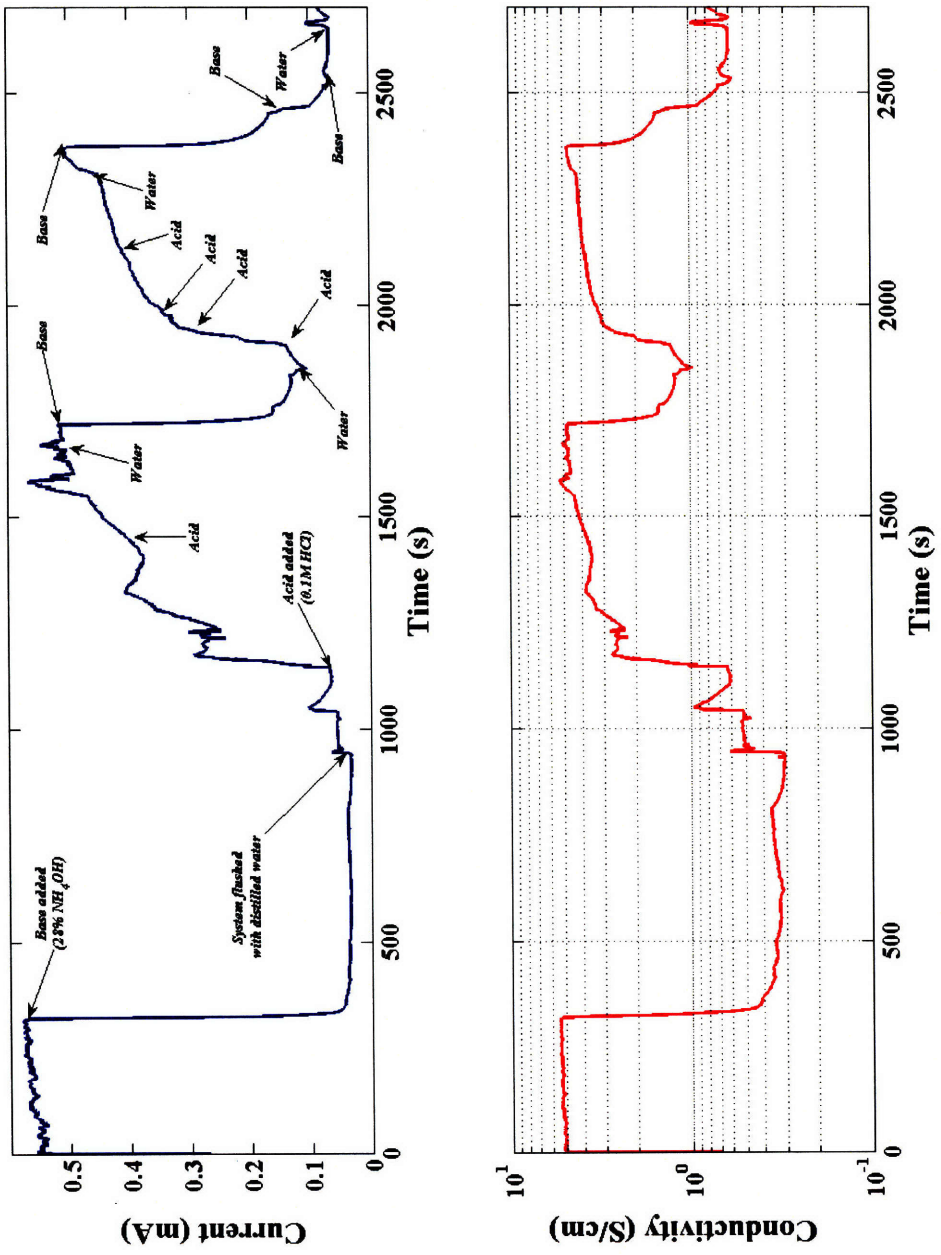

Figure 4-7: Using the bath shown in Figure 4-6, a polypyrrole sample was exposed to successive solutions. Annotations reflect the timing of these different solutions. The sample conductivity was reduced by a factor of 12 when immersed in a basic solution. This conductivity was recoverable when submerged in an acidic solution.

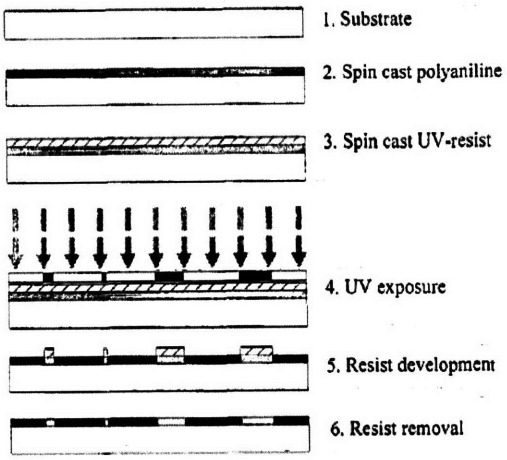

Figure 4-8: Photolithographic techniques can be used to selectively passivate underlying conducting polymer. Developing the photoresist deprotonates the unprotected conducting polymer, creating a conductive pattern within a non-conductive matrix. From [67].

This resulted from the deintercalation of anions [24], essentially actuating the material. This was unacceptable for the current application and work was discontinued in this area.

Makela et al. applied this deprotonation technique using photolithographic patterning methods [67]. After spin casting the conducting polymer polyaniline and a coating of ultraviolet photoresist, the resist was exposed to ultraviolet light through a mask (see Figure 4-8). The subsequent development of the photoresist in a strongly alkaline solution rendered the exposed regions of polyaniline ten orders of magnitude less conductive.

The selective passivation patterning technique is simple in that it patterns an existing continuous deposition of conducting polymer. However, the residual stresses left by the treatment with a basic solution prevent the use of this technique in the current work.

4.1.4 Contact or Screen Printing

Holdcroft [58] wrote an excellent review of the various techniques available for patterning conducting polymers. He goes into some detail on several printing techniques.

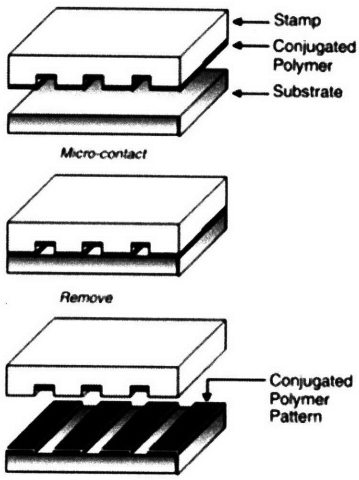

Figure 4-9: Using microcontact printing, a thin layer of conducting polymer can be transferred to a substrate. This requires patterning of the mask from an elastomer such as PDMS. From [58].

The first of these, microcontact printing (or μCP), is shown schematically in Figure 4-9. By patterning a stamp from an elastomer such as polydimethylsiloxane (PDMS), a precise pattern of an organothiol can be transferred to a surface. If, for example, the surface is gold, the exposed gold can be etched away, leaving a pattern of conducting electrodes for ECD. Alternatively, a thin layer (on the order of a few nanometers) of conducting polymer can be directly transferred to a substrate surface.

μCP has the drawback of requiring the photolithographic patterning of either the stamp itself or the pattern to be transferred, necessitating clean room conditions for fabrication. Additionally, the dynamic physical contact and mechanical pressure applied between stamp and substrate mitigate against using this technique for the current application.

Similarly, screen printing also requires dynamic mechanical pressure between pattern and substrate, as well as a squeegee device to transfer the pattern. Further, screen printing requires a soluble material for deposition [58, 59]. While the conducting polymer poly (3,4-ethylenedioxythiophene) (PEDOT) is soluble (when combined with polystyrene sulfonic acid) and can be patterned this way, the conductivities achieved are lower than with other deposition methods [68].

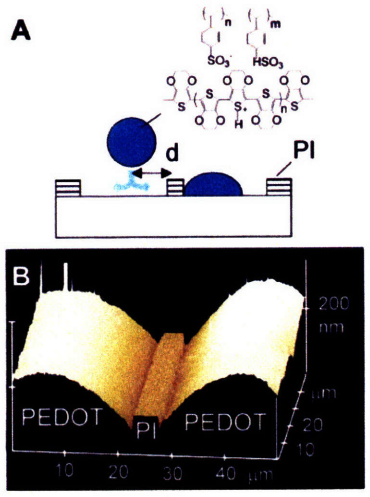

Figure 4-10: Using photolithographic techniques, Sirringhaus et al. were able to achieve high resolution with an inkjet printing process. Figure A is a schematic of how the droplet of PEDOT/PSS is limited by the hydrophobic patterned PI. Figure B was created using atomic force microscopy and shows the profile of the PI-limited deposition. From [69].

4.1.5 Inkjet Printing

Some soluble conducting polymers have been patterned using modified inkjet printing equipment [58, 69–74]. By patterning the target substrate with selective hydrophilic and hydrophobic regions, Sirringhaus et al. were able to achieve resolutions of 5 μm (see Figure 4-10) [69]. The conducting polymer in this case was PEDOT doped with polystyrene sulfonic acid (PSS), which makes the PEDOT soluble in organic solvents such as chloroform, and the hydrophobic boundaries were fabricated via photolithographic patterning of polyimide.

This method was rejected due to the need to construct a system for inkjet printing an appropriate conducting polymer onto the desired polymeric substrate. The polymer to be used had to be soluble, and while the PEDOT-PSS system is soluble, as mentioned above it has lower conductivities than other methods.

4.1.6 Vapor Phase Deposition

There has been considerable work using films of pentacene (an organic semiconductor) deposited using a process called organic vapor phase deposition (OVPD) [75–78]. This

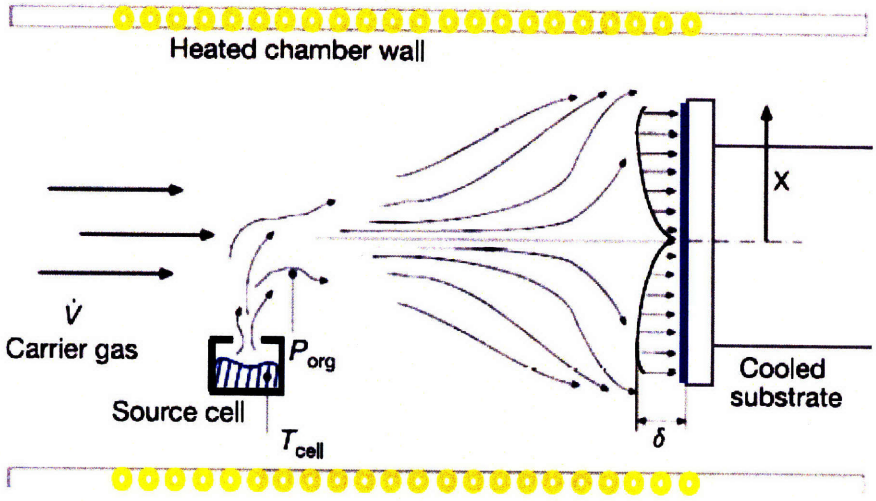

Figure 4-11: Schematic shows cross-section of a hot-walled organic vapor phase deposition (OVPD) reactor. An inert gas, saturated with the vapor of the organic source material, carries them downstream to the cooled target substrate. The hydrodynamic boundary layer of thickness δ is shown, which depending upon reactor conditions can be varied to control deposition speed and thickness. $\dot{V}$ is the gas volumetric flow velocity, T_{cell} is the organic source cell temperature, P_{org} is the partial pressure of the organic material vapor, and X is the position relative to substrate axis. From [76].

is primarily utilized in fabricating organic thin film transistors (OTFT). A schematic of the OVPD process is shown in Figure 4-11.

The OVPD process is useful for some organic materials, but it is not generally suitable to deposit conducting polymers. However, a variation of this process known as organic chemical vapor deposition (oCVD) can do so [79,80]. During the oCVD process, the conducting polymer is polymerized and deposited onto the target substrate in one straightforward step (see Figure 4-12). The oCVD process allows line-of-sight deposition without significant lateral migration, so the polymer can be patterned using a simple shadow mask. Additionally, oCVD is the most gentle process for the target substrate of all those examined. For these reasons, oCVD was the best methods to deposit the control electronics in the current work.

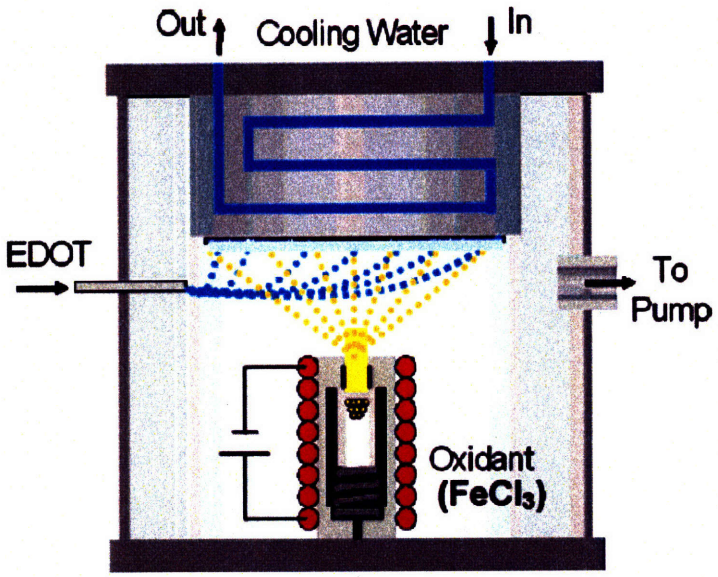

Figure 4-12: In oxidative chemical vapor deposition (oCVD), the EDOT monomer flows in from the left, making contact with the sublimated oxidizing agent. Polymerization occurs, and the PEDOT deposits onto the target substrate. The target is held on the underside of a temperature-controlled platform at the top of the chamber. From [80].

4.2 Oxidative Chemical Vapor Deposition

As discussed in the previous section, oCVD was the deposition process most suited for the current application. The process can be used to deposit many different conducting and non-conducting polymers, and is extremely gentle to the target substrate. Patterning can be accomplished with simple shadow masks, with resolution limited only by the mask fabrication process.

4.2.1 Experimental Setup

The oCVD process was pioneered in the Chemical Engineering Department at MIT in the lab of Professor Karen Gleason. Thanks to a collaboration via MIT's Institute for Soldier Nanotechnologies, Professor Gleason graciously allowed this work to be done using her facilities. The depositions were conducted in the vacuum chamber system shown in Figure 4-13.

The equipment consists of a vacuum chamber (drawn schematically in Figure 4-

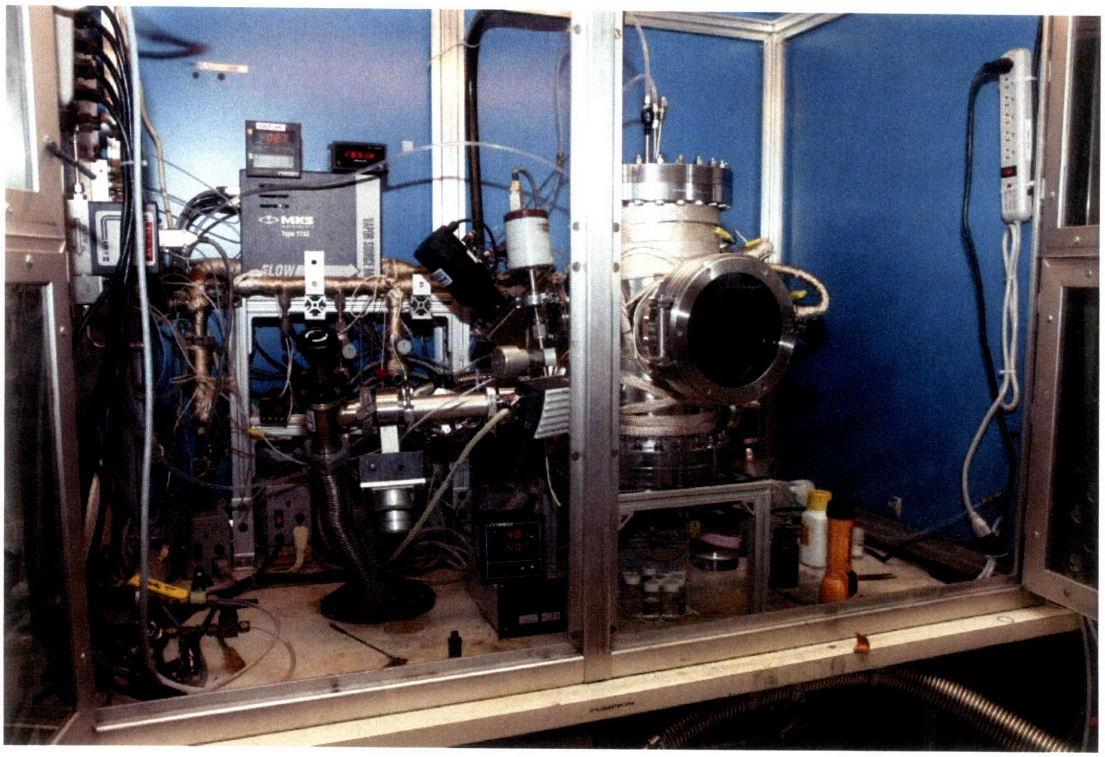

Figure 4-13: The oCVD experimental setup shown is centered around the vacuum chamber (large circular window). Monomer flow is controlled at the upper left, and the oxidant temperature is controlled at the bottom center. Photo taken in the Gleason Lab at MIT.

12) with a heated crucible into which an oxidant (usually Fe(III)Cl_3) is placed. Upon achievement of pressures below 150 mTorr, the oxidant is heated to approximately 240 °C at which point it sublimates to vapor form. The heated conducting polymer monomer (normally ethylenedioxythiophene, or EDOT) is introduced in vapor form. The target substrate - normally polyethelyne terephthalate (PET) film - is maintained at a constant temperature (normally 85 °C), as this is used to control the conductivity of the deposited film [80]. At this temperature, conductivities of $10^3 \frac{S}{m}$ were regularly achieved.

When the monomer and oxidant make contact in the deposition chamber, PEDOT is formed and deposits directly onto the target substrate (see Figure 4-14). Following deposition, the system is allowed to cool before venting. After removal from the chamber, residual monomer and oxidant are washed off the target substrate with methanol.

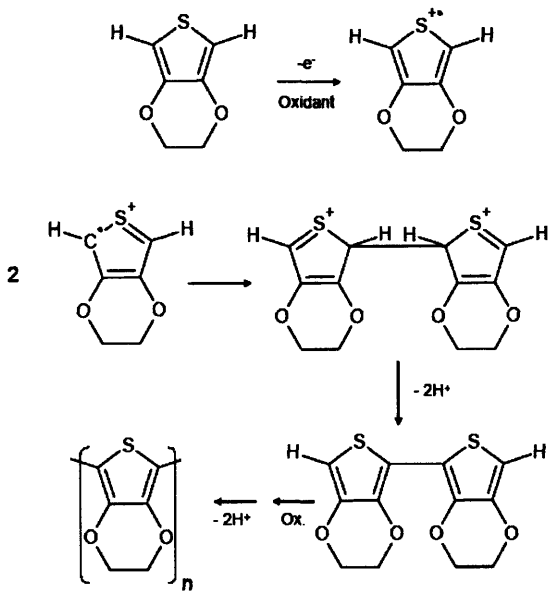

Figure 4-14: The mechanism of PEDOT polymerization in the oCVD process actually favors longer polymer chains. The EDOT dimers oxidize more readily than the monomer, driving the process to longer chains. From [68].

As discussed in Chapter 6, co-fabrication of the programmable material required insulative polymer layers that provided both ionic and electronic barriers between the actuator, sensor, and electronics layers. This was accomplished by patterned deposition of polystyrene using a plasma-polymerization process in the Gleason lab.

The reason polystyrene was used as the barrier material was not only for its barrier characteristics but also for the ability to 'graft' subsequent oCVD layers of PEDOT onto the polystyrene surface. Grafting was first used in oCVD by Im et al. [80], allowing strong attachment of the deposited film onto a substrate with a molecular structure containing aromatic rings. As part of the oxidative deposition process, these aromatic rings form attachment sites for the PEDOT (see Figure 4-15).

4.2.2 Patterning

One of the advantages of the oCVD process was that patterning the conducting polymer could be accomplished with shadow masks. This was done using both metal and adhesive masks. The metal masks were used initially to achieve good resolution

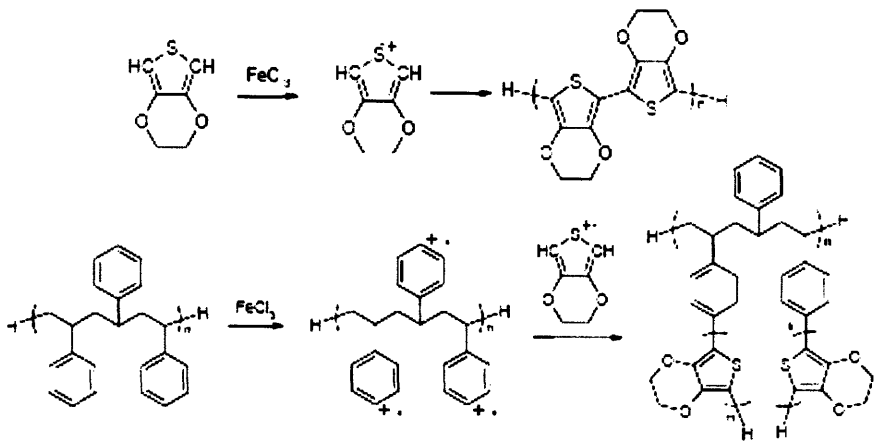

Figure 4-15: Starting with polystyrene (lower left), the oxidative chemical vapor deposition process activates sites on the aromatic rings for PEDOT attachment and polymerization. The attachment (grafting) that results is excellent. From [68].

(see Figure 4-16), but the external manufacturer was slow to provide completed masks. For this reason, many depositions were completed using adhesive paper masks, which were much simpler, cheaper, and faster to fabricate, though they did not provide the resolution of metal. An internal fabrication method for metal masks was devised, and later depositions were again completed with metal masks.

The pattern designs were dictated by the requirements of the control electronics needed to implement the feedback loop. Each design was completed using SolidEdge® 19.

The masks had to meet certain criteria:

- Withstand temperatures of 85 °C.
- Did not damage fragile substrate.
- Thin enough to prevent significant shadowing of PEDOT deposition.
- Either adhesive (and thus conformal) or else rigid (and thus statically clamped tightly to substrate).
- Reusable masks are preferable to one-time use.
- Inert (with respect to oCVD conditions).

(a) (b) (c)

Figure 4-16: Metal masks in subfigures a and c were for oCVD of PEDOT, while mask in b was for plasma-polymerization of polystyrene. These masks were produced by outside manufacturer Stencils Unlimited, and are each 50 mm square.

Adhesive Masks

In order to accelerate the prototyping cycle, adhesive masks were used for many early depositions. It was important to find a masking material that could be accurately cut with a pattern and still be able to withstand the conditions of the oCVD process. Several adhesive tapes were tested, and many of them reacted poorly to the elevated temperature of the oCVD chamber.

The final adhesive mask design used 3M® 9415 repositionable tape and heavy paper. The tape was double-sided, with one high tack surface which was adhered to the paper. The distal surface of the tape was coated with a low tack adhesive to allow repositioning of the mask if necessary.

The adhesive masks were fabricated using a Trotec® laser engraver. While the resolution of the cut patterns did not match that of the externally fabricated metal masks, as shown in Figure 4-17, the 100 μm spot size of the laser was adequate for most patterning tasks.

An unforeseen advantage of the 3M® 9415 tape was that these masks lifted off the substrate very easily when washed in methanol following deposition. If handled carefully, the paper/adhesive masks could be reused several times. Unfortunately, it was discovered that a significant amount of adhesive remained on the substrate following mask removal. This did not hinder early tests, but was a factor in the discontinuance of adhesive mask usage.

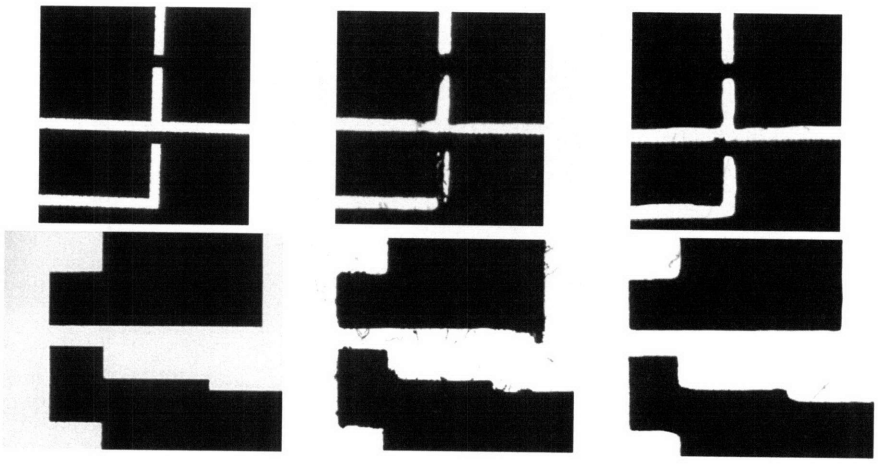

Figure 4-17: Comparing adhesive masks fabricated on the laser engraver with the metal masks shown in Figure 4-16 shows that adequate resolution is achievable with adhesive masks for initial design iteration.. The leftmost pair of photos show close-ups of components of the metal masks. The small bridges are 200 μm in width. The center pair of photos shows an adhesive mask after a single pass of the laser engraver, while the rightmost pair of photos shows an adhesive mask after two passes using the final cutting settings.

Metal Masks

Once the designs for the electronic components had been refined, it was necessary to achieve greater accuracy and repeatability than could be accomplished with adhesive/paper masks. Parallel to the several depositions conducted using the adhesive masks, a metal mask fabrication method was devised that could be completed in-house. While these rigid masks were clamped to the substrate (and were thus in physical contact with the deposition target), this contact was static. This made the impact on and risk to the fragile substrate much less than techniques such as contact printing or screen printing, which required dynamic contact with the substrate.

Using wire electrical discharge machining (wire EDM), metal masks were fabricated from 120 μm thick stainless steel (see Figure 4-18). Since the wire EDM equipment needed access paths to the patterned cutouts, Kapton® tape was used to block unwanted gaps in the mask (this tape was used due to its chemical inertness) and improve the mask stiffness. All mask designs were created using SolidEdge® software and programmed for the wire EDM in G-code.

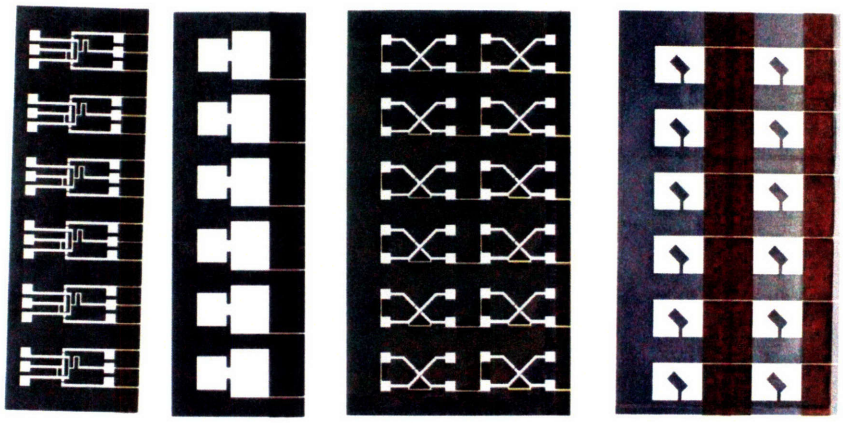

Figure 4-18: This set of metal masks was fabricated on the wire EDM equipment in the BioInstrumentation Lab at MIT. The left pair are for deposition of electrochemical differential amplifiers (mask for PEDOT at far left, mask for ionic barrier polystyrene second from left). The right pair are for deposition of electrochemical transistors (mask for PEDOT second from right, mask for polystyrene at far right). Each mask is 8 cm in height.

4.2.3 Results

An example of an oCVD fabrication is shown in Figure 4-19. Using the patterning techniques discussed above, it was found that features 200 μm in width were achievable, while attempts 100 μm features had poor results due to the mask thickness. Future work should leverage the ability of the wire EDM to produce angled cuts. The v-shaped openings in the mask which would result should reduce the shadowing which prevented implementation of smaller features.

Examination of the components fabricated using oCVD shows that the metal masking techniques used as previously described were effective. Scanning electron microscopy reveals the good definition of both the PEDOT and polystyrene layers (see Figure 4-20). The device shown, while somewhat dirty, performed well on testing.

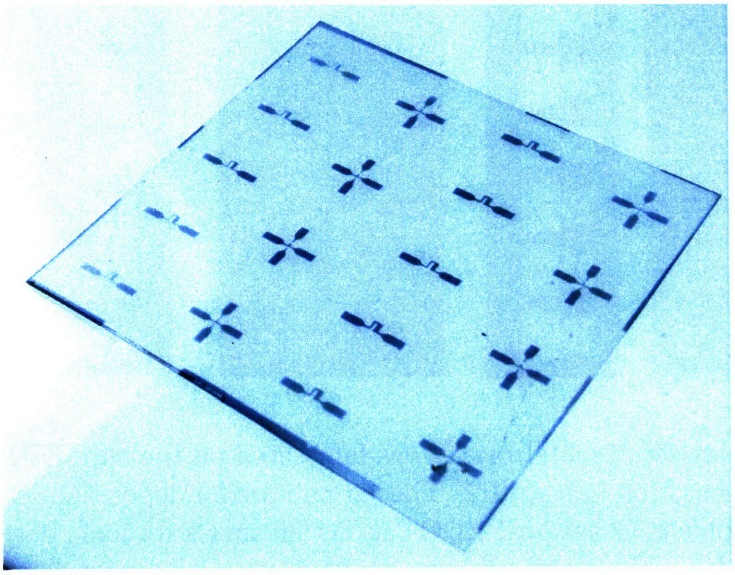

Figure 4-19: This figure shows a 100 mm square substrate of PET with depositions of PEDOT and polystyrene. The large areas of PEDOT are contact pads for testing purposes. The polystyrene can be faintly seen masking portions of the PEDOT deposition.

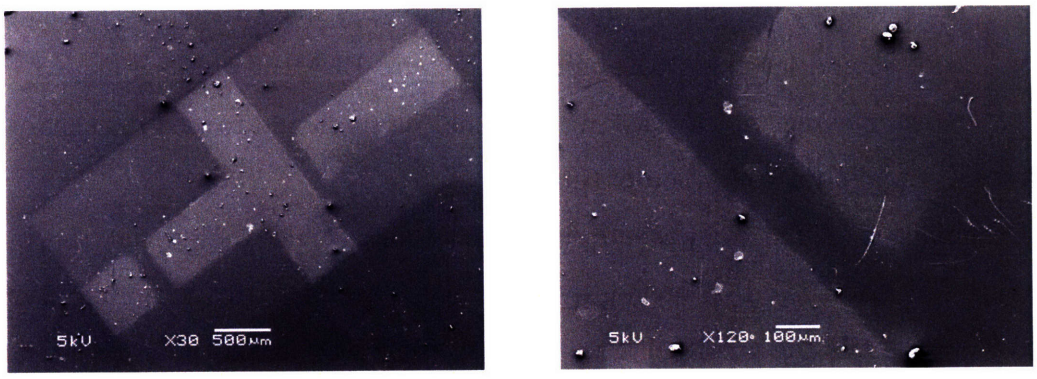

(a) (b)

Figure 4-20: Subfigure (a) shows an overview of a component deposited using oCVD. The PEDOT pattern is readily apparent, as is the polystyrene barrier layer over the outer portions of the device. Subfigure (b) shows a close-up of a gap of the same component, demonstrating the excellent definition of the PEDOT deposition achieved using wire EDM-fabricated masks.

Chapter 5

Feedback Electronic Components

5.1 Feedback System Requirements

In order to close the control loop in the device, a component is needed which will drive the error between the desired actuator strain and the actual strain of the device to zero. As shown in Figure 5-1, the desired strain is provided as an input to the system. A signal corresponding to the actuator strain is output by the sensor. These two signals must be compared and the difference between them amplified to provide an input to the actuator itself.

The simplest component for accomplishing this task is a differential amplifier (DA) [81]. This can be implemented with two transistors as shown in Figure 5-2. The theory of the DA is examined in a later section, but it is enough to know at this point that it is necessary to fabricate transistors in order to implement the feedback loop.

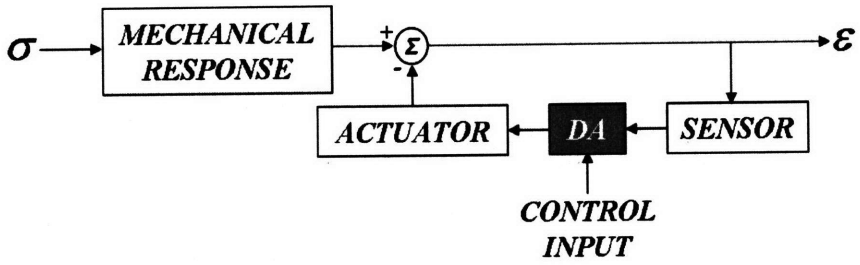

Figure 5-1: System block diagram.

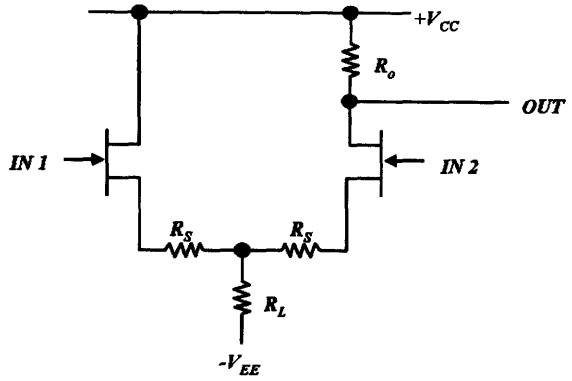

Figure 5-2: A "long-tailed pair" is a simple way of implementing a differential amplifier. This circuit uses only two transistors to amplify the difference between two input voltages [81].

Future work may examine implementation of PID (proportional - integral - derivative) control elements using operational amplifiers and other, passive, components such as capacitors and inductors, but the scope of this work was limited to the DA.

5.2 Previous Work

Many researchers have done work in the area of creating functional electronic components and devices using conducting polymers [51, 76, 82–88]. The first transistors incorporating conducting polymers were fabricated by Ebisawa et al. [89] in 1983 using polyacetylene as a semiconductor material in an organic field effect transistor (OFET), as shown in Figure 5-3. Continued research has led to the use of other conducting polymers as channel materials [90–94] within silicon-based devices as well as progress towards fully organic components [95–97].

Other work in organic electronics has shown that small organic molecules such as pentacene are more effective as OFET semiconductors than the current state of the art in conducting polymers [83, 97]. The important measure of material performance in this case is the charge carrier mobility, designated μ and measured in $\frac{m^2}{Vs}$. The best and most commonly used conducting polymer for this application is regioregular poly-(3-hexylthiophene) (rr-P3HT), with a charge carrier mobility on the order of 2×10^{-6} [98]. Mobilities of up to 1.1×10^{-4} have been demonstrated with pentacene [98]. Figure 5-4

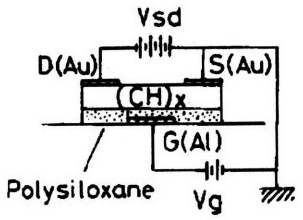

Figure 5-3: The first organic transistor utilized conducting polymer (labeled $(CH)_x$ in the figure) only for the semiconductor channel. All other components were non-organic. From [89].

gives an idea of the mobility ranges achievable with these materials relative to that currently available with silicon-based components.

As can be seen, even the best organic components are only beginning to compete with silicon-based electronics. As a result, most of the current research is directed to areas where silicon components have traditionally been unsuited such as low-cost, flexible, and large-area applications [97].

One of the most prominent of these organic electronics applications is the OLED, or organic light emitting diode. Since the early 1990's [99] such progress has been made in OLED design and fabrication [93] that OLED devices have begun to reach the commercial market (see Figure 5-5) [100].

Unfortunately, OFET's are currently impractical for a programmable material. The deposition methods and patterning techniques required to successfully fabricate an OFET (see Chapter 4) are too harsh to successfully deposit these components

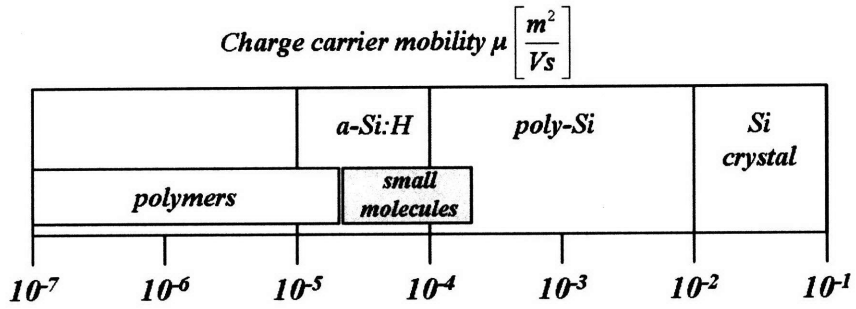

Figure 5-4: Conducting polymers are currently incapable of achieving charge carrier mobilities that are competitive with silicon-based components. The dark box represents organic small molecules such as pentacene. From [97].

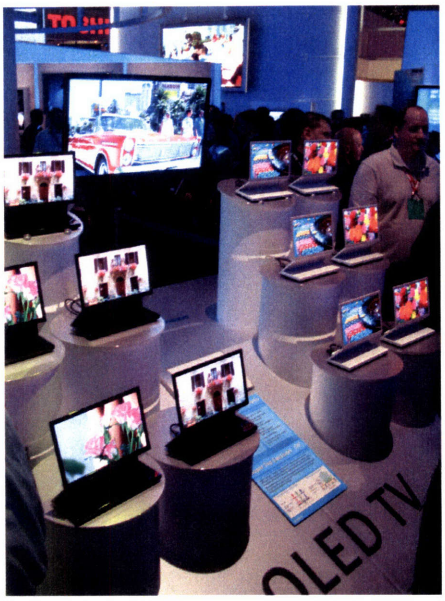

Figure 5-5: . These OLED high definition televisions from Sony® have a contrast ratio of $10^6 : 1$ and were first displayed at the 2007 Consumer Electronics Show.

onto a polypyrrole actuator backing. Simpler components are called for, such as electrochemical transistors.

Rather than depending on a very sensitive and difficult to deposit organic semiconductor layer as the channel material (as in an OFET), electrochemical transistors (ECT) are simply appropriately patterned traces of conducting polymer within an electrolyte [30, 95, 101, 102]. The electrolyte allows the establishment of electrochemical cells within the transistor, and the conductivity drain-source path can then be switched on and off electrochemically.

Wrighton et al. [103] were the first to create an ECT, using polypyrrole as the active material (see Figure 5-6(a)). These devices are not self-contained, however, as they require an external counter electrode. This research was refined by Schuhmann et al. [104], who miniaturized the device by writing polypyrrole lines across 100 μm gaps between source, gap, and drain using a scanning electrochemical microscope (see Figure 5-6(b)). Again, these devices required an external counter electrode.

As the ultimate goal is to create a programmable material that does not need to be immersed in electrolyte with a separate counter electrode nearby, ECT designs by Chen et al. were of great interest [71, 105]. These devices, discussed further below,

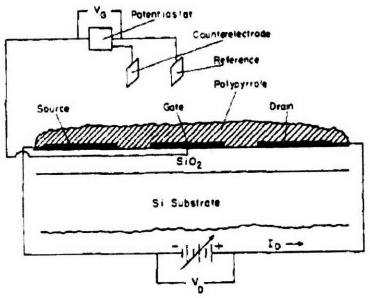

(a) Wrighton et al. (from [103]).

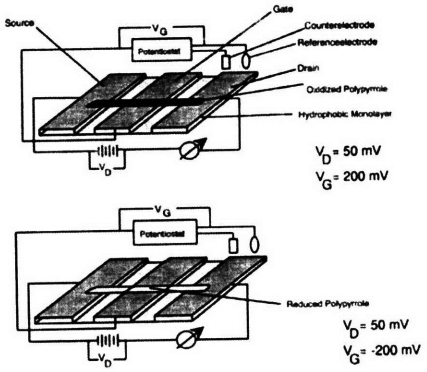

(b) Schuhmann et al. (from [104]).

Figure 5-6: Wrighton and Schuhmann created early electrochemical transistors using polypyrrole as the channel material. As can be seen, both devices must be submerged in electrolyte and require an external counter electrode.

obviate the need for an external counter electrode through the use of two separate electrochemical cells.

Chen's ECT were fabricated by first spin-coating a surface with a solution of PEDOT:PSS. The patterns were made by scoring the surface with a plotter, removing the conducting polymer from unwanted areas. This technique is unsuited to the current application, but patterning these devices can be accomplished in an oCVD deposition using shadow masking (see Chapter 4).

5.3 Diodes

5.3.1 Device Design

As a step to creating functional electrochemical transistors, electrochemical diodes were first designed and tested. Based on Chen's work [71], these diodes contain a single electrochemical cell. As shown in Figure 5-7, a positive potential applied between points a and b ($V_a > V_b$) causes a redox reaction to occur in the cell at c and d. As c is at a higher potential than d, c oxidizes and d is reduced. The conductive path $a - c - b$ is enhanced and current flows.

Conversely, reversing the potential between a and b reverses the redox reaction at c and d. In this case, c is reduced, and the conductive path is interrupted. These

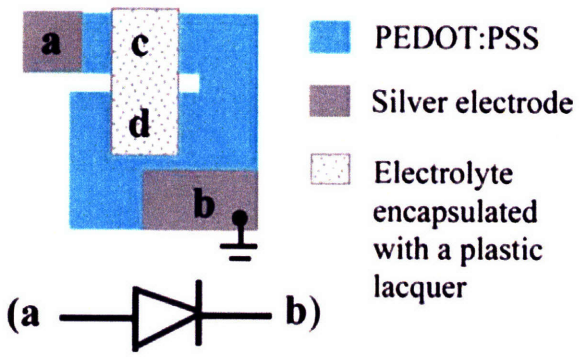

Figure 5-7: Chen's electrochemical diode design was implemented using spin-coated PEDOT which was subsequently patterned using a plotter. The electrolyte between c and d forms an electrochemical cell.

diodes were found to have rectification ratios on the order of 100 for $\pm 3V$ input.

5.3.2 Component Testing

For ease of testing, diodes were designed to be submerged in an electrolyte solution. Figure 5-8 shows a successful diode based upon Chen's design. The overlay shown represents the deposition of ionic barrier material (polystyrene, in this case) which established the electrochemical cell in the exposed regions of PEDOT. The diode was submerged with the two lead traces (on the left of the figure) oriented upwards. The electrolyte solution level was not allowed to go higher than the polystyrene barrier deposition.

Using this diode design, a sinusoidal voltage input was applied and the response measured. The input was generated by an Agilent® 33220A signal generator, and the output was measured using a National Instruments® PCI 6289 Data Acquisition Board (18-bit analog input resolution) with BNC 2110 Connector Block. A computer running Microsoft® Windows XP was used to collect the data using software written in Microsoft® Visual Basic.

The diode was submerged in a solution of tetrabutylammonium hexafluorophosphate in propylene carbonate to determine the diode's rectification capabilities. The input consisted of a 0.1 Hz $\pm 3V$ sine wave. Output data is shown in Figure 5-9 for a diode with 500 μm features.

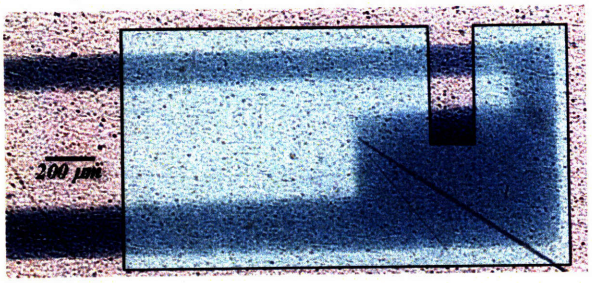

Figure 5-8: This electrochemical diode was fabricated using the oCVD process. Component with 200 μm feature sizes shown. Shaded region designates area covered by polystyrene deposition.

As shown in the figure, the solid line represents the actual time response of the diode. The dashed line is the integral of the time response. The upward trend of this integral plot indicates that rectification is occurring.

The fact that current reduction is evident for a foward bias (positive voltage values) indicated that the polystyrene deposition was either poorly patterned or was insufficiently ionically insulative to prevent reduction of the conductive path under a forward bias (in other words, area *d* in Figure 5-7 extended across the path between *c* and *b*). In addition to these difficulties, it was later discovered that the propylene carbonate solvent in the electrochemical test environment was gradualing degrading the polystyrene layer, exposing the PEDOT and de-localizing the electrochemical cell.

Figure 5-10 shows the current-voltage relationship for the 200 μm diode (the 500 μm sample was damaged prior to this test). As can be seen, a rectification ratio of 2.5 was achieved. While this does not match Chen's ratio of 100, this is the first time a functional diode-like device has been manufactured using the oCVD process.

Several design iterations were undertaken to improve the performance and repeatability of the diode performance. By using a plasma-polymerization process to deposit the polystyrene, forward-bias cutoff due to current path reduction was eliminated (see Figure 5-11). Later experiments utilized different electrolyte in an effort to improve the biocompatibility of the system (see Chapter 7), so the diode response shown in Figure 5-11 is from a test performed in an aqueous solution of sodium dodecylbenzensulfonate (NaDBS). As can be seen, an improved rectification ratio in excess of 4 has been achieved.

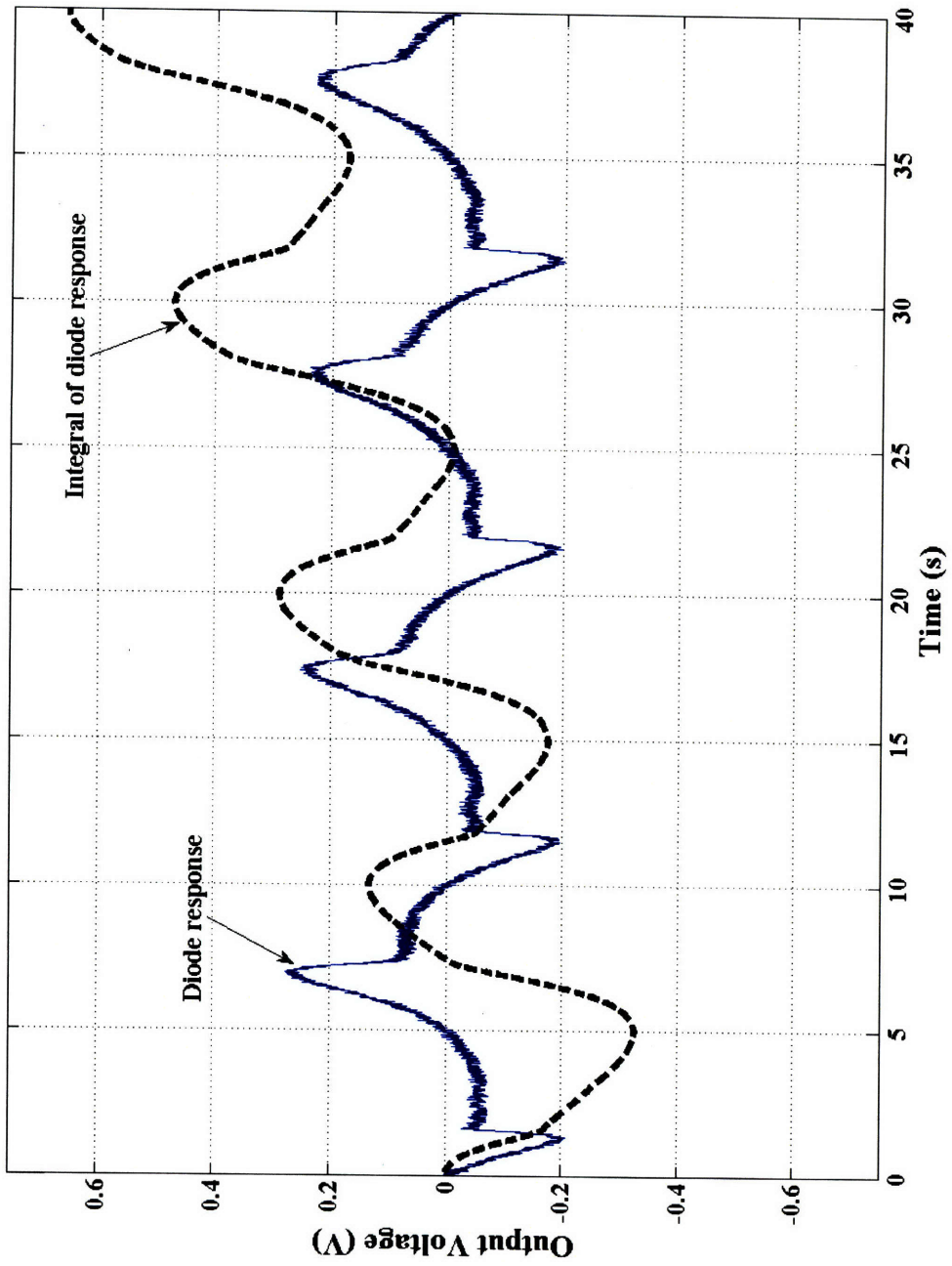

Figure 5-9: A 500 μm EC Diode was tested with a sinusoidal voltage input. The integral of the diode response is also shown, verifying that rectification is occuring.

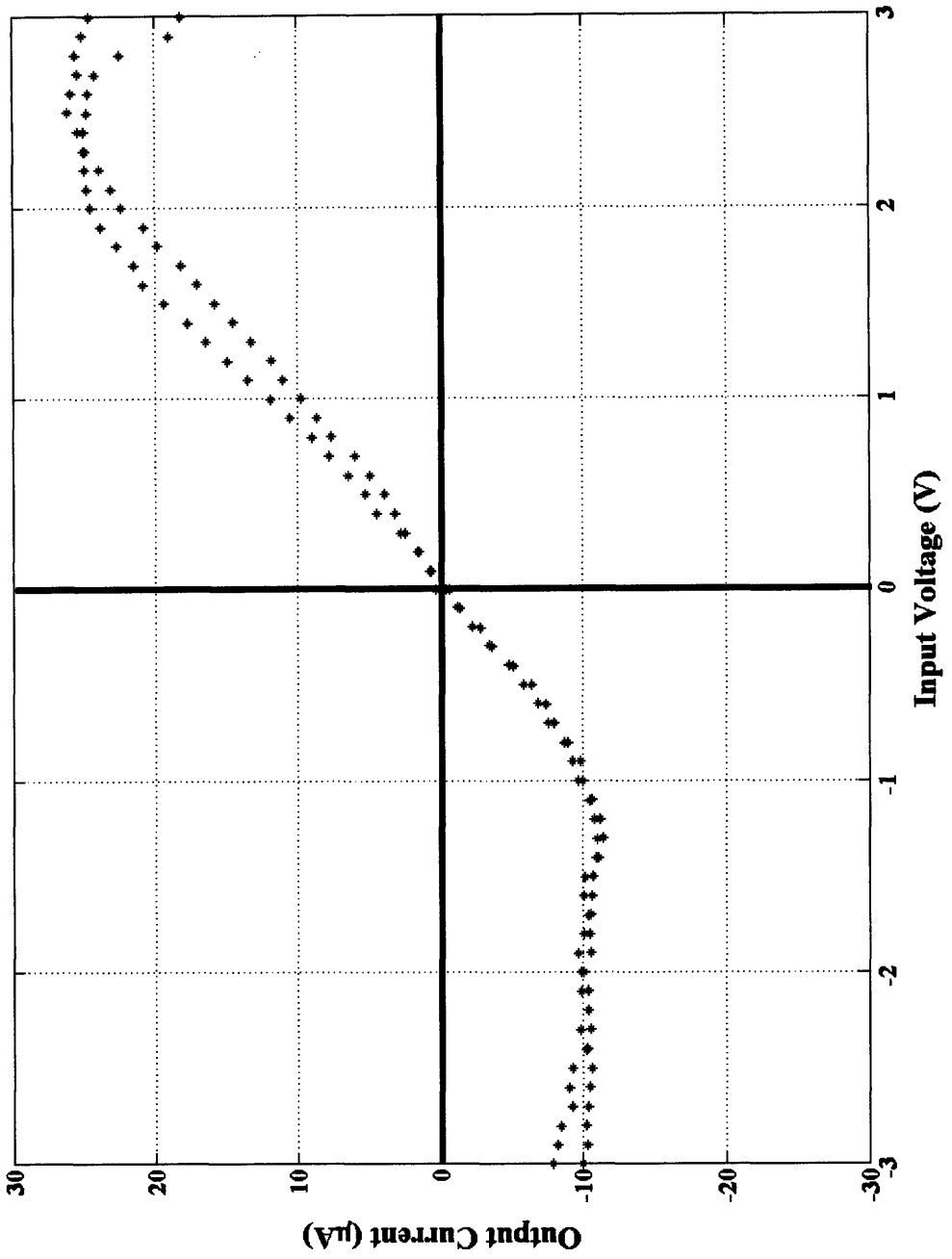

Figure 5-10: The performance of this EC diode is not strictly linear for positive voltages due to the unwanted current path reduction on forward biasing. A rectification ratio of 2.5 is achieved.

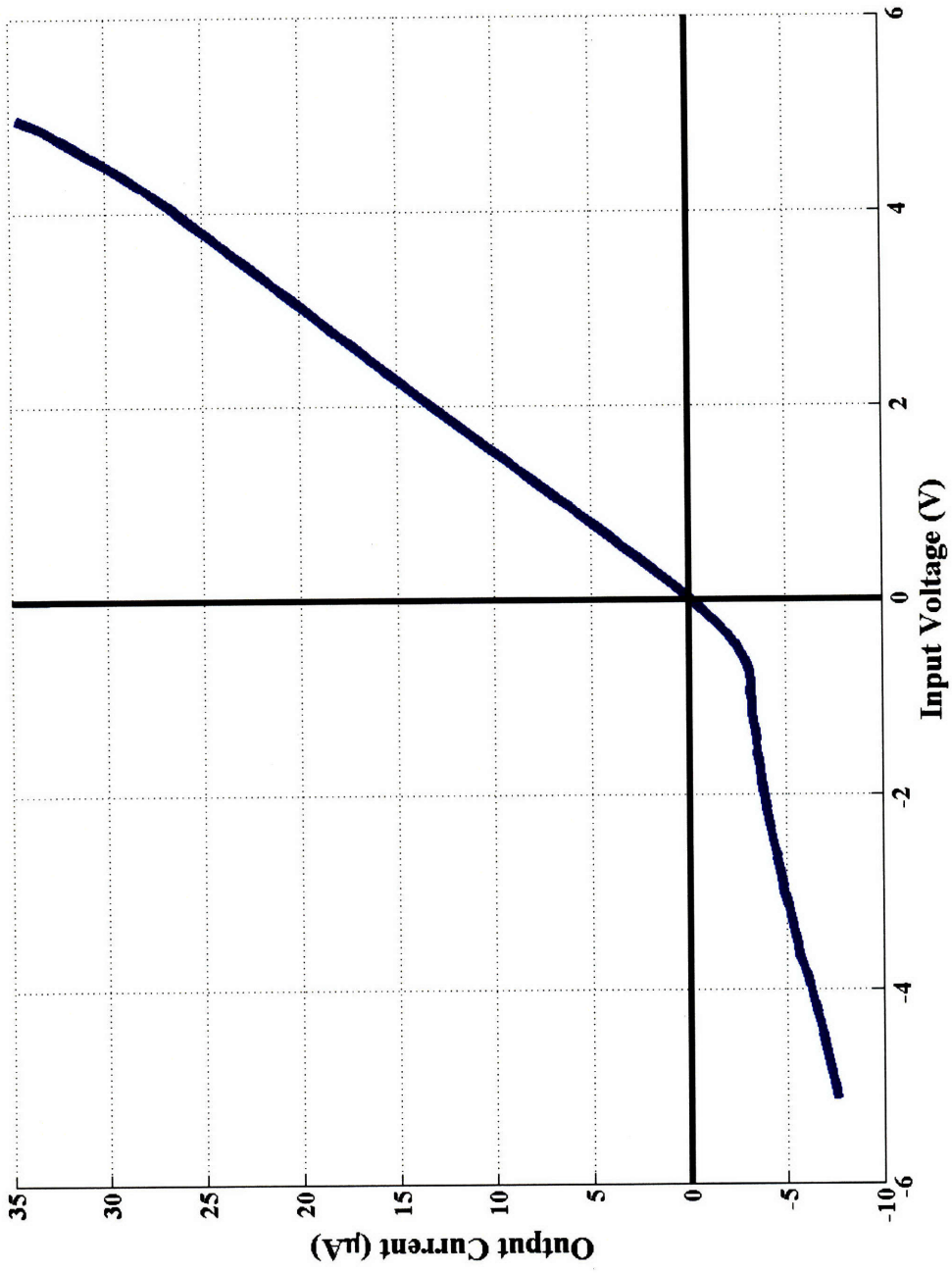

Figure 5-11: Improvement in fabrication and testing techniques resulted in an electrochemical diode with a rectification ratio in excess of 4.

5.4 Transistors

The key element in the implementation of the feedback loop, transistors were a significant research focus in this work. Considerable effort went into deciding what type of transistor to use and what design would best satisfy the device requirements.

Most silicon-based transistors in use today are one of two types: bipolar junction transistors and field effect transistors. Significant work has been done in the area of organic field effect transistors [83], as discussed above. For the purposes of this work, OFET's require deposition and patterning methods that are too harsh. Further, OFET performance is highly dependent upon the surface morphology of the organic semiconductor material used [75]. In order to achieve repeatably usable components, extremely precise deposition conditions are required.

Electrochemical transistors (ECT), on the other hand, can be deposited and patterned using the oCVD technique with a shadow mask. Several alternating layers of conducting and non-conducting polymer patterned the right way are all that is required, avoiding the deposition difficulty of an organic semiconductor material.

5.4.1 Device Design

As mentioned previously, Chen et al. [71,105] have created a simple, easily patterned ECT design. As shown in Figure 5-12, these devices modulate the drain-source conductivity through two separate electrochemical cells $a-b$ and $c-d$.

The bias voltage, V_B is maintained at a constant value (3.5 V in this case). For a zero gate voltage V_G and the source lead connected to ground, the $a-b$ cell undergoes a redox reaction. Region a is oxidized while b is reduced, cutting off the drain-source conductive channel. This transistor is thus normally off. Increasing the gate voltage causes a similar redox reaction to occur in the $c-d$ cell. However, in order for c to reduce, it must draw electrons from region b as there is no conductive path beyond b. This effectively oxidizes b, opening the conductive channel between drain and source. In this way the channel can be switched on by changing the gate voltage.

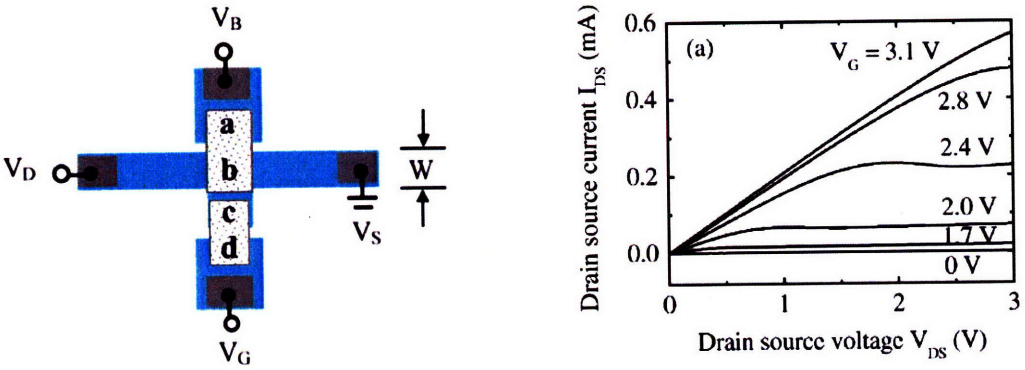

(a) ECT Design.

(b) Current - Voltage characteristic.

Figure 5-12: Chen's design for a fully contained electrochemical transistor uses two electrolyte gel bridges at $a - b$ and $c - d$ to create two separate electrochemical cells. Modifying the gate voltage switches the conductivity of the drain-source path on and off [105].

5.4.2 Component Testing

Transistor testing was completed using instrumentation similar to that for the diode component testing. Potentials were applied by two Agilent® E3631A triple-DC power supplies and the tests were controlled using Visual Basic software (shown in Appendix A). Tests were initially conducted with ECT submerged in TBAP/PC electrolyte, while later tests used aqueous solutions of NaDBS or NaCl.

These initial tests did not exhibit channel conductivity modulation. It was later discovered that the PEDOT leads were actuating (swelling and contracting) with potential changes at places where they were submerged in the electrolyte and not protected by the polystyrene barrier layer. When these leads passed out of the electrolyte into air, where the test sample was clamped to the test instrumentation, breaks would develop at the liquid free surface and destroy the sample (see Figure 5-13).

For example, one test conducted in the NaDBS electrolyte actually broke down mid-test, as shown in Figure 5-14. As the drain-source voltage was cycled from low to high for each successive increase in gate voltage, a lead clearly breaks near the end of the third gate voltage run and no further useful information is gained.

This testing difficulty was overcome by changing the electrolyte system to one containing a smaller anion (Cl^-) to minimize actuation changes and fully submerging

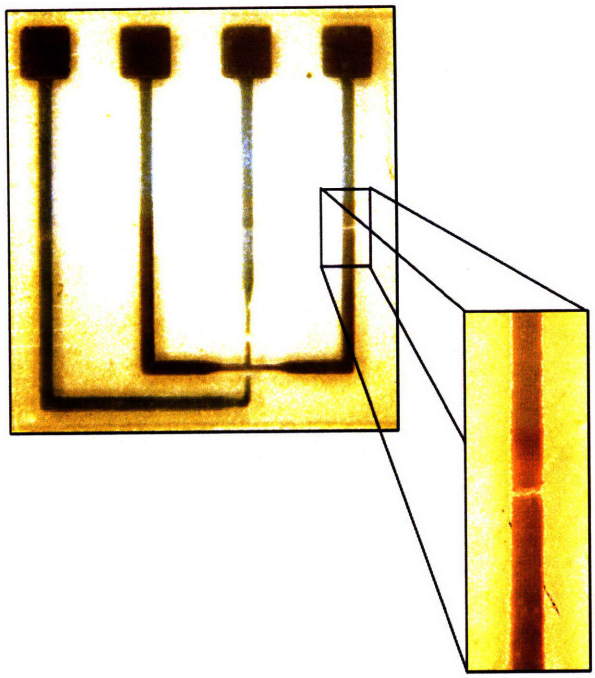

Figure 5-13: Poor ionic barrier layer deposition and the resulting differential actuation of the underlying PEDOT resulted in path breakage at the electrolyte free surface.

the test sample in the electrolyte to remove the free surface. This required permanently attaching lead wires to the sample and then sealing them to prevent parasitic electrochemical activity. This process was slower and more difficult than the previous clamping protocol.

Some successful tests were run in the NaDBS system, as shown in Figure 5-15, demonstrating that electrolyte systems suitable for actuation could be used for channel modulation in the ECT component as well. This result was the first demonstration of an electrochemical transistor fabricated using the oCVD method.

Based on these results, an empirical model of the drain-source channel resistance was derived for use in predicting the performance of integrated circuits containing these ECT's. For a constant drain-source voltage in the saturation region, the drain-source channel resistance R_{ds} is an exponential function of the gate-source voltage V_{gs}:

$$R_{ds} = \left(6 \times 10^{6}\right) e^{-2.3 V_{gs}}. \tag{5.1}$$

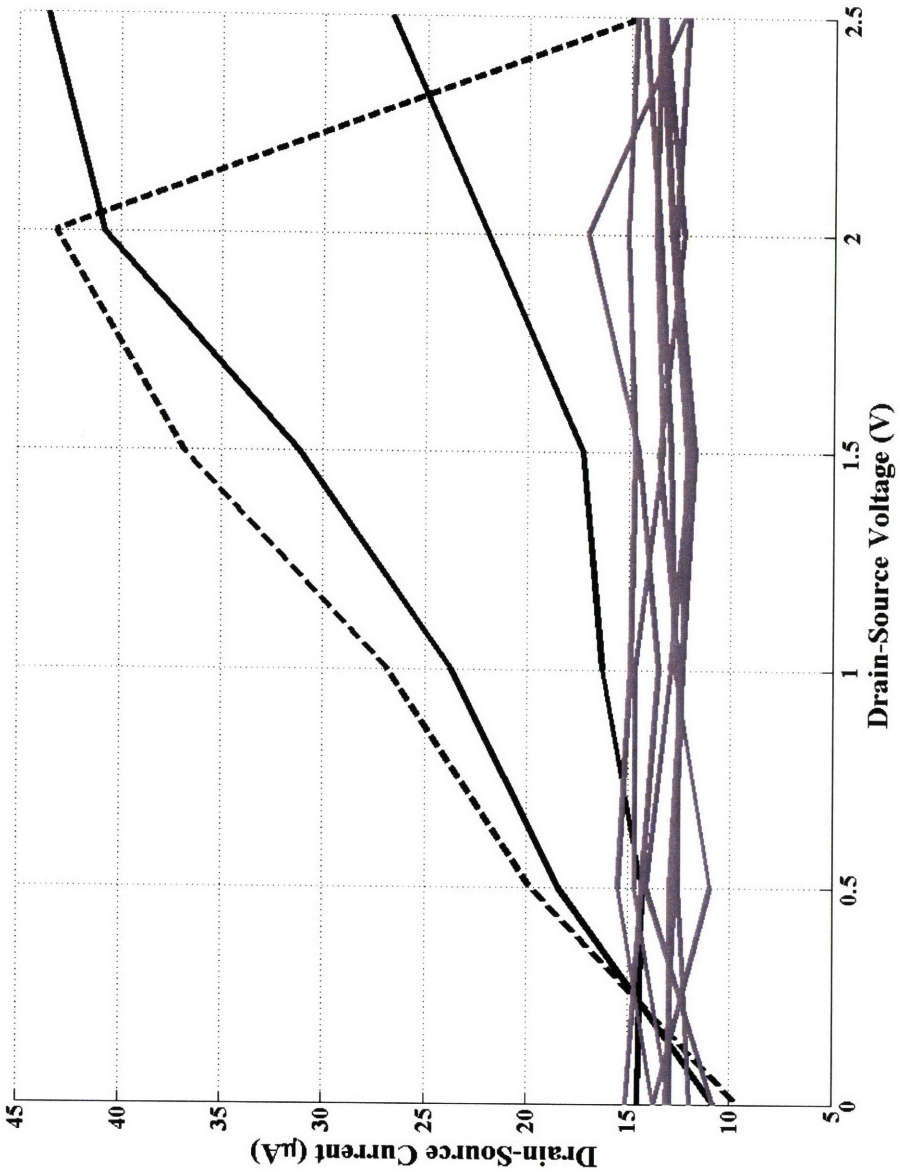

Figure 5-14: As a result of the breakage shown in Figure 5-13, many samples failed before modulation was apparent. The sample test result shown here demonstrates channel modulation (darker lines) until a lead breaks during the test of the third gate voltage value (dashed line). At this point no response is measured for any further gate voltage value (lighter lines).

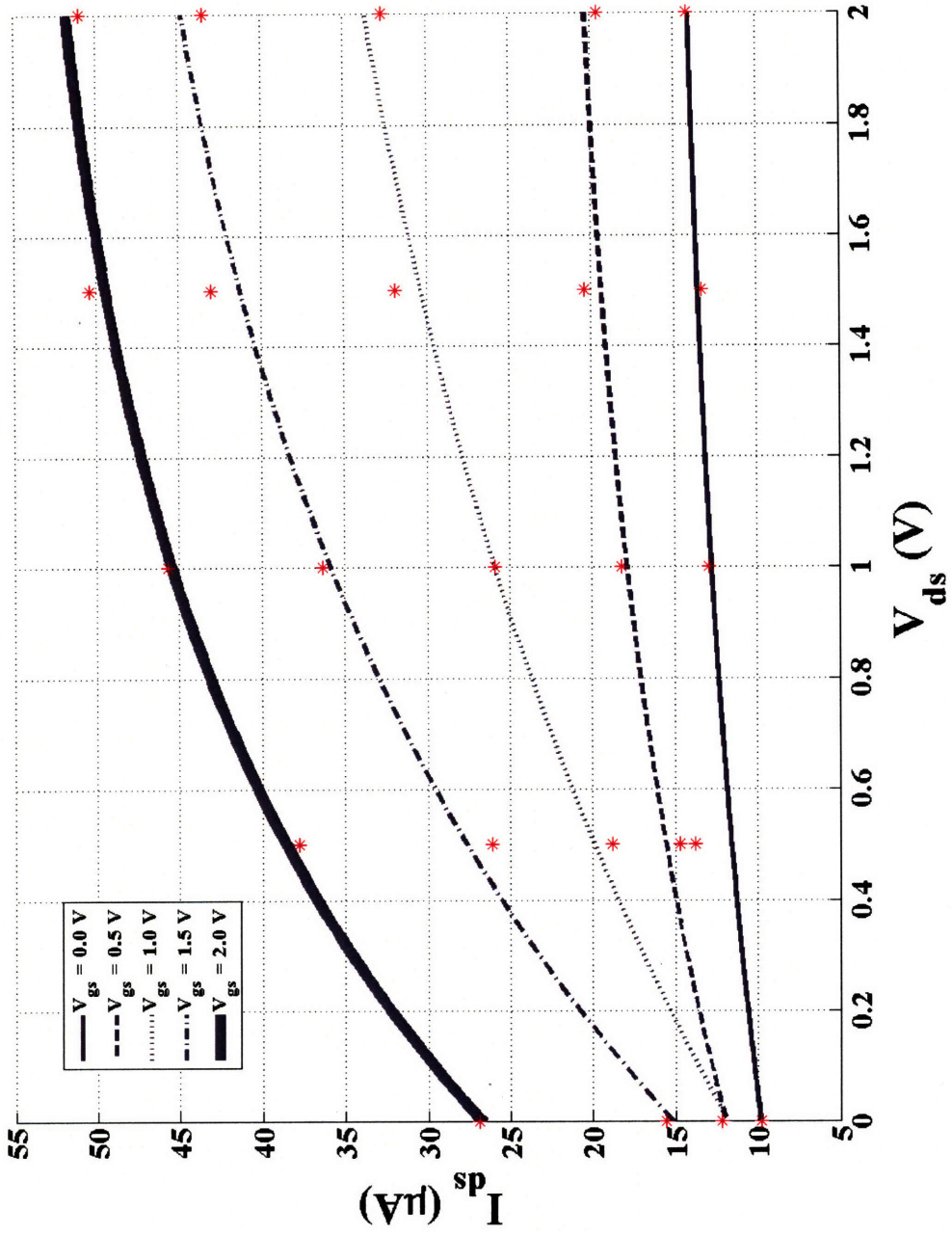

Figure 5-15: Once improvements were made to the barrier material deposition process, the electrolyte free surface was removed, and the solvent was changed, excellent drain-source channel conductivity modulation was achieved. This transistor behavior is empirically modeled using Equation 5.1.

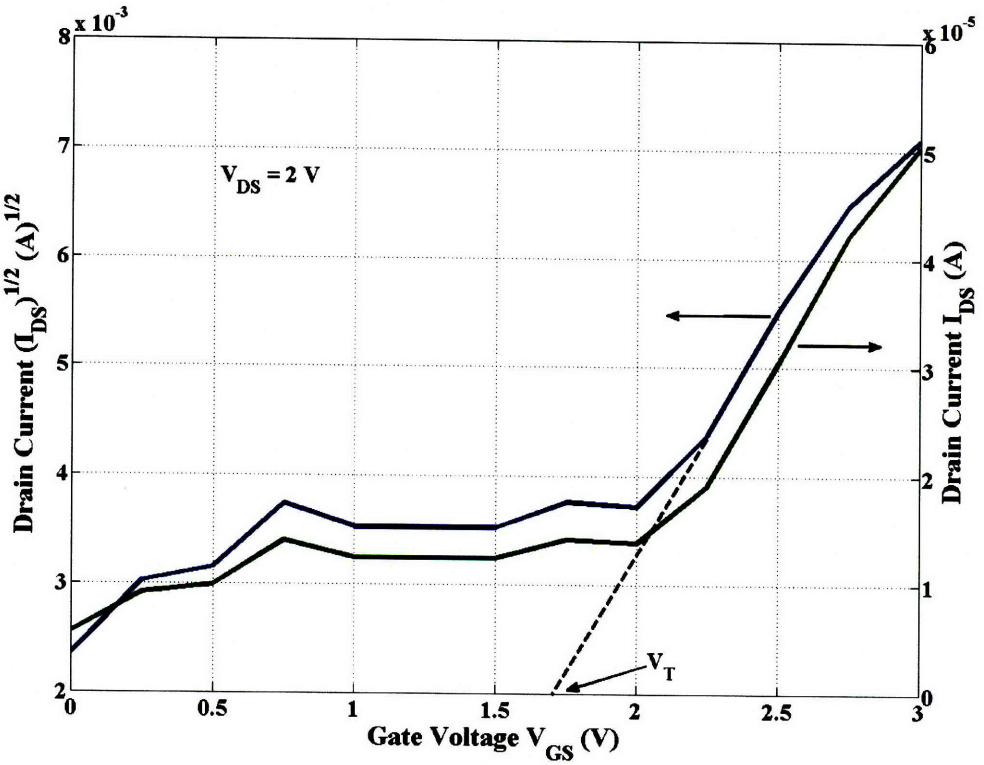

Figure 5-16: The transistor from Figure 5-15 showed a threshold voltage of 1.7 V and a transconductance of 0.046 mS.

The transconductance of a transistor is defined as

$$g_m = \left(\frac{\partial I_{DS}}{\partial V_{GS}}\right)_{V_{DS}}. \tag{5.2}$$

Transconductances of 1 mS were achieved with these components, though most were on the order of 0.1 mS. As shown in Figure 5-16, the ECT from Figure 5-15 has a transconductance of 0.046 mS and a threshold voltage of 1.7 V. These results are compared with other electrochemical transistors in Figure 5-17.

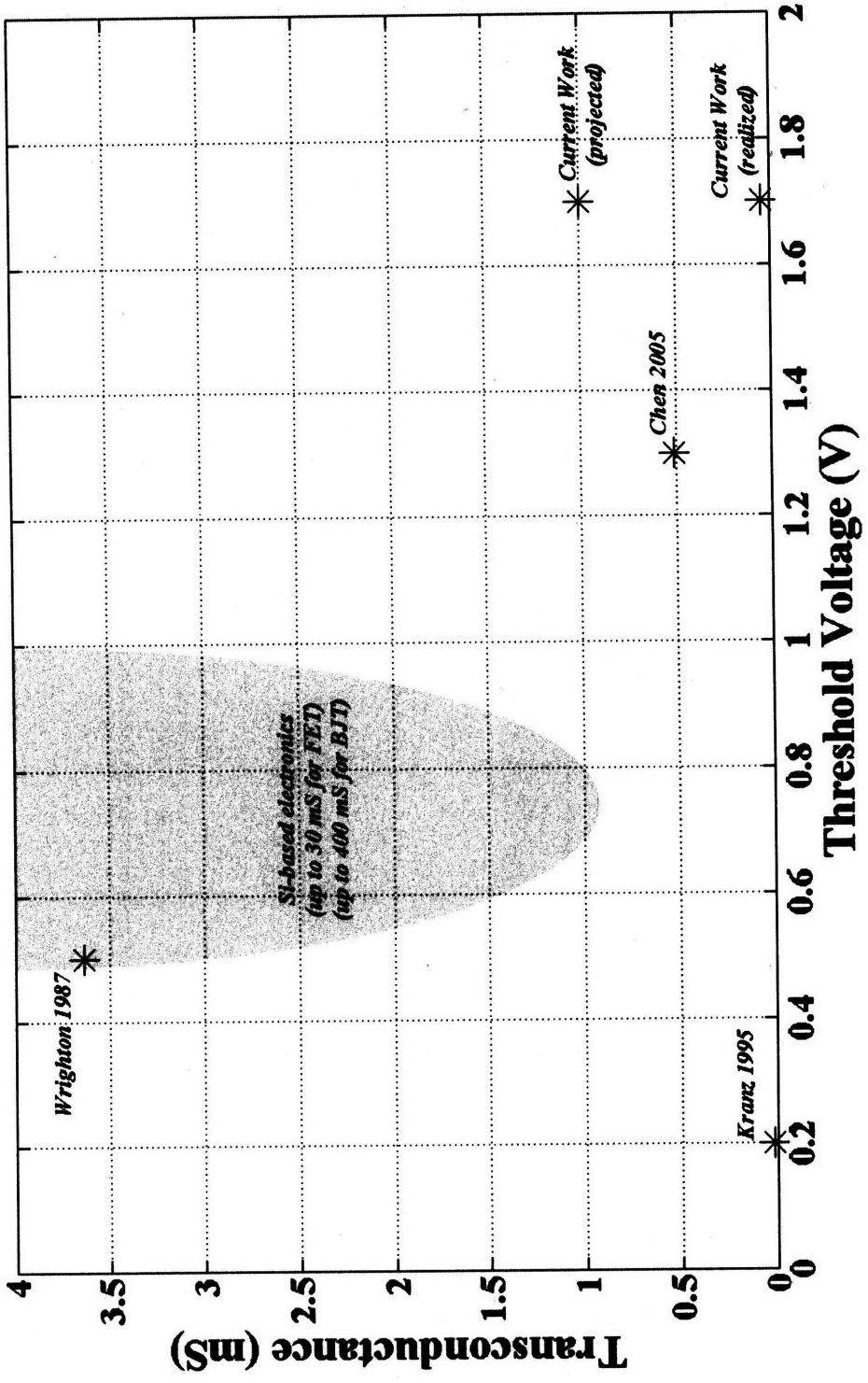

Figure 5-17: Several previous researchers' electrochemical transistors are shown (with silicon-based component values as a reference comparison). The current work can be feasibly extended to obtain transconductances of 1 mS.

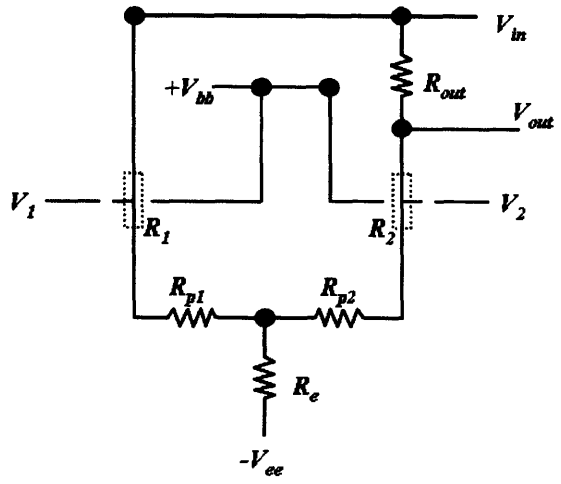

Figure 5-18: A differential amplifier can be implemented using electrochemical transistors as shown here. The bias voltage V_{bb} serves both as the high input voltage and the bias input for the ECT's.

5.5 Differential Amplifiers

5.5.1 Circuit Design

In order to effectively utilize an electrochemical differential amplifier (ECDA) in the programmable material (Figure 5-18), the theoretical behavior of the circuit must first be understood. By incorporating the empirical transistor model (Equation 5.1), the ECDA model can be derived.

As shown in Figure 5-18, calling the node between the paired resistors x gives

$$\frac{V_x - V_{ee}}{R_e} = \frac{V_{in} - V_x}{R_1 + R_{p1}} + \frac{V_{in} - V_x}{R_{out} + R_2 + R_{p2}}, \tag{5.3}$$

which when solved for V_x gives

$$V_x = a_1 V_{ee} + a_2 V_{in}, \tag{5.4}$$

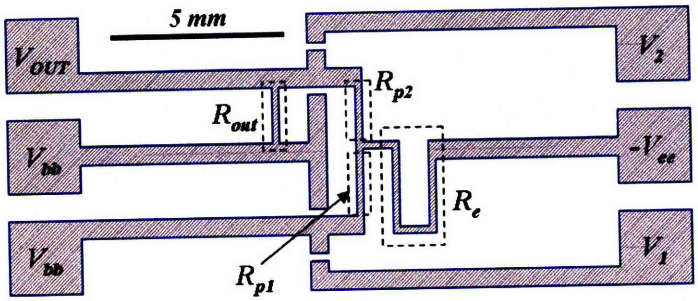

Figure 5-19: To implement an ECDA using the oCVD process, the pattern shown is used. Narrow regions implementing resistors are labeled. There are two V_{bb} inputs to allow ease of manufacture on the wire EDM.

where

$$\begin{aligned} a_1 &= \frac{(R_1 + R_{p1})(R_{out} + R_2 + R_{p2})}{a_d}, \\ a_2 &= \frac{R_e(R_{out} + R_1 + R_2 + R_{p1} + R_{p2})}{a_d}, \text{ and} \\ a_d &= R_e(R_1 + R_{p1}) + (R_e + R_1 + R_{p1})(R_{out} + R_2 + R_{p2}). \end{aligned} \tag{5.5}$$

This is then used to solve for V_{out}:

$$V_{out} = V_{in} - R_{out}\left(\frac{V_{in} - V_x}{R_{out} + R_2 + R_{p2}}\right). \tag{5.6}$$

Using these equations and the known values of internal resistances of the ECDA circuit, testable predictions can be made regarding the behavior of a fabricated ECDA.

Physical implementation of the ECDA using oCVD is shown in Figure 5-19. Narrow conductive regions were used to implement the needed resistors. Polystyrene barrier material was deposited on all areas other than the test access pads and the two ECT, so that they might be open to the electrolyte.

5.5.2 Circuit Testing

ECDA circuits were tested using an application written in Visual Basic code (shown in Appendix B). Early samples were wired for testing using conductive epoxy to

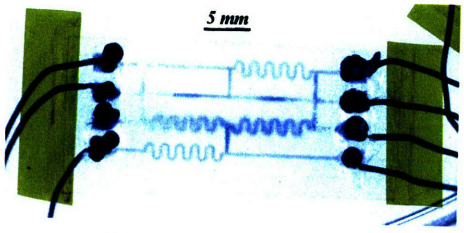

(a) Individually wired.

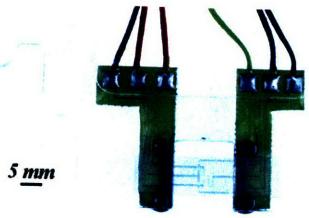

(b) Test clamps.

Figure 5-20: Early ECDA designs were tested using individual wires attached to the sample, as shown in (a). Later, more effective designs were tested in a custom-built clamping system as shown in (b).

Table 5.1: ECDA Internal Resistances.

R_e	1.04 MΩ
R_{out}	144 kΩ
R_{p1}	144 kΩ
R_{p2}	40 kΩ

make electrical contact and inert epoxy to seal the contacts and prevent unwanted electrochemical activity as shown in Figure 5-20(a). Later samples were tested using a custom-designed clamping system (see Figure 5-20(b)) which greatly sped up the testing cycle.

The given sample's internal resistors were measured (see Table 5.1). Using V_1 as the control input and holding it constant while varying V_2 (treated as the sensor output signal), tests were conducted of the circuit behavior. These results are shown in Figure 5-21 along with the theoretical predictions. The theoretical predictions differed by a constant DC value from the experimental results, and this has been removed.

As can be seen, the theoretical predictions match the experimental results. An attenuation of 4.7 dB of the difference between V_1 and V_2 is expected and seen. This is the first operational electrochemical differential amplifier fabricated using the oCVD process.

Improvement of the ECDA performance can be accomplished through several means. First, and easiest to implement, better control of the resistor values resulting

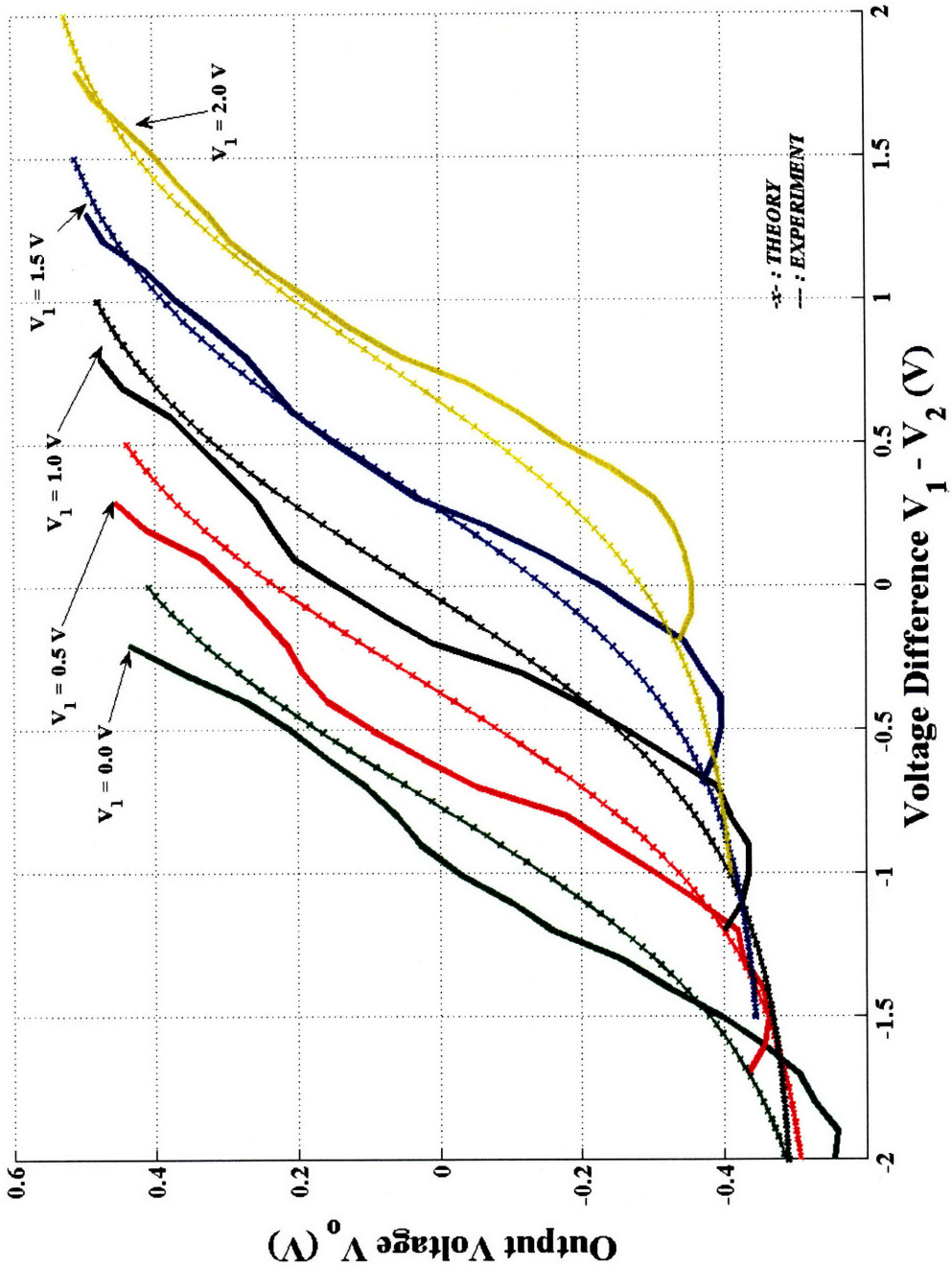

Figure 5-21: The experimental and theoretical ECDA performances are shown side by side. With a constant DC offset removed from the theoretical results, the experimental data matches well.

Table 5.2: ECDA Internal Resistances for Improved Amplification.

R_e	500 kΩ
R_{out}	1 MΩ
R_{p1}	100 kΩ
R_{p2}	100 kΩ

from deposition and patterning of the ECDA can result in significant increases in amplification. For example, a careful deposition resulting in resistor values shown in Table 5.2 (and an appropriate choice of voltages to ensure the operating point is at the origin) results in amplification of 7.5 dB. By increasing R_{out} to 10 MΩ and increasing the value of V_{in} to 12.6 V, the amplification can be increased further to 21 dB.

The second possibility for improvement of ECDA amplification is through improvement of the electrochemical transistors themselves. Increasing the value of the exponent, k, in the transistor relationship, $R_{ds} = R_t e^{-kV_{gs}}$, can improve the amplification more significantly than refinement of resistor values. Using the resistor values in Table 5.2, an increase of k from 2.3 to 5 increases the amplification from 7.5 dB to 14 dB. A further increase to 10 results in a gain of 18 dB. Combining this value of k with the improved settings above (V_{in} = 12.6 V and R_{out} = 10 MΩ) gives an amplification of 34 dB.

In order to achieve this improvement in k, the ECT deposition must be further refined. More precise control of the polystyrene ionic barrier layer will improve the electrochemical cells, better defining the areas of the PEDOT cell components exposed to the electrolyte. Reduction in the size of the cell gap width will increase the cell electrical field, speeding diffusion and increasing the response speed. This will of course require smaller mask features, which can be accomplished through reduction of the cutting wire size in the wire EDM.

These improvements in ECT performance are summarized in Table 5.3. Other ECT internal resistances remain constant as given in Table 5.2, V_1 has be set to zero to maintain the operating point, and $-V_{ee}$ has been set to -10 V. The actual voltage

Table 5.3: ECDA Parameter Sets for Improved Amplification.

Parameter Set	k	R_{out} (MΩ)	V_{in} (V)	Gain (dB)
1	2.3	1	1.4	7.5
2	5	1	1.4	14
3	10	1	1.4	18
4	2.3	10	12.6	21
5	5	10	12.6	28
6	10	10	12.6	34

output for these various parameter sets is shown in Figure 5-22.

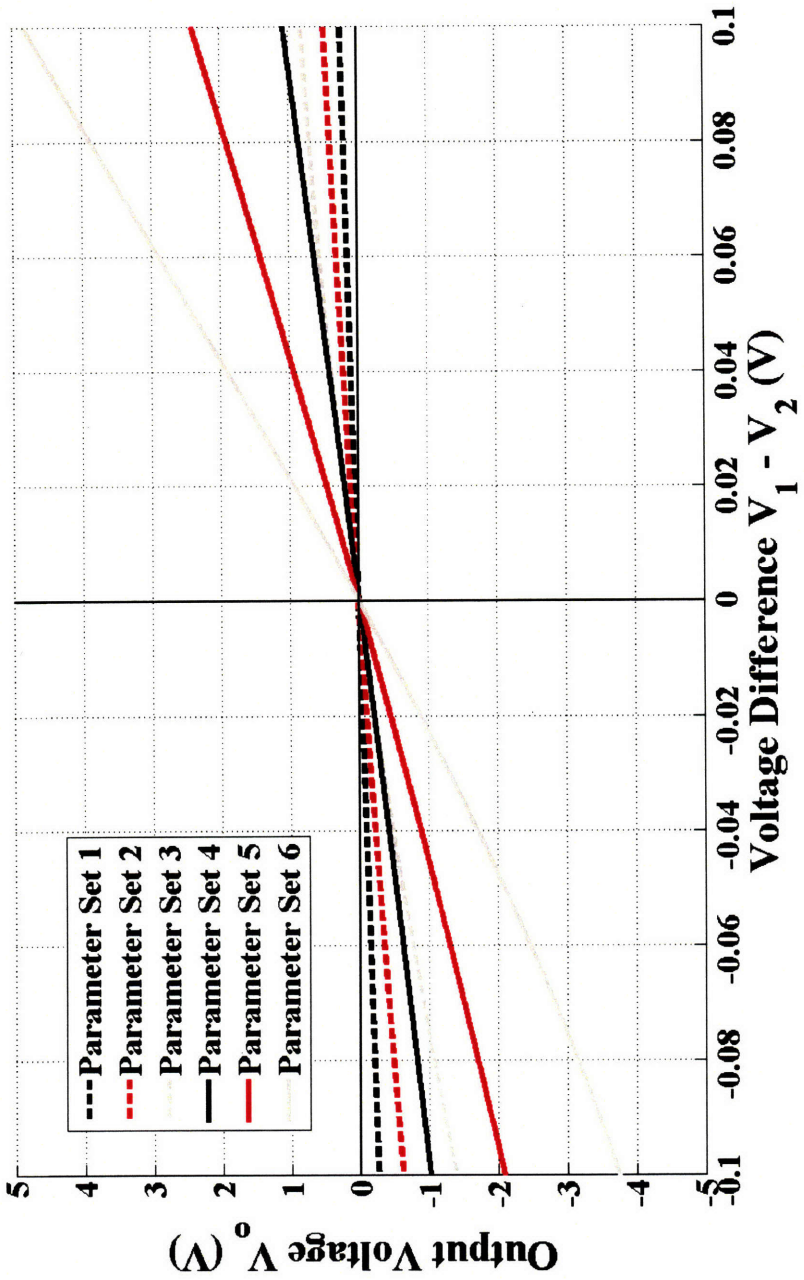

Figure 5-22: By modifying the transistor exponential response, the output resistor value, and the input supply voltage, much higher gains can be achieved with the electrochemical differential amplifier. Parameter sets in the legend match those in Table 5.3.

Chapter 6

System Integration

The key to creating a programmable material is the co-fabrication of all the pieces in one seamless, integrated device. In this chapter the design integration, experimental work, and mathematical system integration will be examined.

In the 30 years since the discovery of conducting polymers [17] and 25 years since the first organic transistor [89], few devices incorporating organic electronics have seen commercial success. This is due in large part to the manufacturing challenges and integration difficulties faced. As Stephen Forrest wrote in 2004,

> "... the ultimate test of this technology lies less in the reliability and performance of the organic components, which in some cases has already approached or even exceeded the requirements of a particular application, but rather in the ability to manufacture products at very low-cost. Although the cost of the organic materials used in most thin-film de-

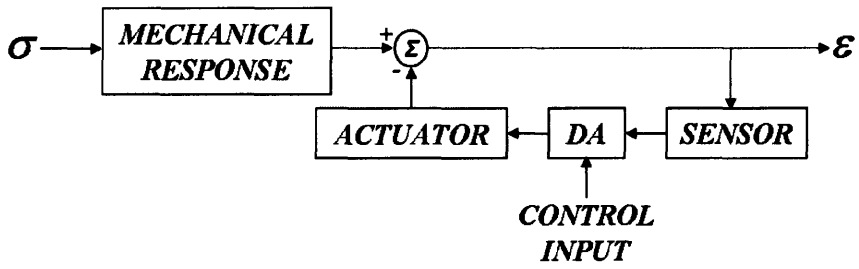

Figure 6-1: System block diagram.

vices is low, in electronics the materials cost rarely determines that of the end product, where fabrication and packaging costs typically dominate. Hence, the successful application of this interesting materials platform will depend on capturing its low-cost potential through the innovative fabrication of devices on inexpensive, large-area substrates." [76]

The fabrication of a programmable material in this work is an attempt to deal with some of these challenges by simplification of the manufacturing and integration processes.

6.1 Previous Work

Over the past decade, significant work has been done in the area of organic integrated devices [97, 106]. De Leeuw et al. created all-polymer logic circuitry based on PAN [82,84], including inverters, NAND gates, and ring oscillators. Crone et al. built shift registers based on polythiophene and pentacene [85].

Sirringhaus, et al. [93] used regio-regular poly(3-hexylthiophene) (rr-P3HT) to create organic light-emitting diodes (OLEDs), as shown in Figure 6-2. Other OLED work includes that by Rogers and Bao (paperlike displays based on OFET design [86]), and Forrest [76]. The OLED display shown in Figure 5-5 is the most successful application of an organic device, though it is of course not entirely organic in its components.

None of the previous research examined the possibility of creating an integrated controlled organic actuation device. This research is the first to attempt to bring together the actuation, sensing, and electronics capabilities of conducting and non-conducting polymers. Additionally, no previous research has explicitly examined the questions of co-fabrication that arise from this study of programmable materials.

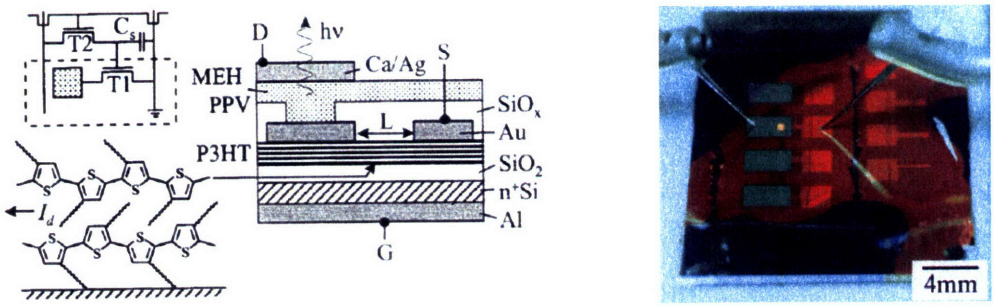

(a) (b)

Figure 6-2: Sirringhaus et al. [93] were able to fabricate an organic light emitting diode using some conducting polymer components. This design utilizes a FET with rr-P3HT as the semiconductor material. Note the many components not fabricated with polymeric materials.

6.2 Device Design

Creating the programmable material as an integrated device required the ability to deposit multiple functional layers in a mechanically an electronically robust fashion. As alluded to in Chapter 2, the first iteration of the device will be a linear configuration (see Figure 6-3). Later work should include the construction of a trilayer device to amplify the actuator strain through bending tip displacement.

The starting point for co-fabrication of this device is a free-standing polypyrrole film. This film will serve as the actuator layer shown in Figure 6-3. This film is first coated with a barrier layer of polystyrene, which serves to electronically and ionically isolate the actuator from the sensor. Patterning of this layer is necessary to allow electrical communication between the actuator and the control electronics on the far side of the sensor. The only direct energetic coupling between the sensor and actuator is mechanical, as shown in the bond graph in Figure 6-4.

In order to deposit the sensor layer electrochemically, a conductive surface must be emplaced to serve as the working electrode. This is done through oCVD of PEDOT on top of the polystyrene insulator layer. Both the polystyrene and PEDOT layers are approximately 200 nm thick. Once a sensor layer (approximately 25 μm thick) is deposited, another insulating layer of polystyrene is deposited to isolate the sensor from the electronics. This is again patterned to allow electrical contact between the

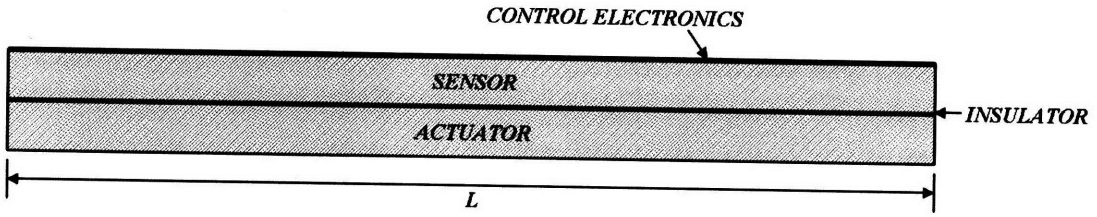

Figure 6-3: This is a side view along the length of a proposed design of a programmable material. Gray regions represent polypyrrole layers, while layers deposited using oCVD and plasma polymerization are labeled. Fabrication begins with the actuator layer, building upwards by depositing insulator, sensor, and electronics.

sensor and electronics.

The control electronics layer is the outermost layer of the programmable material. Consisting of up to two layers of PEDOT and two layers of polystyrene, the entire layer is less than 1 μm thick. As previously mentioned, electrical connectivity must be maintained between the control electronics and the sensor (to receive and utilize the position sense signal) and actuator (to provide a driving input) layers.

As mentioned in previously in Chapter 2, to produce a programmable material to serve as a position-controlled feedback device with usable deformations, a trilayer geometry is envisioned. A linear programmable material fabricated using the process discussed above will be used for one of the actuators in the trilayer, with a gel electrolyte separating it from a second actuator layer comprised of a single layer of polypyrrole. Initially, the difficulty of making electrical contact with the opposing actuator layer may lead to using a stiff, non-polymer conducting material such as platinum or gold in place of the far actuator to form a bilayer device. This would simplify early design and allow refinement prior to creation of a full trilayer device.

6.3 Co-fabrication

An important part of the fabrication process is the deposition of the polystyrene barrier layers. These had to be shown first to be sufficiently ionically and electronically insulative to prevent system shortouts. To test this, samples were made with PEDOT on a substrate of polyethylene terephthalate (PET). One sample was left with bare

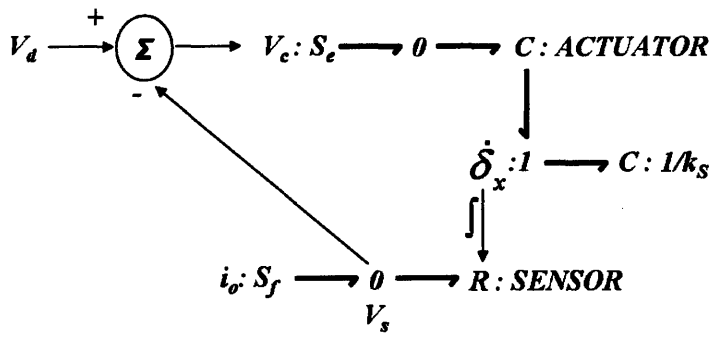

Figure 6-4: The system bond graph shows the energy flow between components. The system desired position is an input, V_d. The differential amplifier provides a control input V_c, to the actuator. The system deformation is mechanically transmitted from the actuator to the sensor, which then returns a position feedback V_s via resistance modulation.

PEDOT, while another was then coated with polystyrene.

These samples were then tested via cyclic voltammetry (CV) in an aqueous solution of NaDBS to examine the ionic activity of the depositions. As can be seen from Figure 6-5 the sample coated with polystyrene showed significantly less activity than the bare PEDOT, exhibiting lower current densities and preventing the redox reaction at $\pm 0.25\ V$.

To examine the ability to deposit polypyrrole electrochemically using vapor deposited PEDOT as a working electrode, samples were fabricated with PEDOT deposited via oCVD onto PET and polypyrrole (see Figure 6-7(a)). To determine the appropriate voltage for the ECD, CV tests were conducted with and without pyrrole monomer in solution. As shown in Figure 6-6, an oxidation peak is clearly visible at $3\ V$ when the monomer is present in solution.

ECD was carried out under the TBAP/PC conditions described in Chapter 2 (modified to be potentiostatic at the desired deposition voltage) and polypyrrole was successfully deposited (see Figures 6-7(b) and 6-7(c)). Unfortunately, the propylene carbonate-based electrolyte damaged the polystyrene layer, causing separation of the polypyrrole substrate and the newly deposited polypyrrole layer.

This was remedied in a later co-fabrication test using an aqueous solution, as shown in Figure 6-8. Even though the deposition had to take place at a higher

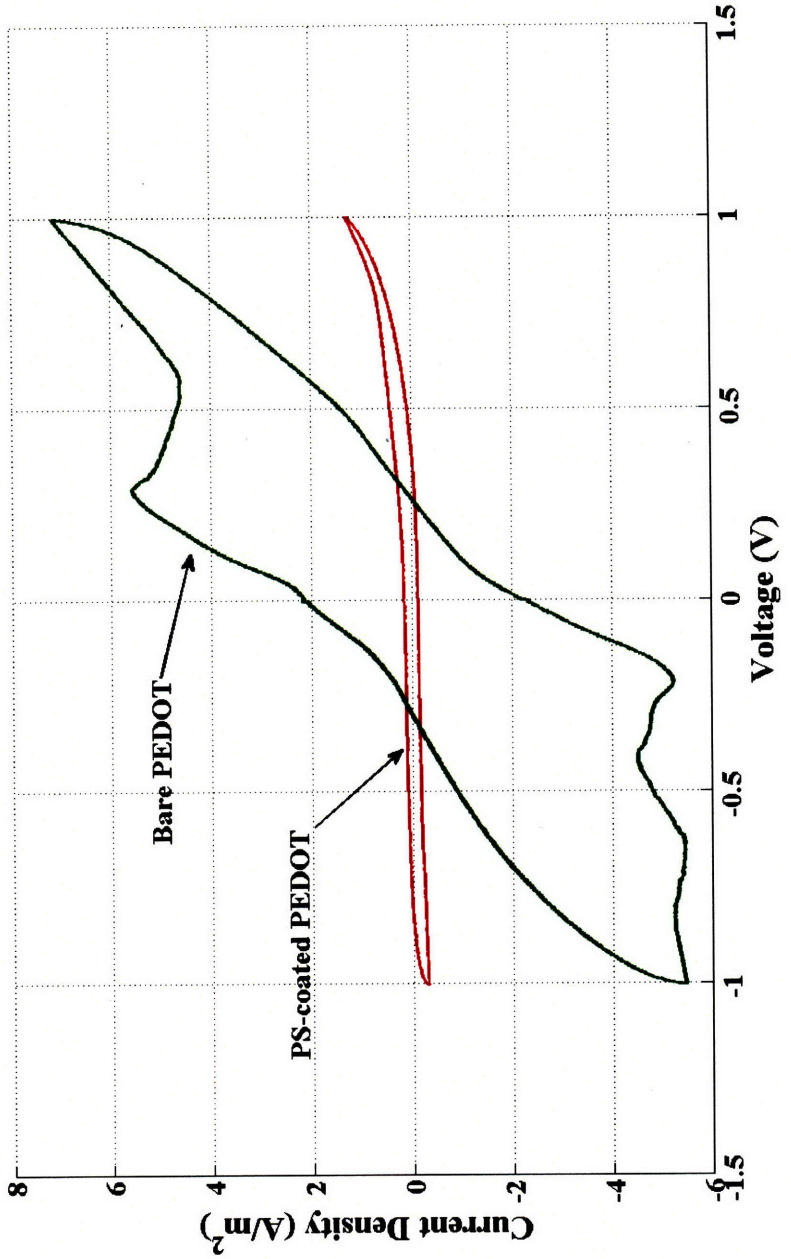

Figure 6-5: By comparing the system response to cyclic voltammetry testing, the effectiveness of the polystyrene ionic barrier is demonstrated. The large curve shows the much higher current density (indicating significant electrochemical activity) of the bare PEDOT film when compared to the polystyrene-coated PEDOT.

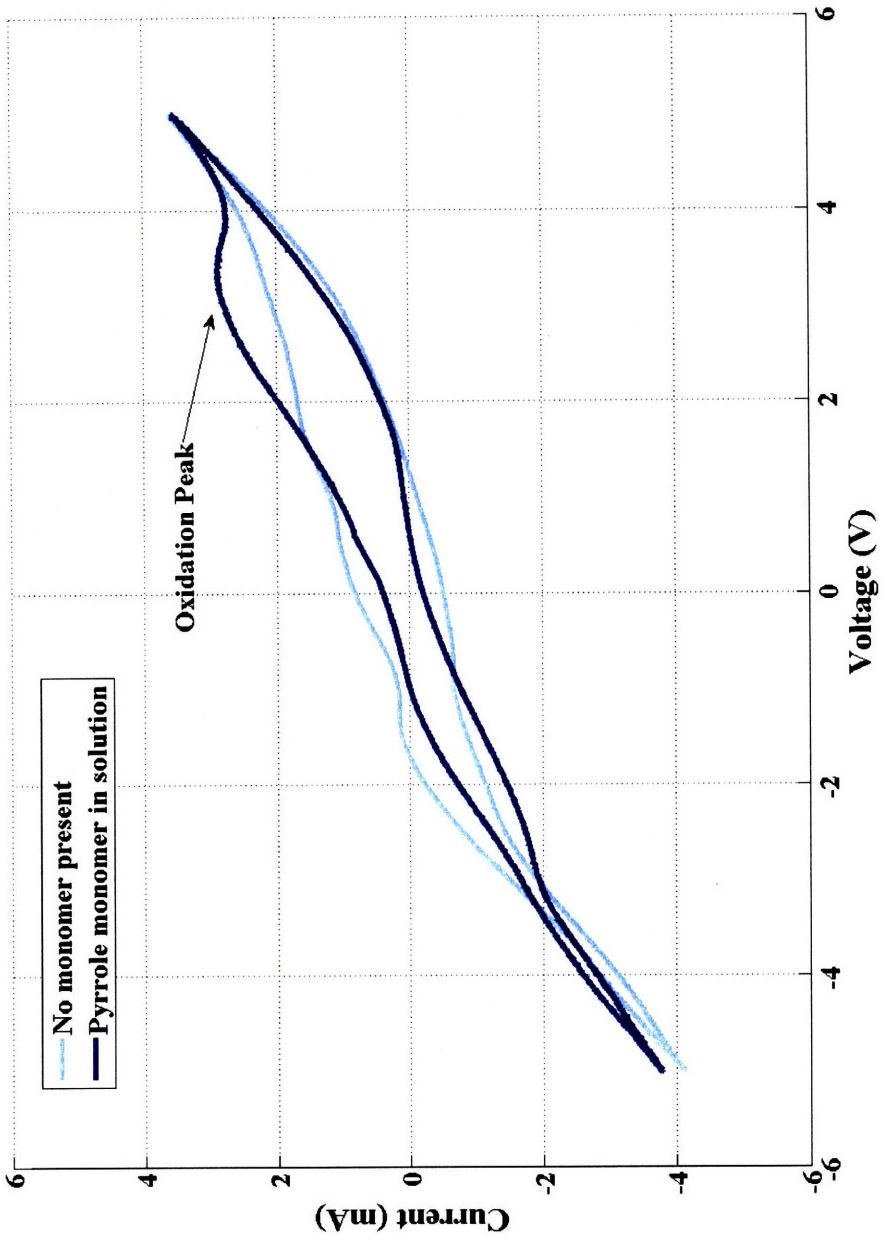

Figure 6-6: Cyclic voltammetry of the PEDOT target in an electrolyte solution containing pyrrole monomer shows an oxidation deposition peak at 3 V that is not apparent in the absense of monomer.

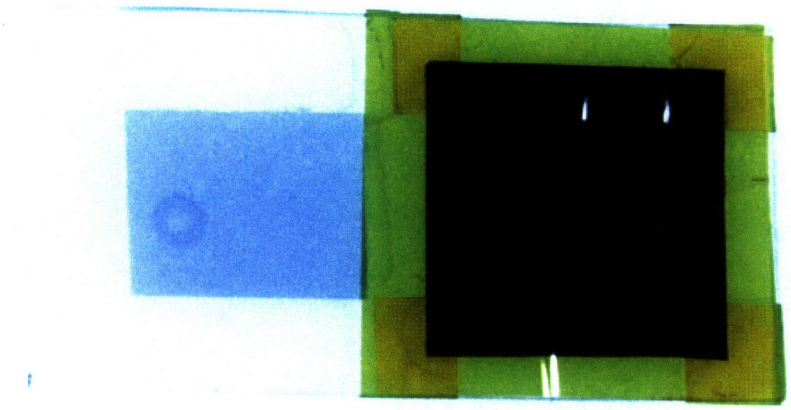

(a)

(b)

(c)

Figure 6-7: Polypyrrole was successfully deposited on a PEDOT target (b) and polypyrrole-polystyrene-PEDOT target (c). Unfortunately, the propylene carbonate electrolyte damaged the polystyrene ionic barrier layer, causing separation of the polypyrrole layers in (c).

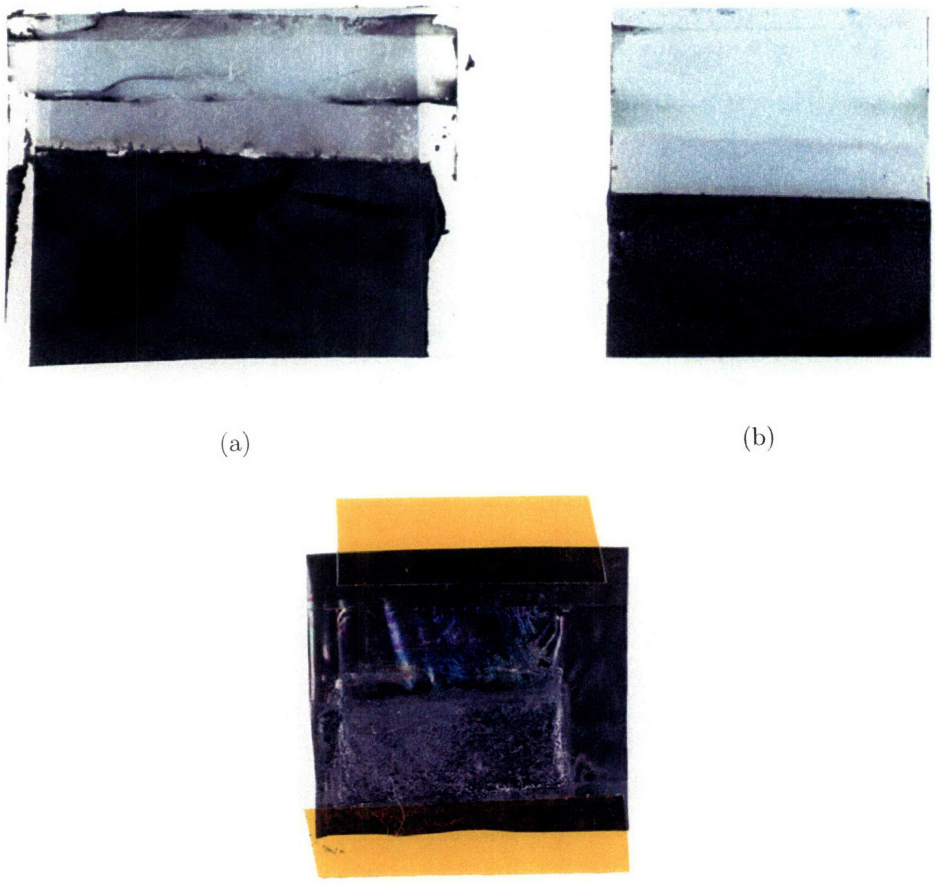

Figure 6-8: Polypyrrole deposited on PEDOT (a), polystyrene-PEDOT (b), and polypyrrole-polystyrene-PEDOT (c). By changing the electrolyte solvent from propylene carbonate to water, layer separation was avoided. This was also a significant improvement in the biocompatibility of the device (see Chapter 7).

temperature (4°C rather than the -40°C used with PC electrolyte), the deposition was successful enough for further work.

6.4 System Model

Having demonstrated that the fabrication methodology for constructing the programmable material is feasible, it is now necessary to synthesize the previous mathematical component models into an overall system theoretical construct. This model

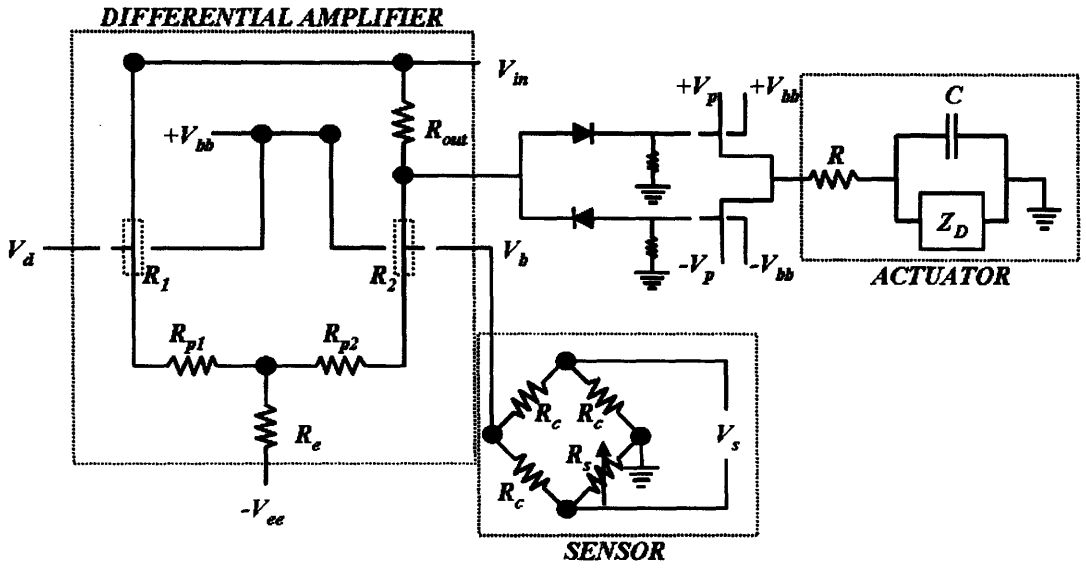

Figure 6-9: In this lumped parameter model, the actuator has been modeled as a resistance (representing the electrolyte/contact resistance) in series with a capacitor (representing the double layer capacitance) in parallel with the diffusion impedance [15]. The electrochemical differential amplifier is shown to the left, and the Wheatstone bridge containing the sensor variable resistor is shown to the lower right. A pair of transistors is used between the amplifier and the actuator to provide the necessary driving current.

will incorporate the experimentally verified representations of the actuator, sensor, and control electronics.

The integrated system can be represented as a lumped parameter model as shown in Figure 6-9. The actuator consists of a resistance in series with a capacitance and diffusion impedance in parallel [15]. The sensor resistor is shown as one leg of a Wheatstone bridge configuration. The electrochemical transistors are embedded within the differential amplifier, which receives the desired input signal, V_d, and the sensor output, V_b, and outputs a control voltage. This output voltage directs the flow of current from a bipolar source through two transistors, which provides the current to drive the actuator.

To review, the mechanical response of the device (which consists primarily of polypyrrole) is modeled by

$$\epsilon(t) = C_1 e^{-\tau_1 t} + C_2 e^{-\tau_2 t} + C_3, \tag{6.1}$$

where

$$
\begin{aligned}
C_1 &= \frac{E_c\left(E_b\eta_f - E_c\eta_d\right)}{\eta_d\eta_f\left(E_a + E_b\right)}, \\
C_2 &= \left[\frac{1}{E_a + E_b + E_c} - \frac{E_b}{\eta_d\left(E_a + E_b\right)}\right]\sigma_o + \left[\frac{E_c\left(E_b\eta_f - E_c\eta_d\right)}{\eta_d\eta_f\left(E_a + E_b\right)}\right]\epsilon_o, \\
C_3 &= \left(\frac{E_b}{\eta_d\left(E_a + E_b\right)}\right)\sigma_o, \\
\tau_1 &= \frac{E_c}{\eta_f}, \text{ and} \\
\tau_2 &= \frac{E_a E_b}{\eta_d\left(E_a + E_b\right)}.
\end{aligned}
\tag{6.2}
$$

The actuator is represented using Madden's diffusive elastic metal (DEM) model (see Chapter 2 for a more detailed discussion):

$$
Y(s)\cdot R = s\cdot\frac{\frac{1}{\sqrt{\tau_C}}\cdot tanh\left(\sqrt{s\tau_D}\right) + \sqrt{s}}{\frac{\sqrt{s}}{\tau_{RC}} + s^{3/2} + \frac{1}{\tau_C}\cdot s\cdot tanh\left(\sqrt{s\tau_D}\right)},
\tag{6.3}
$$

where

$$
\begin{aligned}
\tau_D &= \frac{a^2}{4D}, \\
\tau_{RC} &= RC, \text{ and} \\
\tau_C &= \frac{\delta^2}{D}.
\end{aligned}
\tag{6.4}
$$

For the purposes of this simulation, a pole-zero-gain approximation is used to represent the DEM transfer function (shown in Equation 6.5). This approximation was derived by matching the frequency response of the DEM model over a useful range of frequencies (10^{-2} to 10^3 Hz) for the actuator parameter values given in Table 6.1. Of course, the precise value of the transfer function is dependent upon the parameters of the actuator used.

$$
Y(s) = \frac{0.028\left(s + 1\times 10^{-5}\right)\left(s + 1.3\right)\left(s + 22\right)}{\left(s + 0.2\right)\left(s + 2.5\right)\left(s + 30\right)}
\tag{6.5}
$$

Table 6.1: Actuator Parameters.

Symbol	Represents	Value
L	Actuator length	50 mm
W	Actuator width	3 mm
T	Actuator thickness	25 μm
α	Strain-to-charge ratio	500×10^{-12} $\frac{m^3}{C}$
D	Ion diffusion coefficient in polypyrrole	10^{-11} $\frac{m^2}{s}$
R	Actuator internal resistance	25 Ω
C	Actuator internal capacitance	0.25 $\frac{F}{m^2}$
δ	Capacitive double layer thickness	2 nm

This is an impedance relationship which, when integrated, gives the charge injected into the actuator based on the voltage applied.

Once the charge is known, the overall strain resulting from actuation under loaded conditions is

$$\epsilon = \frac{\alpha q}{LWT} + \frac{\sigma}{E}, \tag{6.6}$$

where L, W, and T are the length, width, and thickness of the polymer, respectively, σ is the applied stress, and E is the polymer Young's modulus. This equation is used to represent the actuator performance under uniaxial stress conditions.

Knowing the actuator strain then gives the strain experienced by the sensor layer. The change in resistance resulting from this strain (see Chapter 3 for greater detail) is given by

$$R_s = R_c \frac{1+\epsilon_x}{(1-\nu\epsilon_x)^2}. \tag{6.7}$$

To utilize this sensor output, the variable resistor of the sensor forms one leg of a Wheatstone bridge. Assuming the resistors in the remaining three legs have constant and equal values (R_c), the voltage output from the sensor is

$$V_b = \left(\frac{R_s}{R_s + R_c} - \frac{1}{2}\right) V_s, \tag{6.8}$$

where V_s is the bridge input voltage and V_b is the bridge output voltage.

The control electronics consist of an electrochemical differential amplifier. The

performance of this circuit (see Chapter 5 for greater detail) is given by

$$V_{out} = V_{in} - R_{out}\left(\frac{V_{in} - V_x}{R_{out} + R_2 + R_{p2}}\right). \tag{6.9}$$

where

$$V_x = a_1 V_{ee} + a_2 V_{in}, \tag{6.10}$$

and

$$\begin{aligned} a_1 &= \frac{(R_1 + R_{p1})(R_{out} + R_2 + R_{p2})}{a_d}, \\ a_2 &= \frac{R_e(R_{out} + R_1 + R_2 + R_{p1} + R_{p2})}{a_d}, \text{ and} \\ a_d &= R_e(R_1 + R_{p1}) + (R_e + R_1 + R_{p1})(R_{out} + R_2 + R_{p2}). \end{aligned} \tag{6.11}$$

These component equations were synthesized into a single system model using the MATLAB® code shown in Appendix C. Table 6.2 lists the component values used for the device system simulation. The transistor characteristics are what has been currrently achieved, while the resistor values given are for easily achievable values. All simulation results use these component values unless otherwise stated.

The overall system response time is limited primarily by the actuator. The 19 second settling time of the actuator is lengthened slightly by the electrochemical activation times of the transistors, but the actuator response is still by far the slowest component of the system response.

Using the values given in Table 6.2, a 1 MPa step stress input results in a mechanical strain response (ϵ_m) of 1.61% before creep effects set in. This mechanical response is what the programmable material would experience in the absense of any feedback behavior. The charge-driven strain (ϵ_q) reaches 0.26% after the actuator settling time. This gives a resultant strain (ϵ_r) of approximately 1.35% (see Figure 6-10). This resultant strain causes the apparent stiffness of the programmable material to increase over the unactuated stiffness of the polypyrrole layers comprising the bulk of the device. The ratio of the apparent stiffness to the unactuated stiffess,

Table 6.2: System Component Values for Simulation.

Symbol	Represents	Value
V_d	System operating point voltage	0 V
V_{in}	System input voltage	1.39 V
V_s	Sensor bridge input voltage	20 V
R_c	Sensor bridge constant resistors	100 Ω
R_i	Sensor resistor initial value	100 Ω
R_e	ECDA long tail resistor	500 $k\Omega$
R_{out}	ECDA output resistor	1 $M\Omega$
R_{p1}	ECDA pair resistor 1	100 $k\Omega$
R_{p2}	ECDA pair resistor 2	100 $k\Omega$
L	Device length	50 mm
W	Device width	3 mm
T	Sensor thickness	25 μm
E	Actuator and Sensor modulus	800 MPa
k	ECT on/off exponent	2.3 V
R_t	ECT rest resistance	6 $M\Omega$

termed K_E, is 1.18 in this case (as shown in Figure 6-10 inset).

In Chapter 5, projections were made for improvements to the performance of the ECDA. By implementing the parameter values that provide the best ECDA performance, the apparent stiffness of the programmable material can be increased by a factor greater than 7. As shown in Figure 6-11, the mechanical response does not change for the given 1 MPa stress step input, but the improved ECDA performance significantly increases the charge-driven strain response.

Finally, it is important to note that the apparent stiffness change is dependent primarily upon the parameters of the programmable material rather than the mechanical input. As shown in Figure 6-12, progressively increasing the stress input by 1 MPa steps only slightly changes the apparent stiffness (allowing for system settling time following each step). The original system parameters shown in Table 6.2 are used.

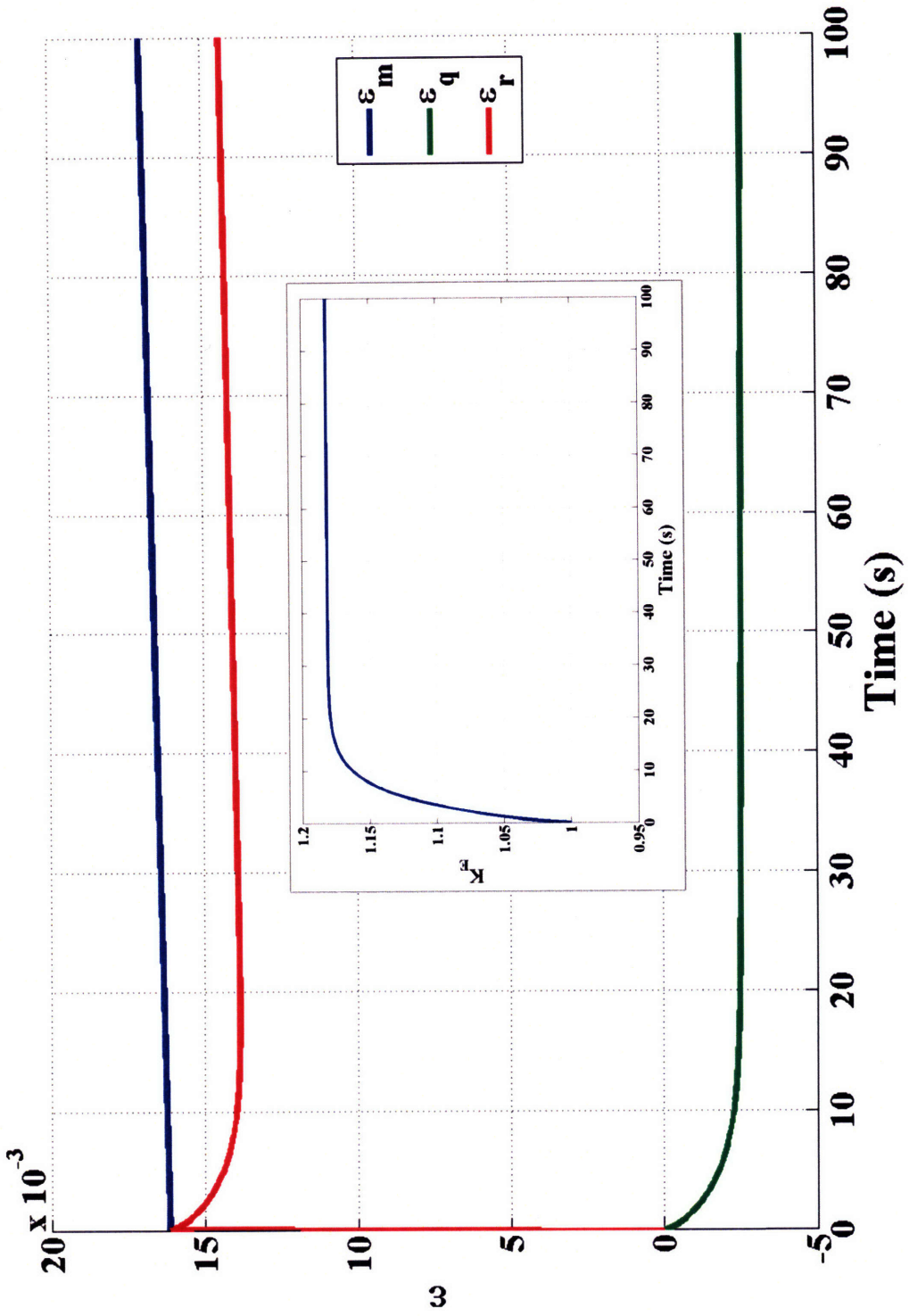

Figure 6-10: This plot shows the system response for a 1 MPa stress step input. The mechanical strain, ϵ_m, is offset by the charge-driven strain, ϵ_q, to give a resultant strain of ϵ_r. For the system parameters given in Table 6.2, the programmable material increases the apparent stiffness by 18% (inset).

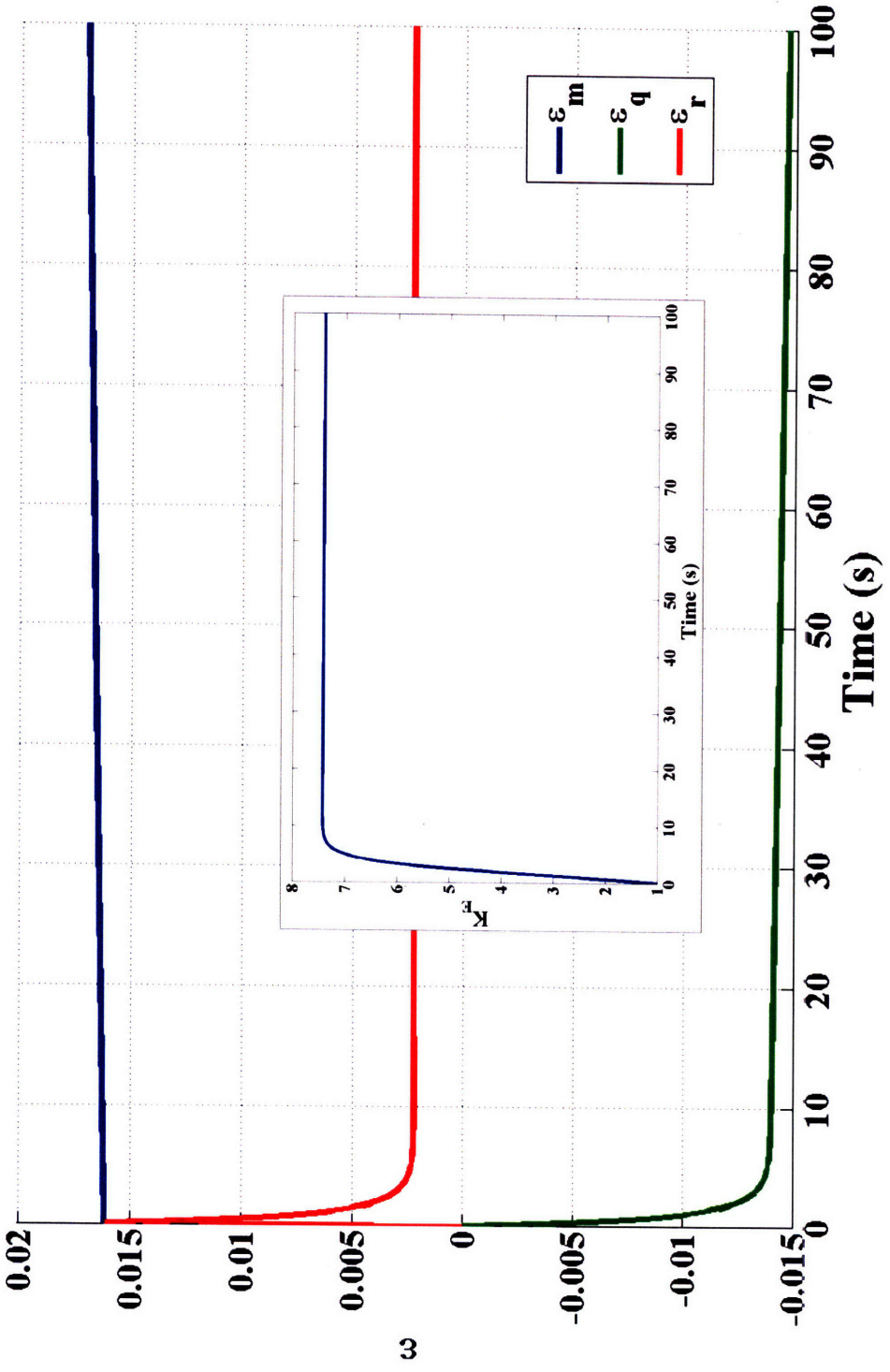

Figure 6-11: Using the projected best-case parameters for the programmable material ECDA, an increase in apparent stiffness of a factor greater than 7 is achievable (inset).

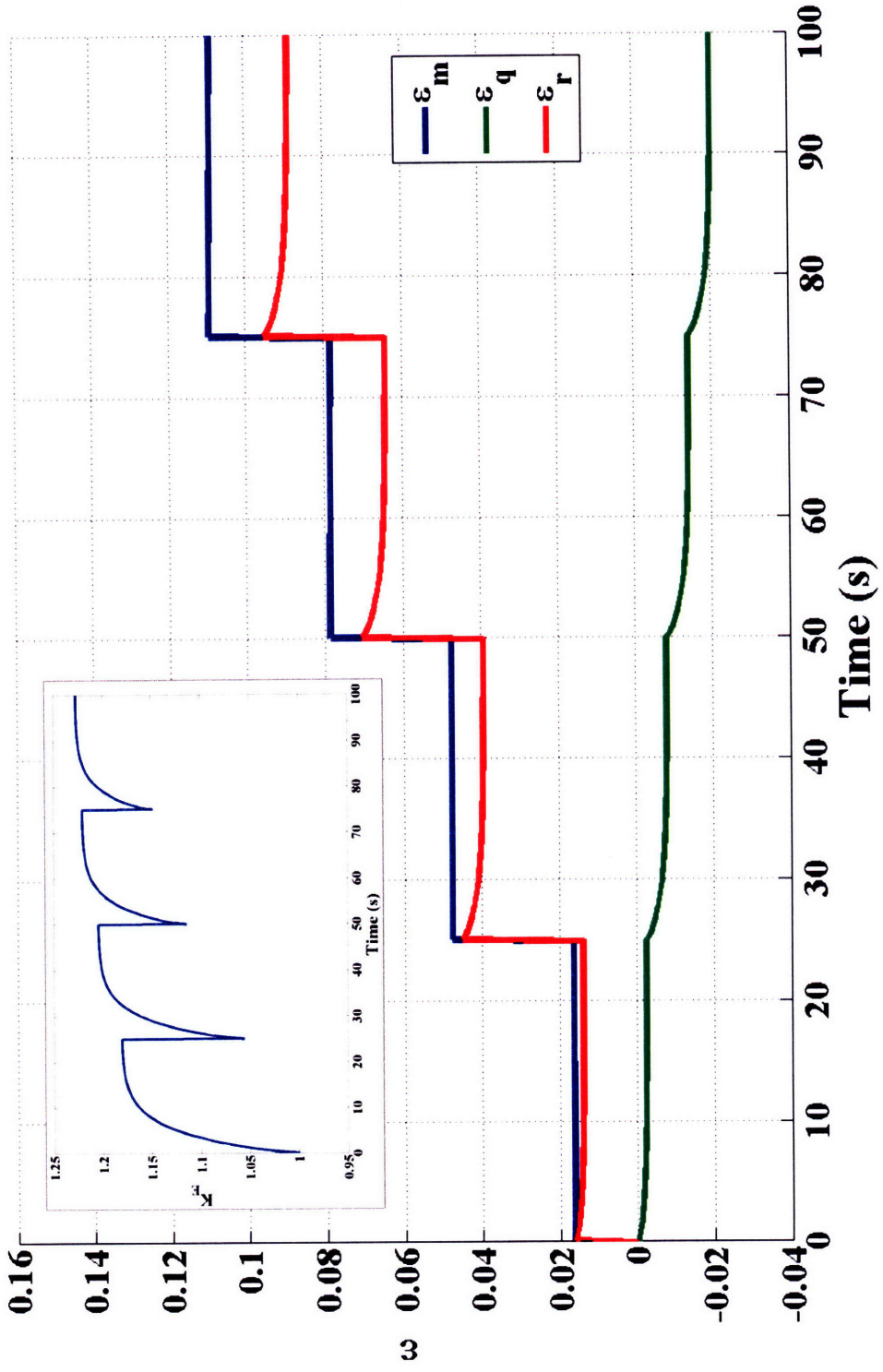

Figure 6-12: As shown in the inset, the programmable material's apparent stiffness increases only slightly when the mechanical input magnitude is increased by a factor of four. The margin of increase drops as the input magnitude rises.

Chapter 7

Biostability

The biological realm is a field which has received significant attention for conducting polymer applications [36,107,108]. The potential to create sensors, probes, actuators, and electronics from conducting polymers requires an understanding of the interaction between these polymers and the biological environment. This work utilizes polypyrrole due to the significant work done both within the MIT BioInstrumentation Lab and in the literature using this polymer.

This portion of the current research is focused on finding the optimal deposition conditions for creating biologically compatible polypyrrole that will retain actuation functionality and conductivity after significant periods of time in a biological environment. Once potentially biostable samples have been fabricated, they are then tested in instrumentation custom built for this work.

7.1 Previous Work

Many researchers have examined the prospects for using polypyrrole-based devices as biological sensors, actuators and drug delivery mechanisms. This requires understanding the biocompatibility of polypyrrole (defined as the ability of the biological system to function in the presence of the polymer) as well as the biostability of polypyrrole (defined the ability of polypyrrole to retain its relevant material properties while exposed to a biological environment).

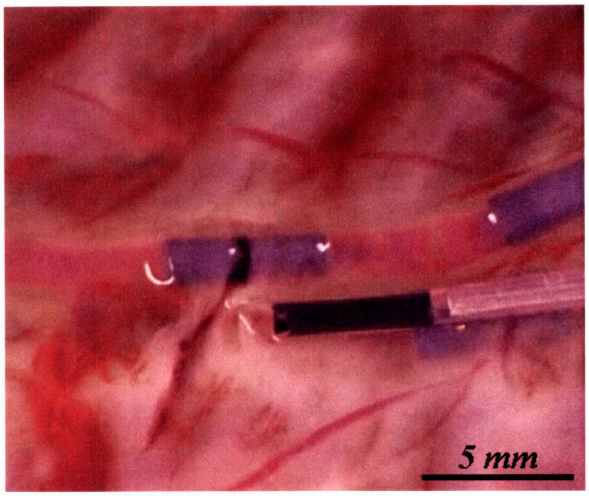

Figure 7-1: Immerstrand et al. used a polypyrrole bilayer actuator to repair a severed blood vessel. The bilayer is reduced (and thus contracted) prior to insertion. After placement, the polypyrrole returns to its oxidized state and the bilayer expands to hold the blood vessel together. A second insert is shown for comparison. From [107].

In order to use polypyrrole (and other conducting polymers) in biological environments, they must first be fabricated in biologically friendly ways. Since polypyrrole incorporates anions and solvent from the electrolyte solution during deposition, those ions and that solvent must not be harmful to the subsequent biological environment. While solvent choices are limited (nearly all work has been done in aqueous solutions, as biological systems are aqueous by nature), the choice of dopant ions is nearly endless [108–121].

Much of the work done examining biodopant anions was performed with a focus on either the biocompatibility [108–119] of the resulting material or the ability to functionalize the polypyrrole surface for drug delivery [113, 121–123].

Polypyrrole has also been used for cell matrix substrate formation [120, 124, 125], miniature biosensors [126], and neural regeneration [112, 127]. Immerstrand et al. [36, 107] used a gold/polypyrrole bilayer shaped into a tube to repair a severed blood vessel (see Figure 7-1). The bilayer only has to actuate once, does not biodegrade, and is eventually incorporated into the vessel wall.

7.2 Experimental work

For the initial set of biostability tests, a vial array was constructed containing 25 vials. This allowed for five sets of five test vials, each set with the same biological fluid in each of the five vials. Acrylic inserts were fabricated that held the film within the fluid. These inserts had gold contacts and integrated lead wires which enabled a four point resistance measurement to be taken each hour over several weeks. Figure 7-2 shows the completed vial array.

The polypyrrole samples used were all cut from the same film, which was deposited electrochemically using the process described in Chapter 2. After the film deposition was completed, the film was allowed to dry in a fume hood for several days, then removed from the crucible and cut to individual sample sizes. These were manually attached to the vial inserts, using plastic clamps to ensure good contact between the sample and electrodes.

Once the samples were mounted and the vials filled, the array was placed in an incubator and the entire apparatus was maintained at 37°C and 95% humidity for the duration of the test. The lead wires for each vial were connected to two channels within an Agilent® 34970A Data Acquisition / Switch Unit (two channels of two wires each were required for the four-wire resistance measurement). Measurements were taken once per hour and recorded on a PC running the Agilent BenchLink Data Logger software.

The biological solutions used were corn oil, Ringer's lactate, fetal bovine serum (FBS), and pig's blood treated with ethylenediaminetetraacetic acid (EDTA) to prevent clotting. The FBS was used in both active and heat inactivated forms.

Initial results for films deposited using the standard deposition conditions showed poor biostability in blood and serum (see Figure 7-3). The delayed start of the pig's blood samples was moved to the origin for comparison. Since these results showed less biostability than was desired, current work focuses on modifying the films to improve this.

To verify that the change in resistance shown in the first set of testing was not

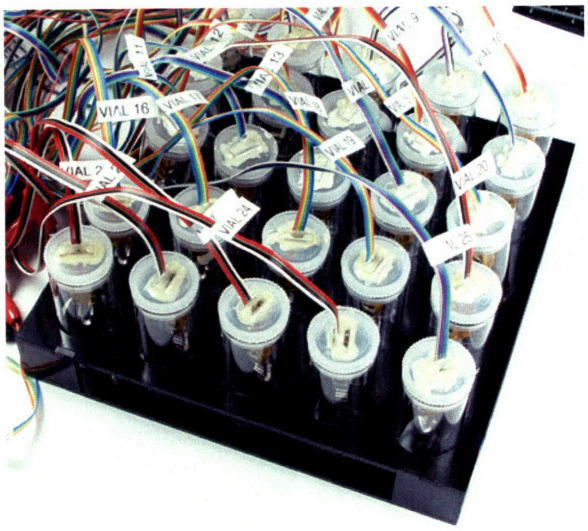

(a)

(b)

Figure 7-2: Each vial in this array contained a polypyrrole sample clamped to electrical contacts. The sample was sumberged in a small amount of biological fluid while keeping the contact points above the surface.

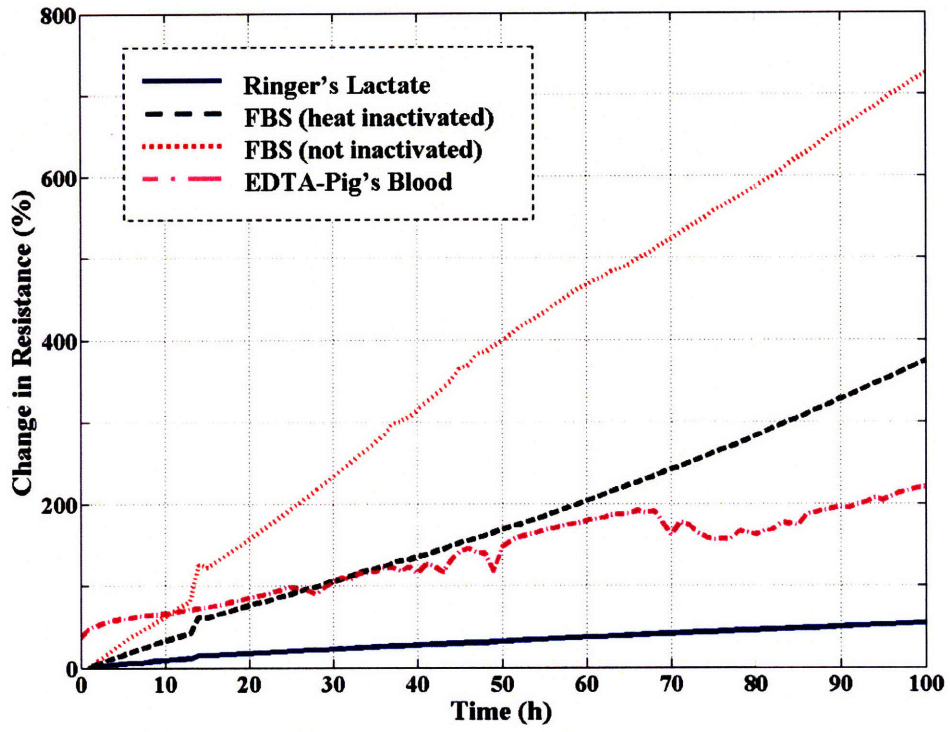

Figure 7-3: Significant changes in resistance were observed for polypyrrole samples submerged in fetal bovine serum (FBS) and pigs blood.

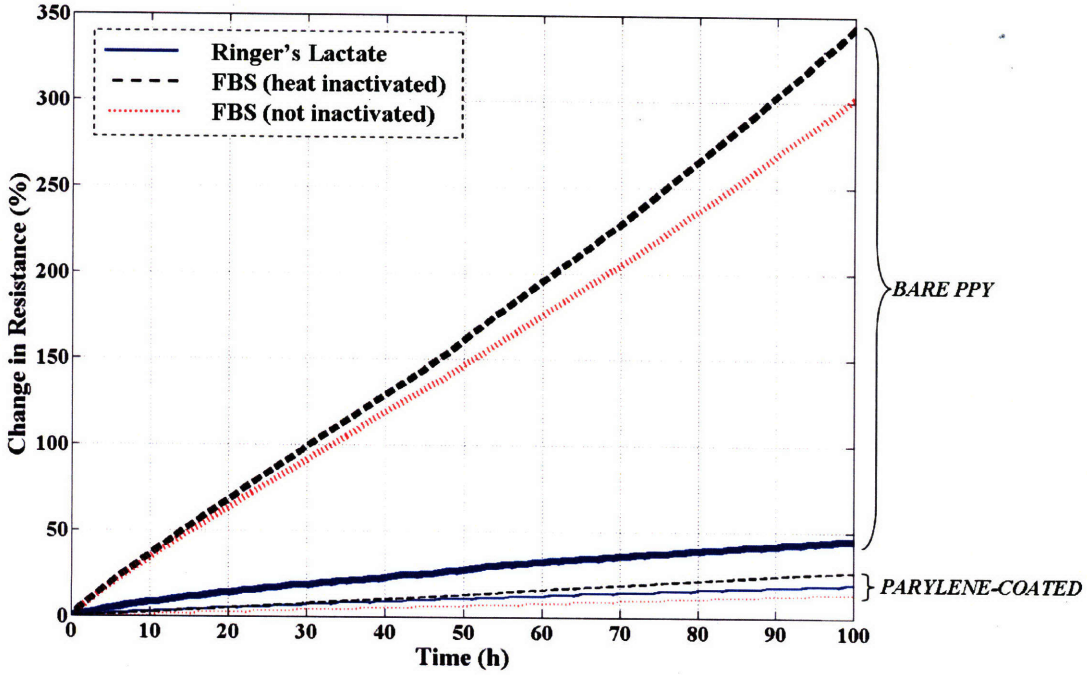

Figure 7-4: This assay verified that the polypyrrole samples themselves were being degraded rather than the test equipment. The parylene-coated samples showed no evidence of instrumentation fouling.

due to fouling of the custom-built instrumentation, a second assay was run with some samples coated in parylene. As can be seen in Figure 7-4, the parylene-coated samples maintained constant resistances, demonstrating that it was in fact the polymer being affected in earlier tests rather than the instrumentation.

7.3 Ongoing Research

7.3.1 Test Chamber Design

To test these new films' biostability, impedance measurements will be taken while they are submerged in the same set of biological fluids as used in the previous testing. A new test chamber is being fabricated (see Figure 7-5) which significantly reduces the fluid volume required while adding the capability to circulate the fluid over the samples. This chamber will hold nine samples with four point lead wires extending outside the incubator. The sample leads will be multiplexed to an impedance analyzer,

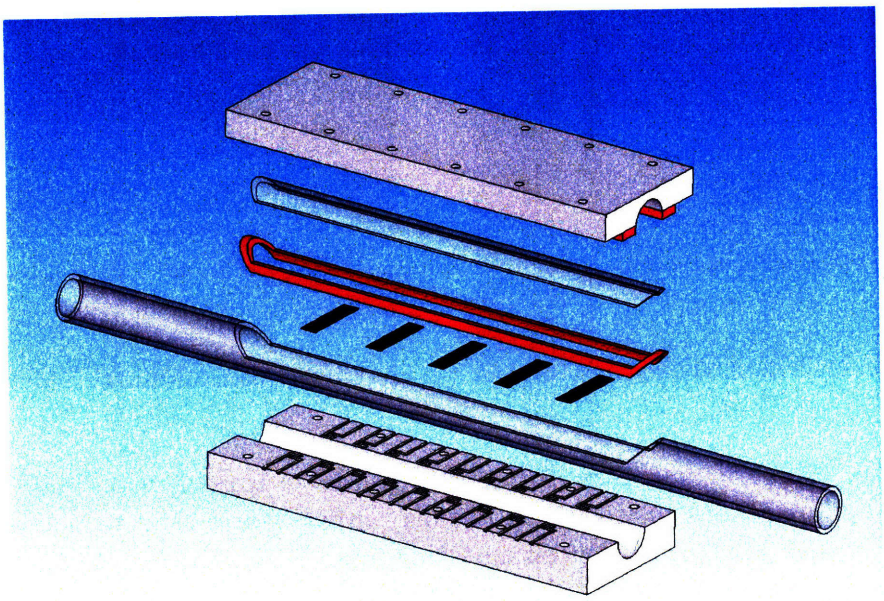

Figure 7-5: This chamber design allows several testing improvements over earlier setups. Each of the nine samples is held in place by the clamping of the two blocks. The samples extend through the Teflon® tube, which allows the solution to be circulated through the test region. (Diagram by Nate Sharpe, MIT BioInstrumentation Lab.)

which will take measurements every hour for approximately four weeks.

7.3.2 Biodopant Study

In order to function reliably in a biological environment, polypyrrole must retain both its conductivity and actuation capability. Both of these properties are highly dependent upon the conditions under which the polypyrrole was initially electrochemically fabricated. The dopant anion used in deposition enables the polymer to be conductive, and the mobility of that anion (along with the relative mobilities of ions in the final device environment) dictates the actuation characteristics of the polypyrrole. Therefore, the dopant ion used in deposition must be such that (1) it is non-toxic to the biological environment, and (2) it is either immobile within the polymer or is a functional part of the actuation ion-exchange.

For the second series of biostability tests, various candidate biodopant ions will be used: Cl^-, dodecyl benzene sulfonate (DBS), ClO_4, poly styrene sulfonate (PSS),

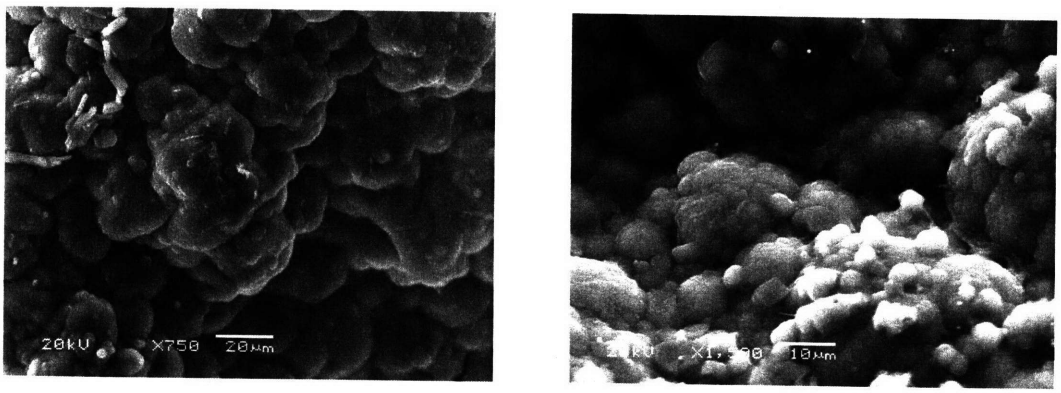

(a) (b)

Figure 7-6: These figures show SEM photographs of a polypyrrole film deposited using ClO_4 dopant ions. Note the nodule-like surface morphology, which is common with traditional polypyrrole deposition techniques.

p-toluene sulfonate (PTS), poly vinylsulfonic acid (PVS), and camphorsulfonic acid (CSA). Polypyrrole films will be deposited using these ions under an array of conditions (temperature, concentration, current density). All of the biodopants have been previously utilized in biological environments, demonstrating their biocompatibility [110, 112, 113, 119, 121, 127]. These films will then be characterized for their conductivity, mechanical viability, and surface morphology.

Work done with MIT BioInstrumentation Lab undergraduate researcher Arjun Naskar showed the feasibility of depositing polypyrrole films using these dopants. Among the best films were those made with ClO_4 (shown in Figure 7-6) and Cl^- (shown in Figure 7-7). These films were mechanically robust and had conductivities on the order of 10^3 S/m, but as can be seen from the figures they showed significantly different surface morphology.

The biodopant work is being continued with MIT BioInstrumentation Lab undergraduate researcher Sarah Shieh. The present work if focused on expanding Naskar's results to include different deposition temperatures and durations to examine their effects on film durability and biostability. These films will eventually provide the samples for testing in the new test chamber shown in Figure 7-5.

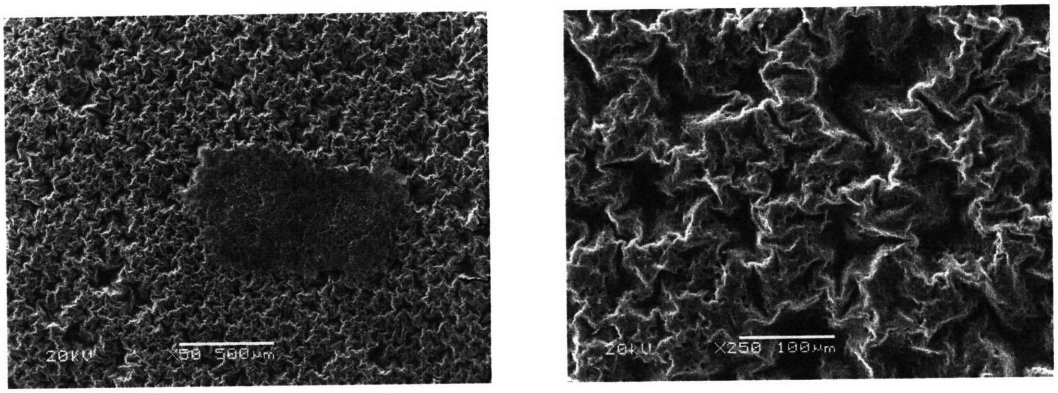

(a) (b)

Figure 7-7: These figures show SEM photographs of a polypyrrole film deposited using Cl^- dopant ions. Note the star-like surface morphology. The increased surface area of the film resulting from this morphology may improve the actuation capabilities of this film.

Chapter 8

Conclusions

This work is the beginning of a quest to create a device which closely replicates the behavior and performance of mammalian skeletal muscle. This incredible actuation device has intricately co-fabricated and integrated actuation, sensory, control, and energy delivery capabilities that has resutled from billions of years of evolution. This research has conceptualized a device, known as a programmable material, which integrates many of these same capabilities and co-fabricates them in such a way as to appear externally to be a single homogeneous material.

By fabricating a feedback loop directly into the device, a programmable material has the ability to modify its material properties based upon the feedback characteristics. Instead of being wholly dependent upon the molecular structure and mechanical arrangement of the device components, the stiffness, damping, and inertia of a programmable material can be 'tuned' by changing a low power input signal to the device.

While a functional device has not yet been realized and a great deal of work remains to be done to do so, many of the initial design and implementation issues have been solved here. At the time of this writing, a preliminary design has been completed for all of the necessary components of the system. Actuators have been demonstrated, and sensors have been tested and their theoretical models verified. Control electronics have been designed and fabricated, using a fabrication process that meets the stringent co-fabrication requirements imposed by the programmable

material design. These components were tested and their theoretical models verified. Layered co-fabrication was demonstrated, which will enable construction of the final device. A full system analysis of the device performance has been completed, utilizing the demonstrated characteristics from experimental tests of each component.

The work that remains is primarily in optimizing the individual device components and integrating them into a fully functional device. Improving the individual components will increase the bandwidth of the programmable material, enabling it to realize a wider range of tunable properties. Extending the co-fabrication work done here will result in the final assembly of the device. Full testing of the completed device is then needed to verify the predictions made here.

8.1 Actuation

First, an actuator was needed. In the interest of recreating the material properties of muscle to the extent possible, conducting polymers have been used to make the various programmable material components. Since it has demonstrated good actuation characteristics in previous research, the conducting polymer polypyrrole was used for the actuator layer of the device. This was chosen over various other 'artificial muscle' technologies as a result of the good compromise polypyrrole represents between total strain, strain rate, and power requirements.

In this work, the actuator model was reviewed and integrated into the overall system model. Several configurations were proposed for a programmable material: linear and trilayer.

The linear device is simpler to fabricate, consisting of an actuator layer, sensor layer, and electronics layer. The relationship between the input current and strain resulting from the actuator was examined closely for this geometry.

A trilayer programmable material serves as a position-controlled device. Using the trilayer arrangement allows significant amplification of the actuator strain into large-scale bending motion. The theoretical relationship between charge injected into the actuator and the resultant device curvature was derived and incorporated into

the system model.

8.2 Sensing

A polypyrrole layer was used as the sensor for the programmable material. This layer serves as a strain gage, transducing the total strain experienced by the device into a voltage usable by the control electronics.

To fully understand the sensor behavior, it was first necessary to model the viscoelastic behavior of the polypyrrole. This was important since it was observed that test samples experienced a creep of nearly 3% over four hours under a 1 MPa load. Two models were proposed, the standard linear solid model and the generalized Maxwell model. Experimental work showed that the Maxwell model more closely represented the actual creep behavior of the sensor.

Having successfully modeled the viscoelasticity, the relationship between the applied strain and the variable resistance of the polypyrrole sensor had to be determined. A mechanical model was proposed which utilized the Poisson effect to predict an increase in resistance under load. A uniaxial stress results in a reduction in the cross-sectional area which can be calculated using the Poisson's ratio of the material. Assuming a constant conductivity of the film (which was reasonable considering the small strains expected), this reduction in area causes a corresponding increase in the sensor resistance. By incorporating this sensor into a full Wheatstone bridge (the othe legs residing in the control electronics), a voltage can be generated which is directly related to the strain experienced by the sensor.

To test this model, appropriate instrumentation was built (to include modification of existing equipment) and test code was written. These tools allowed experimental verification of the Poisson model, which was then incorporated into the system model.

A drawback of the current sensor component is relative the weakness of the sensor. As can be seen in Chapter 3, a typical sensor geometry resulted in a resistance modulation of only 0.38 $\Omega/\%$. In order to turn this into a usable voltage for the control electronics to interpret, a bridge input voltage of 20 V is needed. This large

amplification of a small signal is prone to noise contamination which will result in a reduction in device performance quality.

While a polypyrrole strain gage is a functional sensor for the programmable material, more sensitive alternatives should be pursued. Other conducting polymers may have better strain-resistance relationships without seriously impacting the overall design and fabrication of the device.

8.3 Feedback Electronics

There have been many methods used to deposit and pattern conducting polymers into useful devices. Unfortunately, most of these processes were unsuitable for fabrication of a programmable material. The process used had to allow small feature patterning of the conducting polymer while minimizing the possibility of damage to the underlying polymer substrate. Since the deposition target for the control electronics consists of the actuator and sensor previously co-fabricated, chemicals and processes which damaged these components were unacceptable.

After reviewing many different depsosition and patterning techniques, the oxidative chemical vapor deposition (oCVD) process pioneered by the Gleason lab at MIT was shown to be appropriate for this work. This process deposits poly(3,4-ethylenedioxythiophene) (PEDOT) from the vapor phase, polymerizing the EDOT monomer via an oxidation reaction initated by a sublimated oxidant. This was a gentle and fast procedure which did not require chemical treatment or dynamic contact with the substrate.

By allowing line-of-sight deposition of PEDOT, the oCVD process enabled the use of shadow masks to pattern the components. These masks were custon fabricated first from adhesive material to improve the rapidity of the prototyping process. Once designs were finalized, wire EDM technology was used to fabricate rigid metal masks. The static contact between these masks and the substrate caused no damage to the flexible and somewhat fragile polymer.

Once the deposition and patterning process was refined, electrochemical active

components (diodes and transistors) were fabricated. Purely electrical components were considered, but required compromises in deposition technology which would have rendered the device unusable.

These electrochemical devices were tested, redesigned and refabricated in an iterative process. Custom instrumentation was fabricated to conduct the testing, and various testing algorithms were coded in order to complete the experiments. The electrochemical diodes fabricated have on/off ratios up to 4. These are the first electrochemical diodes to be fabricated using the oCVD process.

A great deal of work was done to realize an electrochemical transistor, as this was the key element to constructing the control electronics that implement the feedback capability of the programmable material. Initial attempts were stymied by insufficient ionic barrier layers, which were needed to isolate and define the two electrochemical cells needed for transistor operation. Another obstacle was the test environment, which consisted of an electrolyte solution with ions to allow electrochemical switching of the conducting polymer. If the solvent or ions were chosen poorly, degradation of the ionic barrier layer (in the case of the solvent) or actuation and breakage of the conducting polymer traces (in the case of the ions) could result.

This work resulted in the first successful fabrication of an electrochemical transistor using the oCVD process. This device demonstrated a threshold voltage of 1.7 V, with a transconductance of 0.046 mS (though transconductances on the order of 1 mS were seen for noisier, less reliable samples). A comparison of these results with other electrochemical (and silicon-based) transistor components was made.

These transistors were then successfully integrated into an electrochemical circuit as part of a fully patterned and deposited differential amplifier. This DA functioned as was theoretically predicted, though imprecise control of some deposition traces resulted in poor resolution of several resistive elements. This caused the DA to attenuate the differential input by 4.7 dB. Nonetheless, the circuit functioned as desired, based on deposited and measured component values.

Future work on the control electronics must focus on the improvement of the transistors as well as the definition of the resistive elements. The DA performance

could easily be improved to provide a 21 dB amplification with reliable resistors. Improvement of the transistors could conceivably improve the amplification to as much as 34 dB.

8.4 Biostability

Since the programmable material is a first step towards a fully functional, controllable, implantable artificial muscle, it was important to examine the survivability of the device in a biological environment. As a result, a study of the biostability of polypyrrole was undertaken as part of this work.

The biocompatibility of polypyrrole has been studied by many researchers prior to this as part of efforts to create polymeric sensors and drug delivery platforms. Biocompatibility characterizes the response of the biological system to the material in question, and was certainly of great interest for the programmable material. In the current research, however, it is necessary for the polypyrrole to actively perform multiple tasks while immersed in a biological environment rather than simply survive implantation. It was therefore of great interest to examine the materials' biostability, which characterizes the ability of the material to survive and retain its useful properties.

Custom instrumentation was fabricated to complete the biostability testing. Initial results using several biological solutions were poor, with the measured resistance of the polypyrrole samples increasing dramatically on submersion in these solutions. All of these polypyrrole samples were fabricated using the standard deposition recipe outlined in Chapter 2.

This study is ongoing, examining several routes for improving the biostability characteristics of polypyrrole. Updated equipment is under construction which will allow more samples to be tested with less solution, as well as enabling circulation of the solution over the samples. Different, more biologically frindly deposition conditions are being examined for their effect on the material performance.

8.5 System Integration

One of the primary advantages of the programmable material design is the co-fabricated nature of the device. This enables the embedding of multiple capabilities into a seemingly homogeneous material with tunable material properties. Thus, the co-fabrication of the system components was of primary importance.

In order to demonstrate the feasibility co-fabricating the programmable material, multiple layers of polypyrrole (forming the actuator and sensor layers) had to be fabricated in such a way as to be electronically and ionically isolated but mechanically bonded.

This was accomplished by first electrochemically depositing a free-standing film of polypyrrole to act as the actuator. One surface of this film was then coated with a barrier material (polystyrene) using a plasma-polymerization process. This barrier material was then coated with a conducting polymer (PEDOT), which served as the working electrode for the electrochemical deposition of a second polypyrrole layer (the sensor). This technique was successfully demonstrated.

Once the co-fabrication process was proven, a full system model was constructed. Using the mathematical models for each of the device components, this model was constructed and evaluated for sensitivity to different variables. It was found that slight improvements to the control electronics (resistor definition, discussed above) would result in a device with an apparent stiffness 18% higher than that of the polypyrrole components. With the largest immediately feasible improvements to transistor performance, an apparent stiffness increase by a factor greater than seven is possible.

8.6 Future Work

The complete fabrication of a programmable material remains to be done. Many of the preliminary issues confounding this effort have been resolved in this work, but problems remain to be solved before full implementation.

Design and fabrication of the control electronics needs refinement. The differential

amplifier behavior is highly dependent upon the internal resistor values, and the masks and deposition process need to be optimized for control of these values. This would allow significant gain values to be achieved rather than the attenuation currently available.

Dual-layer co-fabrication of polypyrrole layers has been demonstrated. It remains to extend this co-fabrication to the entire device. A simpler first device than the trilayer device suggested in this thesis would be a linear device with only one actuator layer. The control electronics and sensor layers would enable the elimination of linear creep behavior when the sample is placed under constant stress. A second step would be creation of an electrolyte-based trilayer device before final creation of an air-functional trilayer.

Finally, the effect of strain on the operation of the control electronics must be examined. The performance of these components have been demonstrated in an unstrained state, but it must be shown that their behavior is not hindered by subjected to strain.

8.7 A Possible Application

Should these questions be answered, and should the integrated capabilities of the programmable material be optimized to their theoretically possible extent, the device would constitute a significant addition to the repertoire of system designers. One possible application that warrants further attention is the concept of adaptable armor.

For soldiers in a combat environment, it is essential that some form of individual ballistic protection be provided. The helmet, of course, serves to protect the head, and some form of body armor protects the torso. This body armor has traditionally been, by necessity, heavy and cumbersome. In order to provide adequate protection against projectiles, this armor is stiff and uncomfortable. In hot environments, wearing the body armor can be extremely challenging.

One technique for improving comfort is to improve the flexibility of the armor. This has been done to some extent through the use of Kevlar® fabrics. Recently,

however, additional protection was needed and so ceramic plates have been added in key locations. These plates are very effective, but make the armor significantly less comfortable.

In order to reduce weight and stiffness, a programmable material could be used to support an array of smaller ceramic plates, as shown in Figure 8-1. If contained between Kevlar fabric front and back layers, the adaptable armor would be able to protect the wearer by activating when needed.

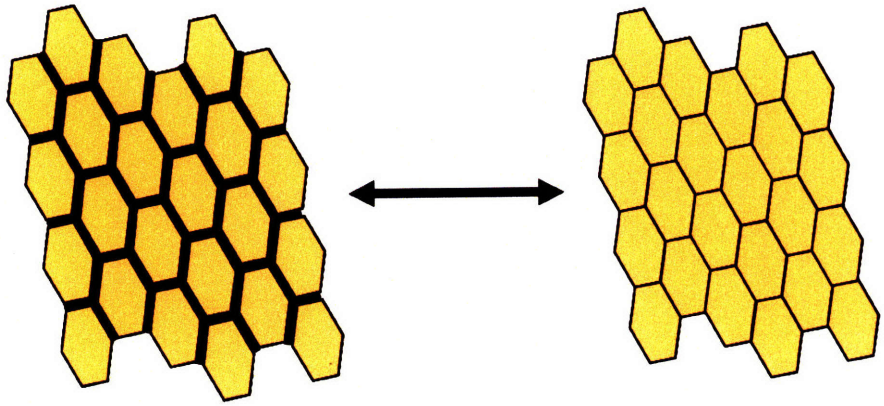

Figure 8-1: To improve comfort and wearability of body armor without sacrificing protection, a programmable material (shown in black) could be used to support an array of ceramic plates. Upon detection of an impact, the programmable material would close the gaps and protect the wearer.

As a projectile strikes the armor, the outer Kevlar layer blunts the impact and slows it down. The impact is detected by the programmable material in the form of the sudden strain increase. The material activates, stiffening and closing the gaps between the ceramic plates. Thus, the stiffness of the armor only appears when needed.

Adaptable armor using programmable materials is not an immediately realizable prospect. However, the path to such a product is clear. A programmable material will provide the ability to create actuation devices unimagined today.

Appendix A

Testing Code for Electrochemical Transistors

```
Imports NationalInstruments.DAQmx
Imports Agilent.TMFramework
Imports Agilent.TMFramework.DataAnalysis
Imports Agilent.TMFramework.DataVisualization
Imports Agilent.TMFramework.InstrumentIO
Imports System.IO
Imports System.Math

Public Class Form1
    Inherits System.Windows.Forms.Form
    Private MeasureThread As New System.Threading.Thread(AddressOf MeasureTime)
    ' powersupply1 is the Drain-Source and Bias voltages (Triple Output PS)
    Dim powersupply1 As New Agilent.TMFramework.InstrumentIO.
     DirectIO("GPIB0::04::INSTR", False, 2000)
    ' powersupply2 is the Gate voltage (Triple Output PS)
    Dim powersupply2 As New Agilent.TMFramework.InstrumentIO.
     DirectIO("GPIB0::05::INSTR", False, 2000)
    Private TaskR1 As Task = Nothing
    Private reader As AnalogMultiChannelReader
    Dim testRunning As Boolean
    Dim timeHack As Date()
    Dim timeN As Date
    Dim startTime As Date
    Dim tStart As Double
    Dim dStart As Double
    Dim hStart As Double
    Dim mStart As Double
```

```
    Dim sStart As Double
    Dim Vg As Double
    Dim Vds As Double()
    Dim Ids As Double()
    Dim Vb As Double
    Dim x As Integer
    Dim y As Double
    Dim z As Double
    Dim j As Integer
    Dim v As Double
    Dim w As Integer = 1
    Dim R As Double
    Dim data As Double()

#Region " Windows Form Designer generated code "
(omitted)

    Private Sub Form1_Load(ByVal sender As System.Object, ByVal e
      As System.EventArgs) Handles MyBase.Load
        testRunning = False
        powersupply1.WriteLine("OUTP OFF")
        powersupply2.WriteLine("OUTP OFF")
        powersupply1.WriteLine("APPL P6V, 0.0, 0.1")
        powersupply1.WriteLine("APPL P25V, 0.0, 0.1")
        powersupply1.WriteLine("APPL N25V, 0.0, 0.1")
        powersupply2.WriteLine("APPL P6V, 0.0, 0.1")
        powersupply2.WriteLine("APPL P25V, 0.0, 0.1")
        powersupply2.WriteLine("APPL N25V, 0.0, 0.1")
        MeasureThread.Start()
        MeasureThread.Suspend()
    End Sub

    Private Sub StartButton_Click(ByVal sender As System.Object, ByVal
      e As System.EventArgs) Handles StartButton.Click
        testRunning = True
        v = 0
        Vg = 0
        Vb = txtBias.Text
        R = txtRes.Text
        w = 1
        TotTime.Text = 0
        SecRnd.Text = 0
        powersupply2.WriteLine("APPL P6V, " & Vb & ", 0.1")
        powersupply1.WriteLine("OUTP ON")
        powersupply2.WriteLine("OUTP ON")
```

```
    MeasureThread.Resume()
    txtStatus.Text = "RUNNING"
End Sub

Public Sub MeasureTime()
    Dim d As Double
    Dim h As Double
    Dim m As Double
    Dim s As Double
    Dim StopVds As Double = CDbl(txtVdsMAX.Text) + CDbl(txtStepVds.Text)
    Dim StopVg As Double = CDbl(txtVgMAX.Text)
    Vds = New Double(100000) {}
    Ids = New Double(100000) {}
    timeHack = New Date(100000) {}

    Try
        TaskR1 = New Task
        TaskR1.AIChannels.CreateVoltageChannel("dev1/ai0:1", "",
         CType(-1, AITerminalConfiguration), -1, 10,
         AIVoltageUnits.Volts)
        reader = New AnalogMultiChannelReader(TaskR1.Stream)
        reader.SynchronizingObject = Me
        'Outer loop - Vg is being stepped:
        Do Until testRunning = False
            txtVg.Text = Vg
            If v < StopVds Then
                powersupply1.WriteLine("APPL P6V, " & v & ", 0.1")
                powersupply1.WriteLine("APPL P25V, " & Vg & ", 0.1")
                powersupply1.WriteLine("OUTP ON")
                powersupply2.WriteLine("OUTP ON")
            End If
            startTime = Now
            dStart = Format(startTime, "dd")
            hStart = Format(startTime, "hh")
            mStart = Format(startTime, "mm")
            sStart = Format(startTime, "ss.ffffff")
            tStart = 86400 * dStart + 3600 * hStart + 60 * mStart + sStart
            SecRnd.Text = 0
            x = 1
            y = 0
            z = 0
            j = 0
            'Inner loop - Vds is being stepped:
            Do Until v > StopVds
                timeN = Now
```

```
    d = Format(timeN, "dd")
    h = Format(timeN, "hh")
    m = Format(timeN, "mm")
    s = Format(timeN, "ss.ffffff")
    TotTime.Text = CStr(86400 * d + 3600 * h + 60 * m + s - tStart)
    RunTime.Text = Now
    If TotTime.Text > x Then
        SecRnd.Text = x
        x += 1
    End If
    If TotTime.Text > y Then
        powersupply1.WriteLine("APPL P6V, " & v & ", 0.1")
        v += CDbl(txtStepVds.Text)
        y += CDbl(txtStep.Text)
    End If
    If TotTime.Text > z Then
        data = reader.ReadSingleSample
        Vds(j) = data(1) - data(0)
        Ids(j) = data(0) / R
        txtVds.Text = Math.Round(data(1) - data(0), 5)
        txtIds.Text = Math.Round(data(0) / R, 5)
        timeHack(j) = Now
        z += 1 / CDbl(txtRate.Text)
        j += 1
    End If
Loop

powersupply1.WriteLine("OUTP OFF")
powersupply2.WriteLine("OUTP OFF")
Dim i As Integer
Dim DateTime As Date
Dim FileName As String
DateTime = Now
FileName = "TransistorTest" & CStr(Format(DateTime,
 "MMddyy")) & txtFileMod.Text & "_" & w & ".m"
FileOpen(1, FileName, OpenMode.Output)
PrintLine(1)
PrintLine(1, "% " & FileName)
PrintLine(1)
PrintLine(1, "% Measure transistor response to
 various constant voltages")
PrintLine(1)
PrintLine(1, "Vg = " & Vg & ";")
PrintLine(1)
PrintLine(1, "% Time(s)   Vds (V)  Ids (A)")
```

```
                PrintLine(1)
                PrintLine(1, "Data = [")
                For i = 0 To (j - 1)
                    Print(1, CStr(Format(timeHack(i), "mm")) & "    ")
                    Print(1, CStr(Format(timeHack(i), "ss.ffffff"))
                      & "    ")
                    Print(1, Vds(i) & "    ")
                    Print(1, Ids(i) & "    ")
                    PrintLine(1)
                Next
                PrintLine(1, "];")
                FileClose(1)
                w += 1
                Vg += CDbl(txtStepVg.Text)
                v = 0
                If Vg > StopVg Then
                    testRunning = False
                    powersupply1.WriteLine("OUTP OFF")
                    powersupply2.WriteLine("OUTP OFF")
                    txtStatus.Text = "COMPLETE"
                    MeasureThread.Suspend()
                End If
            Loop
        Catch ex As Exception
            MessageBox.Show(ex.Message)
            powersupply1.WriteLine("OUTP OFF")
            powersupply2.WriteLine("OUTP OFF")
        End Try
        MeasureThread.Sleep(0)
    End Sub

    Private Sub StopButton_Click(ByVal sender As System.Object,
      ByVal e As System.EventArgs) Handles StopButton.Click
        testRunning = False
        powersupply1.WriteLine("OUTP OFF")
        powersupply2.WriteLine("OUTP OFF")
        If Vg < txtVgMAX.Text Then
            MeasureThread.Suspend()
            txtStatus.Text = "ABORTED"
        End If
    End Sub
End Class
```

Appendix B

Testing Code for Electrochemical Differential Amplifiers

```
Imports NationalInstruments.DAQmx
Imports Agilent.TMFramework
Imports Agilent.TMFramework.DataAnalysis
Imports Agilent.TMFramework.DataVisualization
Imports Agilent.TMFramework.InstrumentIO
Imports System.IO
Imports System.Math

Public Class Form1
    Inherits System.Windows.Forms.Form
    Private MeasureThread As New System.Threading.Thread(AddressOf MeasureTime)
    ' powersupply1 is the Bias and Input 1 voltages (Triple Output PS)
    Dim powersupply1 As New Agilent.TMFramework.InstrumentIO.
     DirectIO("GPIB0::04::INSTR", False, 2000)
    ' powersupply2 is the Input 2 and Current Source voltages (Triple Output PS)
    Dim powersupply2 As New Agilent.TMFramework.InstrumentIO.DirectIO
     ("GPIB0::05::INSTR", False, 2000)
    Private TaskR1 As Task = Nothing
    Private reader As AnalogMultiChannelReader
    Dim testRunning As Boolean
    Dim timeHack As Date()
    Dim timeN As Date
    Dim startTime As Date
    Dim tStart As Double
    Dim dStart As Double
    Dim hStart As Double
```

```
    Dim mStart As Double
    Dim sStart As Double
    Dim V1 As Double
    Dim V2 As Double
    Dim V1o As Double()
    Dim Vo As Double()
    Dim Vb As Double
    Dim Vee As Double
    Dim StopV1 As Double
    Dim StopV2 As Double
    Dim x As Integer
    Dim y As Double
    Dim z As Double
    Dim j As Integer
    Dim w As Integer = 1
    Dim data As Double()

#Region " Windows Form Designer generated code "
(omitted)

    Private Sub Form1_Load(ByVal sender As System.Object,
     ByVal e As System.EventArgs) Handles MyBase.Load
        testRunning = False
        powersupply1.WriteLine("OUTP OFF")
        powersupply2.WriteLine("OUTP OFF")
        powersupply1.WriteLine("APPL P6V, 0.0, 0.1")
        powersupply1.WriteLine("APPL P25V, 0.0, 0.1")
        powersupply1.WriteLine("APPL N25V, 0.0, 0.1")
        powersupply2.WriteLine("APPL P6V, 0.0, 0.1")
        powersupply2.WriteLine("APPL P25V, 0.0, 0.1")
        powersupply2.WriteLine("APPL N25V, 0.0, 0.1")
        MeasureThread.Start()
        MeasureThread.Suspend()
    End Sub

    Private Sub StartButton_Click(ByVal sender As
     System.Object, ByVal e As System.EventArgs)
     Handles StartButton.Click
        testRunning = True
        V1 = 0
        V2 = 0
        Vb = txtVb.Text
        Vee = txtVee.Text
        w = 1
        StopV1 = CDbl(txtV1MAX.Text) + CDbl(txtStepV1.Text)
```

```
    StopV2 = CDbl(txtV2MAX.Text)
    TotTime.Text = 0
    SecRnd.Text = 0
    powersupply1.WriteLine("APPL P6V, " & Vb & ", 0.1")
    powersupply1.WriteLine("APPL P25V, 0.0, 0.1")
    powersupply1.WriteLine("APPL N25V, 0.0, 0.1")
    powersupply2.WriteLine("APPL P6V, 0.0, 0.1")
    powersupply2.WriteLine("APPL P25V, 0.0, 0.1")
    powersupply2.WriteLine("APPL N25V, " & -Vee & ", 0.1")
    powersupply1.WriteLine("OUTP ON")
    powersupply2.WriteLine("OUTP ON")
    MeasureThread.Resume()
    txtStatus.Text = "RUNNING"
End Sub

Public Sub MeasureTime()
    Dim d As Double
    Dim h As Double
    Dim m As Double
    Dim s As Double
    Vo = New Double(100000) {}
    V1o = New Double(100000) {}
    timeHack = New Date(100000) {}
    Try
        TaskR1 = New Task
        TaskR1.AIChannels.CreateVoltageChannel("dev1/ai0:1",
         "",CType(-1, AITerminalConfiguration), -1, 10,
         AIVoltageUnits.Volts)
        reader = New AnalogMultiChannelReader(TaskR1.Stream)
        reader.SynchronizingObject = Me
        'Outer loop - V2 is being stepped:
        Do Until testRunning = False
            txtV2.Text = V2
            If V1 < StopV1 Then
                powersupply1.WriteLine("APPL P25V, " & V1 & ", 0.1")
                powersupply2.WriteLine("APPL P6V, " & V2 & ", 0.1")
                powersupply1.WriteLine("OUTP ON")
                powersupply2.WriteLine("OUTP ON")
            End If
            startTime = Now
            dStart = Format(startTime, "dd")
            hStart = Format(startTime, "hh")
            mStart = Format(startTime, "mm")
            sStart = Format(startTime, "ss.ffffff")
            tStart = 86400 * dStart + 3600 * hStart + 60 * mStart + sStart
```

```
SecRnd.Text = 0
x = 1
y = 0
z = 0
j = 0
'Inner loop - V1 is being stepped:
Do Until V1 > StopV1
    timeN = Now
    d = Format(timeN, "dd")
    h = Format(timeN, "hh")
    m = Format(timeN, "mm")
    s = Format(timeN, "ss.ffffff")
    TotTime.Text = CStr(86400 * d + 3600 * h + 60 * m + s - tStart)
    RunTime.Text = Now
    If TotTime.Text > x Then
        SecRnd.Text = x
        x += 1
    End If
    If TotTime.Text > y Then
        powersupply1.WriteLine("APPL P25V, " & V1 & ", 0.1")
        txtV1.Text = V1
        V1 += CDbl(txtStepV1.Text)
        y += CDbl(txtStep.Text)
    End If
    If TotTime.Text > z Then
        data = reader.ReadSingleSample
        Vo(j) = data(0)
        V1o(j) = CDbl(txtV1.Text)
        txtVo.Text = Math.Round(data(0), 5)
        timeHack(j) = Now
        z += 1 / CDbl(txtRate.Text)
        j += 1
    End If
Loop

powersupply1.WriteLine("OUTP OFF")
powersupply2.WriteLine("OUTP OFF")
'Write Data (each file is for a given V2):
Dim i As Integer
Dim DateTime As Date
Dim FileName As String
DateTime = Now
FileName = "DATest" & CStr(Format(DateTime, "MMddyy")) &
 txtFileMod.Text & "_" & w & ".m"
FileOpen(1, FileName, OpenMode.Output)
```

```
            PrintLine(1)
            PrintLine(1, "% " & FileName)
            PrintLine(1)
            PrintLine(1, "% Measure transistor response to
             various constant voltages")
            PrintLine(1)
            PrintLine(1, "Vb = " & Vb & ";")
            PrintLine(1)
            PrintLine(1, "Vee = " & Vee & ";")
            PrintLine(1)
            PrintLine(1, "V2 = " & V2 & ";")
            PrintLine(1)
            PrintLine(1, "% Time(s)   V1 (V)  Vo (V)")
            PrintLine(1)
            PrintLine(1, "Data = [")
            For i = 0 To (j - 1)
                Print(1, CStr(Format(timeHack(i), "mm")) & "    ")
                Print(1, CStr(Format(timeHack(i), "ss.ffffff")) & "    ")
                Print(1, V1o(i) & "    ")
                Print(1, Vo(i) & "    ")
                PrintLine(1)
            Next
            PrintLine(1, "];")
            FileClose(1)
            w += 1
            V2 += CDbl(txtStepV2.Text)
            V1 = 0
            If V2 > StopV2 Then
                testRunning = False
                powersupply1.WriteLine("OUTP OFF")
                powersupply2.WriteLine("OUTP OFF")
                txtStatus.Text = "COMPLETE"
                MeasureThread.Suspend()
            End If
        Loop

    Catch ex As Exception
        MessageBox.Show(ex.Message)
        powersupply1.WriteLine("OUTP OFF")
        powersupply2.WriteLine("OUTP OFF")
    End Try
    MeasureThread.Sleep(0)
End Sub

Private Sub StopButton_Click(ByVal sender As System.Object,
```

```
    ByVal e As System.EventArgs) Handles StopButton.Click
        testRunning = False
        powersupply1.WriteLine("OUTP OFF")
        powersupply2.WriteLine("OUTP OFF")
        If V2 < txtV2MAX.Text Then
            MeasureThread.Suspend()
            txtStatus.Text = "ABORTED"
        End If
    End Sub
End Class
```

Appendix C

MATLAB Code for System Simulation

SystemThesis.m

```
% Overall system model for thesis

clear
clf

%% DEFINE TEST PARAMETERS:
ts=0;       % Start Time
tr=100;      % End Time
dt=0.1;    % Time interval
t=ts:dt:tr;
w=50*2*pi;     % frequency in rad/s
% for j=1:length(t)
%     F(j)=0.05*(1+floor(t(j)./25)); %#ok<AGROW>
% end
F=0.15*ones(1,length(t));
% F=.15+0.05*sin(w*t);

%% DEFINE DEVICE VALUES:
Ep=800e6;   % Polymer base modulus
a=500e-12;  % Strain-to-charge ratio
nu=0.426;   % Poisson's ratio
Ta=25e-6;   % Thickness (single layer)
Wa=3e-3;    % Width
La=5e-2;    % Length
Vol=Ta*Wa*La;
```

```
%% DEFINE SENSOR VALUES:
Vs=20;      % Bridge input voltage
Rc=100;      % Constant resistor value (sensor initial value)

%% DEFINE ECDA VALUES:
Vd=0;       % Set operating point
Vin=1.3925; % High input
Vee=-10;    % Low input
Re=5e5;     % long tail resistor
Ro=1e6;     % output resistor
Rp1=1e5;    % pair resistor (desired input side)
Rp2=1e5;    % pair resistor (bridge side)
Rt=6e6;     % intial resistance of ECT drain-source path
k=2.3;      % exponential coefficient in ECT model

%% DEFINE ACTUATOR:
[A B C D]=tf2ss([.028 .6524 .8008 8.008e-6],[1 32.7 81.5 15 0]);
Ga=ss(A,B,C,D);
eq=0;       % initial value for charge-driven strain
x=zeros(2,4);

%% GENERATE MECHANICAL RESPONSE
s=F./(2*Ta*Wa);
z.em=MechWork(s,t);

for i=1:length(t)
    em=z.em(i);
    er=em+eq;
    z.er(i)=er;
    % SENSOR:
    Rs=Rc*(1+er)/((1-nu*er)^2);
    Vb=(Rs/(Rs+Rc)-.5)*Vs;
    z.Vb(i)=Vb;
    % ECDA:
    R1=Rt*exp(-k*Vd);
    R2=Rt*exp(-k*Vb);
    aden=Re*(R1+Rp1)+(Re+R1+Rp1)*(Ro+R2+Rp2);
    a1=(R1+Rp1)*(Ro+R2+Rp2)/aden;
    a2=Re*(Ro+R1+Rp1+R2+Rp2)/aden;
    Vx=Vee*a1+Vin*a2;
    Vout=Vin-Ro*((Vin-Vx)/(Ro+R2+Rp2));
    z.Vout(i)=Vout;
    % ACTUATOR:
    [q,tt,x]=lsim(Ga,[Vout Vout],[0 dt], x(2,:));
    z.q(i)=q(2);
```

```
    eq=q(2)*a/Vol;
    z.eq(i)=eq;
end

figure(1)
plot(t,z.em,t,z.eq,t,z.er)
legend('\epsilon_m','\epsilon_q','\epsilon_r')
figure(2)
Ke=z.em./z.er;
plot(t,Ke)
```

MechWork.m

```
function em=MechWork(s,t)

% Returns mechanical response for a given strain over given time range

so=1e6;
C1=-2.012;
t1=1.33/3600;
C2=-.462;
t2=16.14/3600;
C3=2.841;
eo=C1+C2+C3;

Ea=so*t2/C3;
star=(C3*Ea*t1^2)/(C3*t1*t2-C1*t2*so);
nf=(1/(star+t1))*(so*Ea/(Ea*(C2-C1*eo)+t2*so));
Ec=t1*nf;
Eb=star*nf-Ea;
nd=Ea*Eb/(t2*(Ea+Eb));

en=zeros(length(t));
ep=zeros(length(t));
e=zeros(length(t));

for i=1:length(t)-1 % this sets t1 (start)
    so=s(i);
    C1=Ec*(Eb*nf-Ec*nd)/(nd*nf*(Ea+Eb));
    C2=so*((1/(Ea+Eb+Ec))-Eb/(nd*(Ea+Eb)))+eo*(Ec*(Eb*nf-Ec*nd)/(nd*nf*(Ea+Eb)));
    C3=so*Eb/(nd*(Ea+Eb));
    t1=Ec/nf;
    t2=Ea*Eb/(nd*(Ea+Eb));
    ep(i,:)=C1*exp(-t1*t)+C2*exp(-t2*t)+C3;

end
en=-ep;

% offset negative strain responses by dt:
for i=1:length(t)
    for j=length(t):-1:1
        if j==1
            en(i,j)=0;
        else
            en(i,j)=en(i,j-1);
        end
    end
```

```
end

ef=en+ep;

% offset each
for i=1:length(t)
    for j=length(t):-1:1
        if j>i
            ef(i,j)=ef(i,j-i);
        else
            ef(i,j)=0;
        end
    end
end

em=sum(ef)/100;
```

Bibliography

[1] Wikipedia. Muscle. *en.wikipedia.org*, May 6, 2008.

[2] Wikipedia. Electric motor. *en.wikipedia.org*, May 6, 2008.

[3] Wikipedia. Strain gauge. *en.wikipedia.org*, May 6, 2008.

[4] Wikipedia. Operational amplifier. *en.wikipedia.org*, May 6, 2008.

[5] J. D. W. Madden, N. A. Vandesteeg, P. A. Anquetil, P. G. A. Madden, A. Takshi, R. Z. Pytel, S. R. Lafontaine, P. A. Wieringa, and I. W. Hunter. Artificial muscle technology: Physical principles and naval prospects. *IEEE Journal of Oceanic Engineering*, 29(3):706–728, 2004.

[6] J. R. Reynolds, C. K. Baker, C. A. Jolly, P. A. Poropatic, and J. P. Ruiz. Electrically conductive polymers. In James M. Margolis, editor, *Conductive polymers and plastics*, pages 1–40. Chapman and Hall, New York, 1989.

[7] R. H. Baughman. Conducting polymer artificial muscles. *Synthetic Metals*, 78(3):339–353, 1996.

[8] M. R. Gandhi, P. Murray, G. M. Spinks, and G. G. Wallace. Mechanism of electromechanical actuation in polypyrrole. *Synthetic Metals*, 73(3):247–256, 1995.

[9] T. F. Otero and H-J Grande. Electrochemomechanical devices: Artificial muscles based on conducting polymers. In T. A. Skotheim, R. L. Elsenbaumer, and J. R. Reynolds, editors, *Handbook of Conducting Polymers*, pages 1015–1028. M. Dekker, New York, 2 edition, 1998.

[10] T. F. Otero and J. M. Sansinena. Soft and wet conducting polymers for artificial muscles. *Advanced Materials*, 10(6), 1998.

[11] A. S. Hutchison, T. W. Lewis, S. E. Moulton, G. M. Spinks, and G. G. Wallace. Development of polypyrrole-based electromechanical actuators. *Synthetic Metals*, 113(1-2):121–127, 2000.

[12] Y. Bar-Cohen. Electro-active polymers: current capabilities and challenges. *Proceedings of SPIE*, Smart Structures and Materials 2002: Electroactive Polymer Actuators and Devices (EAPAD), 2002.

[13] T. Mirfakhrai, J. D. W. Madden, and R. H. Baughman. Polymer artificial muscles. *Materials Today*, 10(4):30 38, 2007.

[14] R. Z. Pytel. *Artificial Muscle Morphology - Structure/Property Relationships in Polypyrrole Actuators.* PhD thesis, Massachusetts Institute of Technology, 2007.

[15] J. D. Madden. *Conducting Polymer Actuators.* PhD thesis, Massachusetts Institute of Technology, 2000.

[16] P. G. A. Madden. *Development and Modeling of Conducting Polymer Actuators and the Fabrication of a Conducting Polymer Based Feedback Loop.* PhD thesis, Massachusetts Institute of Technology, 2003.

[17] H. Shirakawa, E. J. Louis, A. G. Macdiarmid, C. K. Chiang, and A. J. Heeger. Synthesis of electrically conducting organic polymers - halogen derivatives of polyacetylene, (Ch)X. *Journal of the Chemical Society-Chemical Communications*, pages 578 580, 1977.

[18] B. Norden and Krutmeijer. E. The Nobel Prize in chemistry, 2000: Conductive polymers, 2000.

[19] R. Farchioni and Giuseppe Grosso. *Organic Electronic Materials : Conjugated Polymers and Low Molecular Weight Organic Solids.* Springer, Berlin ; New York, 2001.

[20] J. M. Margolis. *Conductive polymers and plastics.* Chapman and Hall, New York, 1989.

[21] G. G. Wallace, G. M. Spinks, L. A. P. Kane-Maguire, and P. R. Teasdale. *Conductive Electroactive Polymers : Intelligent Materials Systems.* CRC Press, Boca Raton, FL, 2nd edition, 2003.

[22] M. Yamaura, T. Hagiwara, and K. Iwata. Enhancement of electrical-conductivity of poly-pyrrole film by stretching - counter ion effect. *Synthetic Metals*, 26(3):209 224, 1988.

[23] P. G. Madden, J. D. Madden, P. A. Anquetil, H. Yu, T. M. Swager, and I. W. Hunter. Conducting polymers as building blocks for biomimetic systems, 2001.

[24] Q. Pei and R. Qian. Protonation and deprotonation of polypyrrole chain in aqueous solutions. *Synthetic Metals*, 45(1991):35 48, 1991.

[25] N. A. Vandesteeg. *Synthesis and Characterization of Conducting Polymer Actuators.* PhD thesis, Massachusetts Institute of Technology, 2007.

[26] Q. B. Pei and O. Inganas. Electrochemical applications of the bending beam method .1. mass-transport and volume changes in polypyrrole during redox. *Journal of Physical Chemistry*, 96(25):10507 10514, 1992.

[27] M. Ue. Mobility and ionic association of lithium and quaternary ammonium-salts in propylene carbonate and gamma-butyrolactone. *Journal of the Electrochemical Society*, 141(12):3336–3342, 1994.

[28] R. H. Baughman, L. W. Shacklette, R. L. Elsenbaumer, E. J. Plichta, and C. Becht. Micro electromechanical actuators based on conducting polymers. In P. I. Lazarev, editor, *Molecular Electronics: Materials and Methods*, Topics in Molecular Organization and Engineering, pages 267–289. Kluwer Academic Publishers, Boston, 1991.

[29] I. W. Hunter and S. Lafontaine. A comparison of muscle with artificial actuators. pages 178–185, 1992.

[30] I. W. Hunter, J. Madden, and P. Madden. Conducting polymer devices for the home. *The Home Automation and Healthcare Consortium*, (Progress Report No. 2-3), 1999.

[31] J. D. Madden, R. A. Cush, T. S. Kanigan, C. J. Brenan, and I. W. Hunter. Encapsulated polypyrrole actuators. *Synthetic Metals*, 105(1):61–64, 1999.

[32] J. D. Madden, R. A. Cush, T. S. Kanigan, and I. W. Hunter. Fast contracting polypyrrole actuators. *Synthetic Metals*, 113(1-2):185–192, 2000.

[33] A. Mazzoldi, A. DellaSanta, and D. DeRossi. Conducting polymer actuators: Properties and modeling. In Y. Osada and D. DeRossi, editors, *Polymer Sensors and Actuators*, Macromolecular systems, materials approach. Springer, New York, 2000.

[34] S. Hara, T. Zama, S. Sewa, W. Takashima, and K. Kaneto. Highly stretchable and powerful polypyrrole linear actuators. *Chemistry Letters*, 32(7):576–577, 2003.

[35] S. Hara, T. Zama, S. Sewa, W. Takashima, and K. Kaneto. Polypyrrole-metal coil composites as fibrous artificial muscles. *Chemistry Letters*, 32(9):800–801, 2003.

[36] E. Smela. Conjugated polymer actuators for biomedical applications. *Advanced Materials*, 15(6):481–494, 2003.

[37] G. M. Spinks, G. G. Wallace, L. Liu, and D. Zhou. Conducting polymers electromechanical actuators and strain sensors. *Macromolecular Symposia*, 192:161–169, 2003.

[38] W. Takashima, S. S. Pandey, and K. Kaneto. Bi-ionic actuator by polypyrrole films. *Synthetic Metals*, 135(1-3):61–62, 2003.

[39] P. A. Anquetil, D. Rinderknecht, N. A. Vandesteeg, J. Madden, and I. W. Hunter. Large strain actuation in polypyrrole actuators. *Proceedings of SPIE*, 5385(Smart Structures and Materials 2004 - Electroactive Polymer Actuators and Devices (EAPAD)), 2004.

[40] J. D. W. Madden, B. Schmid, M. Hechinger, S. R. Lafontaine, P. G. A. Madden, F. S. Hover, R. Kimball, and I. W. Hunter. Application of polypyrrole actuators: Feasibility of variable camber foils. *IEEE Journal of Oceanic Engineering*, 29(3):738 749, 2004.

[41] A. Chen. Large displacement fast conducting polymer actuators. Master's thesis, Massachusetts Institute of Technology, 2006.

[42] S. Hara, T. Zama, W. Takashima, and K. Kaneto. Tris(trifluoromethylsulfonyl)methide-doped polypyrrole as a conducting polymer actuator with large electrochemical strain. *Synthetic Metals*, 156(2-4):351 355, 2006.

[43] Q. B. Pei and O. Inganas. Conjugated polymers and the bending cantilever method: Electrical muscles and smart devices. *Advanced Materials*, 4(4):277 278, 1992.

[44] E. Smela, O. Inganas, Q. B. Pei, and I. Lundstrom. Electrochemical muscles - micromachining fingers and corkscrews. *Advanced Materials*, 5(9):630 632, 1993.

[45] T. F. Otero, J. Rodriguez, E. Angulo, and C. Santamaria. Artificial synthetic metals. 55(557):3713 3717, 1993.

[46] E. Smela, O. Inganas, and I. Lundstrom. Controlled folding of micrometer-size structures. *Science*, 268:1735 1738, 1995.

[47] T. F. Otero and J. M. Sansinena. Artificial muscles based on conducting polymers. *Bioelectrochemistry and Bioenergetics*, 38(2):411 414, 1995.

[48] A. Della Santa, A. Mazzoldi, C. Tonci, and D. De Rossi. Passive mechanical properties of polypyrrole films: A continuum, poroelastic model. *Materials Science and Engineering: C*, 5(2):101 109, 1997.

[49] E. W. H. Jager, E. Smela, and O. Inganas. On-chip microelectrodes for electrochemistry with moveable polypyrrole bilayer actuators as working electrodes. *Sensors and Actuators B*, 56:73 78, 1999.

[50] Y. Wu, G. Alici, G. M. Spinks, and G. G. Wallace. Fast trilayer polypyrrole bending actuators for high speed applications. *Synthetic Metals*, 156(16-17):1017 1022, 2006.

[51] J. Tangorra, P. A. Anquetil, N. S. Wiedenman, T. Fofonoff, and I. W. Hunter. Applications of conducting polymers: Robotic fins and other devices, 2007.

[52] J. Madden, P. Madden, P. A. Anquetil, and I. W. Hunter. Load and time dependence of displacement in a conducting polymer actuator, 2002.

[53] D. De Rossi, A. Della Santa, and A. Mazzoldi. Dressware: wearable hardware. *Materials Science and Engineering C-Biomimetic and Supramolecular Systems*, 7(1):31–35, 1999.

[54] J. Madden, D. Rinderknecht, P. A. Anquetil, and I. W. Hunter. Creep and cycle life in polypyrrole actuators. *Sensors and Actuators A-Physical*, 2006.

[55] J. Madden, P. Madden, and I. W. Hunter. Conducting polymer actuators as engineering materials, 18-21 March 2002.

[56] M. Del Zio. Title. Master's thesis, Massachusetts Institute of Technology, 2006.

[57] E. Smela. Microfabrication of PPy microactuators and other conjugated polymer devices. *Journal of Micromechanical Microengineering*, 9:1–18, 1999.

[58] S. Holdcroft. Patterning pi-conjugated polymers. *Advanced Materials*, 13(23):1753–1765, 2001.

[59] R. Parashkov, E. Becker, T. Riedl, H. H. Johannes, and W. Kowalsky. Large area electronics using printing, methods. *Proceedings of the IEEE*, 93(7):1321–1329, 2005.

[60] L. F. Rozsnyai and M. S. Wrighton. Selective deposition of conducting polymers via monolayer photopatterning. *Langmuir*, 11(10):3913–3920, 1995.

[61] L. M. Dai, A. W. H. Mau, X. Y. Gong, and H. J. Griesser. Electrochemical generation of conducting polymer patterns on plasma modified surfaces. *Synthetic Metals*, 85(1-3):1379–1380, 1997.

[62] D. Hohnholz and A. G. MacDiarmid. Line patterning of conducting polymers: New horizons for inexpensive, disposable electronic devices. *Synthetic Metals*, 121(1-3):1327–1328, 2001.

[63] D. A. LaVan, P. M. George, and R. Langer. Simple, three-dimensional microfabrication of electrodeposited structures. *Angewandte Chemie-International Edition*, 42(11):1262–1265, 2003.

[64] E. W. H. Jager, E. Smela, and O. Inganas. Microfabricating conjugated polymer actuators. *Science*, 290(5496):1540–1545, 2000.

[65] E. Smela, O. Inganas, and I. Lundstrom. Conducting polymers as artificial muscles: challenges and possibilities. *Journal of Micromechanical Microengineering*, 3:203–205, 1993.

[66] W. Takashima, K. Kanamori, S. S. Pandey, and K. Kaneto. Patternable bi-ionic actuator: an example of new functionality of actuation, folding and unfolding of electrochemical spring. *Sensors and Actuators B-Chemical*, 110(1):120–124, 2005.

[67] T. Makela, S. Pienimaa, S. Jussila, and H. Isotalo. Lithographic patterning of conductive polyaniline. *Synthetic Metals*, 101(1-3):705 706, 1999.

[68] K. K. Gleason. Engineering the vapor deposition of conducting polymer nanocoatings. In *Army Nanotechnology Seminars*. MIT Institute for Soldier Nanotechnologies, 2008.

[69] H. Sirringhaus, T. Kawase, R. H. Friend, T. Shimoda, M. Inbasekaran, W. Wu, and E. P. Woo. High-resolution inkjet printing of all-polymer transistor circuits. *Science*, 290(5499):2123 2126, 2000.

[70] R. A. de Barros, C. R. Martins, and W. M. de Azevedo. Writing with conducting polymer. *Synthetic Metals*, 155(1):35 38, 2005.

[71] M. X. Chen, D. Nilsson, T. Kugler, M. Berggren, and T. Remonen. Electric current rectification by an all-organic electrochemical device. *Applied Physics Letters*, 81(11):2011 2013, 2002.

[72] Y. X. Liu, T. H. Cui, and K. Varahramyan. All-polymer capacitor fabricated with inkjet printing technique. *Solid-State Electronics*, 47(5):1543 1548, 2003.

[73] Y. Liu and T. H. Cui. Polymer-based rectifying diodes on a glass substrate fabricated by ink-jet printing. *Macromolecular Rapid Communications*, 26(4):289 292, 2005.

[74] Y. Liu, K. Varahramyan, and T. H. Cui. Low-voltage all-polymer field-effect transistor fabricated using an inkjet printing technique. *Macromolecular Rapid Communications*, 26:1955 1969, 2005.

[75] S.D. Ahn, S.Y. Kang, Y.E. Lee, M.J. Joung, C.A. Kim, and S.S. Suh. Thin film morphology and growth mechanism of pentacene thin film using low-pressure organic vapor deposition. *Materials Research Society Symposium Proceedings*, 769, 2003.

[76] S. R. Forrest. The path to ubiquitous and low-cost organic electronic appliances on plastic. *Nature*, 428(6986):911 918, 2004.

[77] S. W. Pyo, D. H. Lee, J. R. Koo, J. H. Kim, J. H. Shim, and Y. K. Kim. Organic thin-film transistors based on vapor-deposition polymerized gate insulators. *Japanese Journal of Applied Physics Part 1-Regular Papers Brief Communications and Review Papers*, 44(1B):652 655, 2005.

[78] L. Dall'Acqua, C. Tonin, A. Varesano, W. Porzio, and M. Catellani. Vapour phase polymerisation of pyrrole on cellulose-based textile substrates. *Synthetic Metals*, 156(5-6):379 386, 2006.

[79] J. P. Lock, S. G. Im, and K. K. Gleason. Oxidative chemical vapor deposition of electrically conducting poly(3,4-ethylenedioxythiophene) films. *Macromolecules*, 39(16):5326 5329, 2006.

[80] S. G. Im, K. K. Gleason, and E. A. Olivetti. Doping level and work function control in oxidative chemical vapor deposited poly (3,4-ethylenedioxythiophene). *Applied Physics Letters*, 90(15):--, 2007.

[81] P. Horowitz and W. Hill. *The Art of Electronics.* Cambridge University Press, New York, 2nd edition, 1989.

[82] C. J. Drury, C. M. J. Mutsaers, C. M. Hart, M. Matters, and D. M. de Leeuw. Low-cost all-polymer integrated circuits. *Applied Physics Letters*, 73(1):108 110, 1998.

[83] G. Horowitz. Organic field-effect transistors. *Advanced Materials*, 10(5):365 377, 1998.

[84] G. H. Gelinck, T. C. T. Geuns, and D. M. de Leeuw. High-performance all-polymer integrated circuits. *Applied Physics Letters*, 77(10):1487 1489, 2000.

[85] B. K. Crone, A. Dodabalapur, R. Sarpeshkar, R. W. Filas, Y. Y. Lin, Z. Bao, J. H. O'Neill, W. Li, and H. E. Katz. Design and fabrication of organic complementary circuits. *Journal of Applied Physics*, 89(9):5125 5132, 2001.

[86] J. A. Rogers and Z. Bao. Printed plastic electronics and paperlike displays. *Journal of Polymer Science Part a-Polymer Chemistry*, 40(20):3327 3334, 2002.

[87] J. H. Sung, S. J. Kim, and K. H. Lee. Fabrication of microcapacitors using conducting polymer microelectrodes. *Journal of Power Sources*, 124(1):343 350, 2003.

[88] D. Hohnholz, H. Okuzaki, and A. G. MacDiarmid. Plastic electronic devices through line patterning of conducting polymers. *Advanced Functional Materials*, 15(1):51 56, 2005.

[89] F. Ebisawa, T. Kurokawa, and S. Nara. Electrical-properties of polyacetylene polysiloxane interface. *Journal of Applied Physics*, 54(6):3255 3259, 1983.

[90] A. Tsumura, H. Koezuka, and T. Ando. Macromolecular electronic device - field-effect transistor with a polythiophene thin-film. *Applied Physics Letters*, 49(18):1210 1212, 1986.

[91] K. Tada, H. Harada, and K. Yoshino. Polymeric bipolar thin-film transistor utilizing conducting polymer containing electron transport dye. *Japanese Journal of Applied Physics Part 2-Letters*, 35(7B):L944 L946, 1996.

[92] Z. N. Bao, Y. Feng, A. Dodabalapur, V. R. Raju, and A. J. Lovinger. High-performance plastic transistors fabricated by printing techniques. *Chemistry of Materials*, 9(6):1299 1301, 1997.

[93] H. Sirringhaus, N. Tessler, and R. H. Friend. Integrated optoelectronic devices based on conjugated polymers. *Science*, 280(5370):1741 1744, 1998.

[94] G. Horowitz. Organic thin film transistors: From theory to real devices. *Journal of Materials Research*, 19(7):1946 1962, 2004.

[95] M. Halik, H. Klauk, U. Zschieschang, T. Kriem, G. Schmid, W. Radlik, and K. Wussow. Fully patterned all-organic thin film transistors. *Applied Physics Letters*, 81(2):289 291, 2002.

[96] M. Halik, H. Klauk, U. Zshieschang, G. Schmid, W. Radlik, and W. Weber. Polymer gate dielectrics and conducting-polymer contacts for high-performance organic thin-film transistors. *Advanced Materials*, 14(23):1717 1722, 2002.

[97] W. Clemens, I. Fix, J. Ficker, A. Knobloch, and A. Ullmann. From polymer transistors toward printed electronics. *Journal of Materials Research*, 19(7):1963 1973, 2004.

[98] A. Lodha and R. Singh. Prospects of manufacturing organic semiconductor-based integrated circuits. *IEEE Transactions on Semiconductor Manufacturing*, 14(3):281 296, 2001.

[99] J. H. Burroughes, D. D. C. Bradley, A. R. Brown, R. N. Marks, K. Mackay, R. H. Friend, P. L. Burns, and A. B. Holmes. Light-emitting-diodes based on conjugated polymers. *Nature*, 347(6293):539 541, 1990.

[100] R. Lawler. Sony's 1,000,000:1 contrast ratio 27-inch OLED HDTV. *www.endgadget.com*, January 8, 2007.

[101] V. Saxena, V. Shirodkar, and R. Prakash. A comparative study of a polyindole-based microelectrochemical transistor in aqueous and non-aqueous electrolytes. *Journal of Solid State Electrochemistry*, 4(4):231 233, 2000.

[102] M. Taniguchi and T. Kawai. Characteristics of electrochemical transistors. *Molecular Crystals and Liquid Crystals*, 444:61 66, 2006.

[103] H. S. White, G. P. Kittlesen, and M. S. Wrighton. Chemical derivatization of an array of 3 gold microelectrodes with polypyrrole - fabrication of a molecule-based transistor. *Journal of the American Chemical Society*, 106(18):5375 5377, 1984.

[104] C. Kranz, M. Ludwig, H. E. Gaub, and W. Schuhmann. Lateral deposition of polypyrrole lines over insulating gaps - towards the development of polymer-based electronic devices. *Advanced Materials*, 7(6):568 571, 1995.

[105] M. X. Chen. Printed electrochemical devices using conducting polymers as active materials on flexible substrates. *Proceedings of the IEEE*, 93(7):1339 1347, 2005.

[106] J. R. Sheats. Manufacturing and commercialization issues in organic electronics. *Journal of Materials Research*, 19(7):1974 1989, 2004.

[107] C. Immerstrand, K. Holmgren-Peterson, K. E. Magnusson, E. Jager, M. Krogh, M. Skoglund, A. Selbing, and O. Inganas. Conjugated-polymer micro- and milliactuators for biological applications. *MRS Bulletin*, 27(6):461–464, 2002.

[108] P. M. George, A. W. Lyckman, D. A. LaVan, A. Hegde, Y. Leung, R. Avasare, C. Testa, P. M. Alexander, R. Langer, and M. Sur. Fabrication and biocompatibility of polypyrrole implants suitable for neural prosthetics. *Biomaterials*, 26(17):3511–3519, 2005.

[109] E. M. Genies, M. Marchesiello, and G. Bidan. Preparation and properties of polypyrrole made in the presence of biological buffers. *Electrochimica Acta*, 37(6):1015–1020, 1992.

[110] P. Akhtar, C. O. Too, and G. G. Wallace. Detection of amino acids at conducting electroactive polymer modified electrodes using flow injection analysis .1. use of macroelectrodes. *Analytica Chimica Acta*, 339(3):201–209, 1997.

[111] P. Akhtar, C. O. Too, and G. G. Wallace. Detection of amino acids at conducting electroactive polymer modified electrodes using flow injection analysis .2. use of microelectrodes. *Analytica Chimica Acta*, 339(3):211–223, 1997.

[112] C. E. Schmidt, V. R. Shastri, J. P. Vacanti, and R. Langer. Stimulation of neurite outgrowth using an electrically conducting polymer. *Proceedings of the National Academy of Sciences of the United States of America*, 94(17):8948–8953, 1997.

[113] G. Bidan, M. Billon, T. Livache, G. Mathis, A. Roget, and L. M. Torres-Rodriguez. Conducting polymers as a link between biomolecules and microelectronics. *Synthetic Metals*, 102(1-3):1363–1365, 1999.

[114] J. H. Collier, J. P. Camp, T. W. Hudson, and C. E. Schmidt. Synthesis and characterization of polypyrrole-hyaluronic acid composite biomaterials for tissue engineering applications. *Journal of Biomedical Materials Research*, 50(4):574–584, 2000.

[115] L. A. P. Kane-Maguire and G. G. Wallace. Communicating with the building blocks of life using organic electronic conductors. *Synthetic Metals*, 119(1-3):39–42, 2001.

[116] V. Misoska, W. E. Price, S. F. Ralph, G. G. Wallace, and N. Ogata. Synthesis, characterisation and ion transport studies on polypyrrole/deoxyribonucleic acid conducting polymer membranes. *Synthetic Metals*, 123(2):279–286, 2001.

[117] L. Cen, K. G. Neoh, and E. T. Kang. Surface functionalization of electrically conductive polypyrrole film with hyaluronic acid. *Langmuir*, 18(22):8633–8640, 2002.

[118] J. Migdalski, T. Blaz, B. Paczosa, and A. Lewenstam. Magnesium and calcium-dependent membrane potential of poly(pyrrole) films doped with adenosine triphosphate. *Microchimica Acta*, 143(2-3):177 185, 2003.

[119] M. Mattioli-Belmonte, F. Gabbanelli, M. Marcaccio, F. Giantomassi, R. Tarsi, D. Natali, A. Callegari, F. Paolucci, and G. Biagini. Bio-characterisation of tosylate-doped polypyrrole films for biomedical applications. *Materials Science and Engineering C-Biomimetic and Supramolecular Systems*, 25(1):43 49, 2005.

[120] D. D. Ateh, P. Vadgama, and H. A. Navsaria. Culture of human keratinocytes on polypyrrole-based conducting polymers. *Tissue Engineering*, 12(4):645 655, 2006.

[121] P. M. George, D. A. LaVan, J. A. Burdick, C. Y. Chen, E. Liang, and R. Langer. Electrically controlled drug delivery from biotin-doped conductive polypyrrole. *Advanced Materials*, 18(5):577 +, 2006.

[122] Y. L. Li, K. G. Neoh, L. Cen, and E. T. Kang. Physicochemical and blood compatibility characterization of polypyrrole surface functionalized with heparin. *Biotechnology and Bioengineering*, 84(3):305 313, 2003.

[123] S. Geetha, C. R. K. Rao, M. Vijayan, and D. C. Trivedi. Biosensing and drug delivery by polypyrrole. *Analytica Chimica Acta*, 568(1-2):119 125, 2006.

[124] J. Wong, D. Ingber, and R. Langer. Characterization of electrically conducting polypyrrole thin-films for protein adsorption and cell attachment. *Abstracts of Papers of the American Chemical Society*, 206:9 Poly, 1993.

[125] J. Y. Wong, R. Langer, and D. E. Ingber. Electrically conducting polymers can noninvasively control the shape and growth of mammalian-cells. *Proceedings of the National Academy of Sciences of the United States of America*, 91(8):3201 3204, 1994.

[126] S. Cosnier. Biomolecule immobilization on electrode surfaces by entrapment or attachment to electrochemically polymerized films. a review. *Biosensors and Bioelectronics*, 14(5):443 456, 1999.

[127] X. Wang, X. Gu, C. Yuan, S. Chen, P. Zhang, T. Zhang, J. Yao, F. Chen, and G. Chen. Evaluation of biocompatibility of polypyrrole in vitro and in vivo. *Journal of Biomedical Materials Research*, 68A(2004):411 422, 2003.